Computational and Mathematical Methods in Medicine

Computational and Control Methods in Rehabilitation Medicine

Guest Editors: Imre Cikajlo, Takashi Watanabe, and Strahinja Dosen

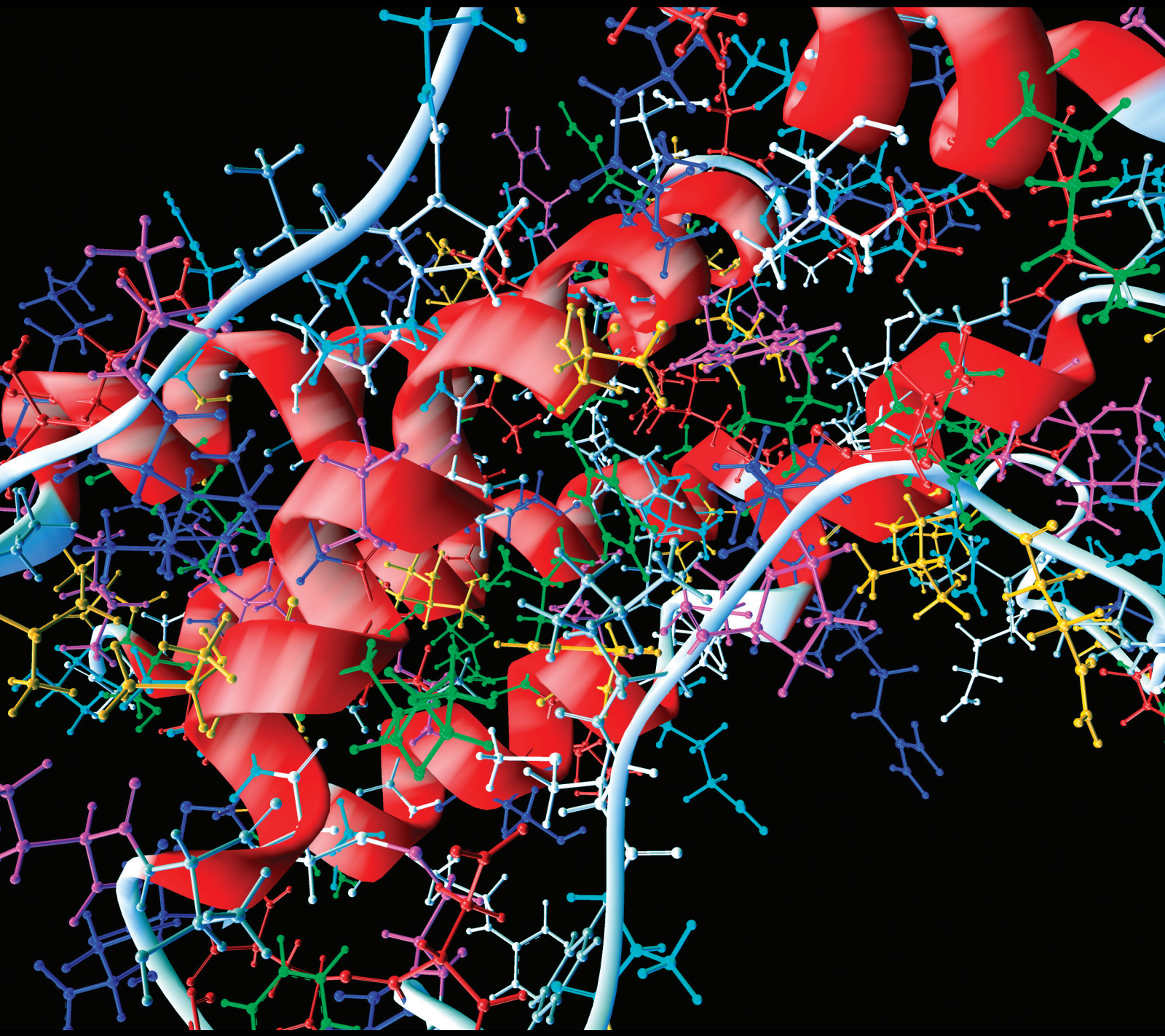

Computational and Control Methods in Rehabilitation Medicine

Computational and Mathematical Methods in Medicine

Computational and Control Methods in Rehabilitation Medicine

Guest Editors: Imre Cikajlo, Takashi Watanabe, and Strahinja Dosen

Editorial Board

Contents

Hindawi Publishing Corporation
Computational and Mathematical Methods in Medicine
Volume 2014, Article ID 707208, 2 pages
http://dx.doi.org/10.1155/2014/707208

Editorial

Computational and Control Methods in Rehabilitation Medicine

Imre Cikajlo,[1] Takashi Watanabe,[2] and Strahinja Dosen[3]

[1] *Research and Development Unit, University Rehabilitation Institute, Linhartova 51, 1000 Ljubljana, Slovenia*
[2] *Division of Biomedical Engineering for Health and Welfare, Graduate School of Biomedical Engineering, Tohoku University, 6-6 Aoba, Aramaki, Aoba-ku, Sendai 980-8579, Japan*
[3] *Department of Neurorehabilitation Engineering, Bernstein Focus Neurotechnology (BFNT) Göttingen, Bernstein Center for Computational Neuroscience (BCCN), University Medical Center Göttingen, University of Göttingen, Von Siebold Street 6, 37075 Göttingen, Germany*

Correspondence should be addressed to Imre Cikajlo; imre.cikajlo@ir-rs.si

Received 18 May 2014; Accepted 18 May 2014; Published 14 July 2014

In recent years the development of human-machine interfaces for medical applications and rehabilitation medicine has rapidly increased and still continues to grow [1]. The main goals have been a novel in-patient and outpatient diagnostics and improved quality of life, especially for the people with neuromuscular impairments or diseases [2]. The research and development in this field require various novel control algorithms and computational tools to extract features from measured biosignals. Some recently developed algorithms and tools may become part of the in-house equipment for hospitals, while some advanced solutions for home applications may also enable telemedical services in the recent future [3].

Before any computation or control of human activity is possible, information on movement of body segments is required. When information from natural sensors is not accessible, external devices such as accelerometers and gyroscopes can provide sufficient information on gait, standing up, balance, or specific motion of lower or upper extremities. However, these sensors are prone to bias, integration, and temperature drift and cannot provide sufficient accuracy for closed-loop control. The use of various mathematical tools, especially extended Kalman filter, can help to partly overcome the specified problem and can assure measurement of selected parameters up to the acceptable level of accuracy [4]. Besides the Kalman filter alternative feature extraction algorithms like discrete Fourier transform, dynamic time warping, or harmonic linear dynamical system are applied [5]. In this special issue we publish an example of electrocardiogram feature extraction.

The accurate and reliable sensory information is a prerequisite for the design of a closed-loop control system, especially when a human is in interaction with the machine in terms of "feeling the environment" or haptics [6]. The word haptic originates from the Greek word haptikos (ἁπτικός) and is related to the sense of touch. This is nowadays particularly important in rehabilitation of patients suffering from stroke. In combination with virtual reality technologies, an upper extremity, and balance, grasping of hand rehabilitation devices can be designed [6]. The haptic robots serving for various rehabilitation purposes are usually complex and intended for the use in clinical environment. However, their simplified passive versions or simple rehabilitation aids equipped with inertial sensory systems are already part of the telerehabilitation systems in function in patients' homes [3] or smart homes. These premises are often well equipped with information-communication technologies and the patients can take full advantage of remote treatment and testing of various novel technologies which may lead to the significant improvement of quality of life [7]. On the other hand, a technological progress, novel computation, and control methods that enable new approaches in rehabilitation medicine require constant clinical evaluation in order to find its way to the everyday clinical practice [8].

We hope the readers of the Journal of Computational and Mathematical Methods in Medicine will find in this special

issue solid theoretical and technological solutions as well as their possible applications in the rehabilitation medicine. However, we would like to encourage the readers to raise new research questions and issues which will significantly contribute to the development and rapid uptake of technologies in rehabilitation medicine.

Imre Cikajlo
Takashi Watanabe
Strahinja Dosen

References

[1] D. Erol and N. Sarkar, "Coordinated control of assistive robotic devices for activities of daily living tasks," *IEEE Transactions on Neural Systems and Rehabilitation Engineering*, vol. 16, no. 3, pp. 278–285, 2008.

[2] I. Cikajlo and Z. Matjačić, "Directionally specific objective postural response assessment tool for treatment evaluation in stroke patients," *IEEE Transactions on Neural Systems and Rehabilitation Engineering*, vol. 17, no. 1, pp. 91–100, 2009.

[3] I. Cikajlo, M. Rudolf, N. Goljar, H. Burger, and Z. Matjačić, "Telerehabilitation using virtual reality task can improve balance in patients with stroke," *Disability and Rehabilitation*, vol. 34, no. 1, pp. 13–18, 2012.

[4] I. Cikajlo, Z. Matjačić, and T. Bajd, "Efficient FES triggering applying Kalman filter during sensory supported treadmill walking," *Journal of Medical Engineering and Technology*, vol. 32, no. 2, pp. 133–144, 2008.

[5] F. Sufi, Q. Fang, I. Khalil, and S. Mahmoud, "Novel methods of faster cardiovascular diagnosis in wireless telecardiology," *IEEE Journal on Selected Areas in Communications*, vol. 27, no. 4, pp. 537–552, 2009.

[6] J. Oblak, I. Cikajlo, and Z. Matjaĉić, "Universal haptic drive: a robot for arm and wrist rehabilitation," *IEEE Transactions on Neural Systems and Rehabilitation Engineering*, vol. 18, no. 3, pp. 293–302, 2010.

[7] M. McCue, A. Fairman, and M. Pramuka, "Enhancing quality of life through telerehabilitation," *Physical Medicine and Rehabilitation Clinics of North America*, vol. 21, no. 1, pp. 195–205, 2010.

[8] D. Kairy, P. Lehoux, C. Vincent, and M. Visintin, "A systematic review of clinical outcomes, clinical process, healthcare utilization and costs associated with telerehabilitation," *Disability and Rehabilitation*, vol. 31, no. 6, pp. 427–447, 2009.

Hindawi Publishing Corporation
Computational and Mathematical Methods in Medicine
Volume 2014, Article ID 761536, 8 pages
http://dx.doi.org/10.1155/2014/761536

Research Article

A Harmonic Linear Dynamical System for Prominent ECG Feature Extraction

Ngoc Anh Nguyen Thi,[1] Hyung-Jeong Yang,[1] SunHee Kim,[2] and Luu Ngoc Do[1]

[1] *Department of Computer Science, Chonnam National University, Gwangju 500-757, Republic of Korea*
[2] *Department of Computer Science, Carnegie Mellon University, Pittsburgh, PA 15213, USA*

Correspondence should be addressed to Hyung-Jeong Yang; hjyang@chonnam.ac.kr

Received 27 September 2013; Revised 6 January 2014; Accepted 10 January 2014; Published 26 February 2014

Academic Editor: Imre Cikajlo

Unsupervised mining of electrocardiography (ECG) time series is a crucial task in biomedical applications. To have efficiency of the clustering results, the prominent features extracted from preprocessing analysis on multiple ECG time series need to be investigated. In this paper, a Harmonic Linear Dynamical System is applied to discover vital prominent features via mining the evolving hidden dynamics and correlations in ECG time series. The discovery of the comprehensible and interpretable features of the proposed feature extraction methodology effectively represents the accuracy and the reliability of clustering results. Particularly, the empirical evaluation results of the proposed method demonstrate the improved performance of clustering compared to the previous main stream feature extraction approaches for ECG time series clustering tasks. Furthermore, the experimental results on real-world datasets show scalability with linear computation time to the duration of the time series.

1. Introduction

Clustering multiple time series data have received considerable attention in recent years in various applications, such as industries of finance, business, science domains, and medicine [1–8]. Clustering in time series is the unsupervised mining of grouping similar time series into a same cluster. Specifically, clustering finds groups of homogenous patterns into a cluster so that these patterns within the cluster bear strong similarity to other ones and dissimilarity to patterns in other clusters [9, 10].

Since the quality of clustering results relies strongly on good features extracted from multiple time series, a very important processing step is to identify compact features extracted from multiple coevolving time series. This step can be used to not only convert a series of original values to more meaningful information, such as more understandable and interpretable information, but it also can lead time series to a lower dimensionality with the most relevant features.

This paper is motivated by mining these essential features of the medicine applications, namely, electrocardiography (ECG) time series. The problems are studied based on the challenges across time series applications such as time shifts effects, nearby frequencies, and harmonics. By exploiting the temporal evolving trends and the correlation characteristics of coevolving time series, meaningful features which help to achieve the best clustering accuracy can be captured.

Feature extraction can efficiently describe time series since suitable representations reduce the feature spaces. This provides highly efficient features for knowledge discovery so that they help to improve performance as well as the speed of the mining algorithms.

Many time series representations have been proposed to extract features. The well-known dimension reduction approaches, namely, Principal Component Analysis (PCA) and Singular Value Decomposition (SVD), are powerful tools to discover linear correlations across multiple time series [11–15]. They effectively give the optimal low-rank approximation of the dataset by removing the variables with lower energy [14]. However, these methods ignore time-evolving patterns since their characteristics are not designed for tracking the ordering of the rows or the columns. Moreover, the projection of the multiple time series into low-dimensional principal components is not easy to interpret. They do not clearly

exhibit the characteristic of each pattern. As a result, applying clustering methodology with these reduction methods to multiple time series leads to poor performance.

One of the popular alternative approaches for feature extraction on multiple time series is Discrete Fourier Transform (DFT), where the original time series data is projected into the frequency domain [16–18]. The main advantage of DFT is to capture frequencies in a single time sequence. However, DFT lacks the dynamics; hence, clustering based on Fourier coefficients is not unsuitable. Another method based on Linear Predictive Coding Cepstrum (LPCC) which also provides distinguished features in time series is well known in signal recognition [8, 19, 20]. It is efficient for clustering performance by means of a few coefficients. However, the representations of achieved LPC cepstrum features are hard to interpret.

The Linear Dynamical System, known as Kalman filters, has been commonly used for time series analysis because of its simple implementation and extensibility [21–23]. Kalman filter can capture correlations among multiple time series and learn their evolving dynamics. However, the time shift effects, which are temporal gaps between two time series, cannot be handled. The representations of the extracted features are not also clear. The resulting model parameters thus lead to poor clustering performance.

Another popular feature extraction method, known as Dynamic Time Warping (DTW), can handle time shifts across the sequences. However, this approach ignores temporal dynamics. Therefore, applying DTW directly for clustering purpose cannot give good results [24].

Autoregression Moving Average (ARMA) is also a method for feature extraction. However, ARMA parameters do not provide a reliable method since different sets of parameters can be obtained even from time series with similar structures. As a result, the clustering performances will be affected dramatically [25, 26].

In this paper, we applied an approach of prominent feature extraction based on a Harmonic Linear Dynamical System (HLDS) [21] for unsupervised learning of time series in biomedical applications, specifically in ECG. Since the applications have characteristics of lag correlation and temporal dynamics, HLDS works well for the prominent feature extraction of the time series in the same period with different lags and light amplitudes. In addition, HLDS is expected to identify periodic patterns and group them into one cluster. These series of frequencies are known as harmonic series which contain several mixtures of frequencies, especially in sensor measurements, such as in human voice and in human motion domain [23, 27].

Our prime objective is to exploit two common characteristics of multiple coevolving time series: correlations and temporal dynamics for meaningful feature extraction. Correlation reflects the relationships among multiple time sequences, while dynamic property discovers the temporal moving trends of multiple time series by automatically identifying a few hidden variables. For example, a particular medical signal of physiological records in ECG application characterizes a specific symptom of a patient such as a malignant ventricular arrhythmia person. Therefore, each time series differs from the others in dynamics since time series encodes temporal dynamics along the time ticks. By capturing correlations, we can achieve good interpretable features in the presence of time shift effects and small shift in frequency. By exploiting the evolving temporal components, we can find the clusters of time series by grouping them with similar temporal patterns.

In order to evaluate the effectiveness of the applied method considering clustering accuracy, reliability, and complexity aspects, this paper demonstrates the clustering results of ECG time series using k-means algorithm. The method we applied discovers useful and understandable features from time series for clustering purposes. Moreover, its computational time scales up to the duration of the time sequences. We demonstrate comparative study to assess the performance of the proposed method against previous feature extraction algorithms such as PCA [11, 12], DFT [17, 18], original Kalman filter [22, 23], and LPCC [19, 20].

The rest of the paper is organized as follows. Background of the underlying Linear Dynamical System theory and the proposed model setup are given in the upcoming Section 2. In Section 3, the experimental time series dataset of ECG used in this paper are illustrated and the empirical evaluations have been conducted to assess effectiveness of the proposed feature extraction method in clustering multiple time series. Finally, we present our conclusions in Section 4.

2. Materials and Methods

2.1. Fundamentals of Linear Dynamical System. Multidimensional time series dataset Y is an ordered sequence of data points measured at equal time intervals, denoted by $Y = \{y_1, y_2, y_3, \ldots, y_T\}$, where each vector $y_1, y_2, y_3, \ldots, y_T$ is formed of M observations recorded at time ticks $t = 1$, $t = 2, \ldots, t = T$, respectively. Time series collections can be formed as the matrix below:

$$Y = \begin{bmatrix} y_1^1 & y_1^2 & \cdots & y_1^i & \cdots & y_1^M \\ y_2^1 & y_2^2 & \cdots & y_2^i & \cdots & y_2^M \\ \vdots & \vdots & & \vdots & & \vdots \\ y_t^1 & y_t^2 & \cdots & y_t^i & \cdots & y_t^M \\ \vdots & \vdots & & \vdots & & \vdots \\ y_T^1 & y_T^2 & \cdots & y_T^i & \cdots & y_T^M \end{bmatrix}. \quad (1)$$

In particular, each row vector includes all of the observations for one certain time tick which is an ordered sequence of T vectors each having dimensionality of M. Each column denotes the observations for one particular measurement, which is an unordered collection of M one-dimensional time series vector [1, 2].

Linear Dynamical System (LDS), known as Kalman filter, has been used to model multidimensional time series data. By taking the definition of time series above as a matrix for a dynamical system, this means that multidimensional time series data can be presented by a matrix $Y_{M\times T}$ of the variables M and observed time ticks T. LDS builds a statistical model to represent the state of the hidden variables

which are evolving to a linear transformation leading to the observed numerical time sequences. LDS captures the correlations among multiple signals by means of choosing a proper number of hidden variables so that the model can learn the dynamics of time series data [13, 14, 28]. LDS for a multidimensional time sequence is modeled by the following equations:

$$z_1 = \mu_0 + \omega_0 \tag{2}$$

$$z_{n+1} = A \cdot z_n + \omega_n \tag{3}$$

$$y_n = C \cdot z_n + \varepsilon_n, \tag{4}$$

where $\theta = \{\mu_0, Q_0, A, Q, C, R\}$ is the set of parameters. Vectors y_n and z_n denote observed data sequences and hidden variables at time n, respectively. μ_0 is an initial state for hidden variables of the whole system. The transition dynamic matrix A relates to the transition of the state from the current time tick to the next time tick with noise $\{\omega_n\}$. The matrix C is the observation projection with noise $\{\varepsilon_n\}$ at each time t. All noise ω_0, ω_i, and ε_i $(i = 1, \ldots, T)$ are zero-mean and normally distributed random variables with covariance matrices Q_0, Q, and R, respectively [29]. The Expectation Maximization (EM) algorithm is utilized to learn the component models and estimate hidden variables [30]. In the model, each row of output matrix C corresponds to one sequence and, therefore, can be used as features in clustering. However, the clustering quality is not good since these features cannot provide high interpretability excluding information of time shift. Time shift effect or phase shift indicates that two time series have the same frequency but different phase lags.

2.2. Proposed Feature Extraction Methodology. In this section, the proposed method for ECG dataset is set up to illustrate how to exploit the interpretability of prominent features extracted from multiple time series in order to improve the clustering quality. Since each row of output transition matrix C of the LDS model does not present distinct characteristic of the corresponding series, we explore further expecting to discover deeper hidden patterns for each sequence of LDS by learning the straight forward transition matrix A and output projection matrix C.

First of all, the hidden dynamics are learned via Linear Dynamical System (LDS), capturing the series of hidden variables which are evolving according to the linear transformation A; they are linearly transformed to the observed numerical sequences [13, 28]. This implies that the series of hidden variables, z_n, are evolving over time ticks with linear transition matrix A. Also, the observed data sequences, y_n, are generated from these series of hidden variables with a linear output projection matrix C [21].

Secondly, after achieving the hidden variables from the LDS system, the canonical form of the hidden variables is identified. However, these hidden variables are hard to interpret since they are mixed in the observation sequences. Therefore, we need to make them compact and uniquely identify. Equation (3) represents the hidden variables depending on the eigenvalues of the transition matrix A [21]. Those eigenvalues can capture the amplitude and frequencies of the underlying signals of hidden variables which are referred to as harmonics. As a result, normalizing the transition matrix can directly reveal the amplitude, frequency, and the mixtures of the given set of sequences. Harmonic Linear Dynamical System (HLDS) uses eigendecomposition on transition matrix A in order to find harmonics as well as the mixing weight of harmonics. The eigendecomposition corresponds to the diagonal matrix (Λ) of eigendynamics and eigenvector (V) of A as follows:

$$A = V \Lambda V^*. \tag{5}$$

In LDS, the output projection matrix C illustrates how the hidden variables are translated into observation sequences with linear combinations. Therefore, we need to compensate C matrix to achieve the harmonic mixing matrix C_h in order to obtain the same observation sequences from eigendynamics (Λ) as the transition matrix:

$$C_h = C \cdot V. \tag{6}$$

The canonical hidden variables will be

$$\begin{aligned} \mu_0^{\text{new}} &= V^* \cdot \mu_0, \\ z_n^{\text{new}} &= V^* \cdot z_n. \end{aligned} \tag{7}$$

V contains conjugate pairs of columns corresponding to the conjugate pairs of eigenvalues in Λ. Therefore, the harmonic mixing matrix C_h must contain conjugate pair of columns corresponding to the conjugate pairs of the eigenvalues in Λ:

$$\begin{aligned} z_n^{\text{new}} &= \Lambda^{n-1} \cdot \mu_0^{\text{new}} + \text{noise}, \\ y_{\text{new}} &= C_h \cdot \Lambda^{n-1} \cdot \mu_0^{\text{new}} + \text{noise}. \end{aligned} \tag{8}$$

From the equation, we can obtain all hidden variables z_n, canonical hidden variables z_n^{new}, and observation y_n. They are mixtures of a set of scaling such as growing, shrinking, or stationary sinusoid signals of data-dependent frequencies which are referred to as harmonics [21]. Their characteristics of frequencies and amplitudes are completely defined by the eigenvalues of the transition matrix A.

Thirdly, the harmonic mixing matrix C_h is calculated in the second step. From here, the contribution of each harmonic to the resulting observation sequences is found. This means that each row of C_h represents the characteristic of each sequence in the domain of the harmonics and thus, it can be used to cluster sequences. However, the harmonic mixing matrix will fail to group similar sequences with phase shifts or time shifts because it tells not only the strength of each eigen dynamic, but also encodes the required phases for different sequences. To eliminate the phase/lag effect by taking the magnitude of the harmonic mixing matrix C_h, we will obtain the same column for the conjugate column of C_h. By dropping these duplicated columns, we will obtain the harmonic magnitude matrix C_m, which tells how strong each harmonic base participates in the observation time sequences and solves lag challenge as well.

Lastly, in order to obtain the interpreted features for each sequence, we apply the dimension reduction approach with

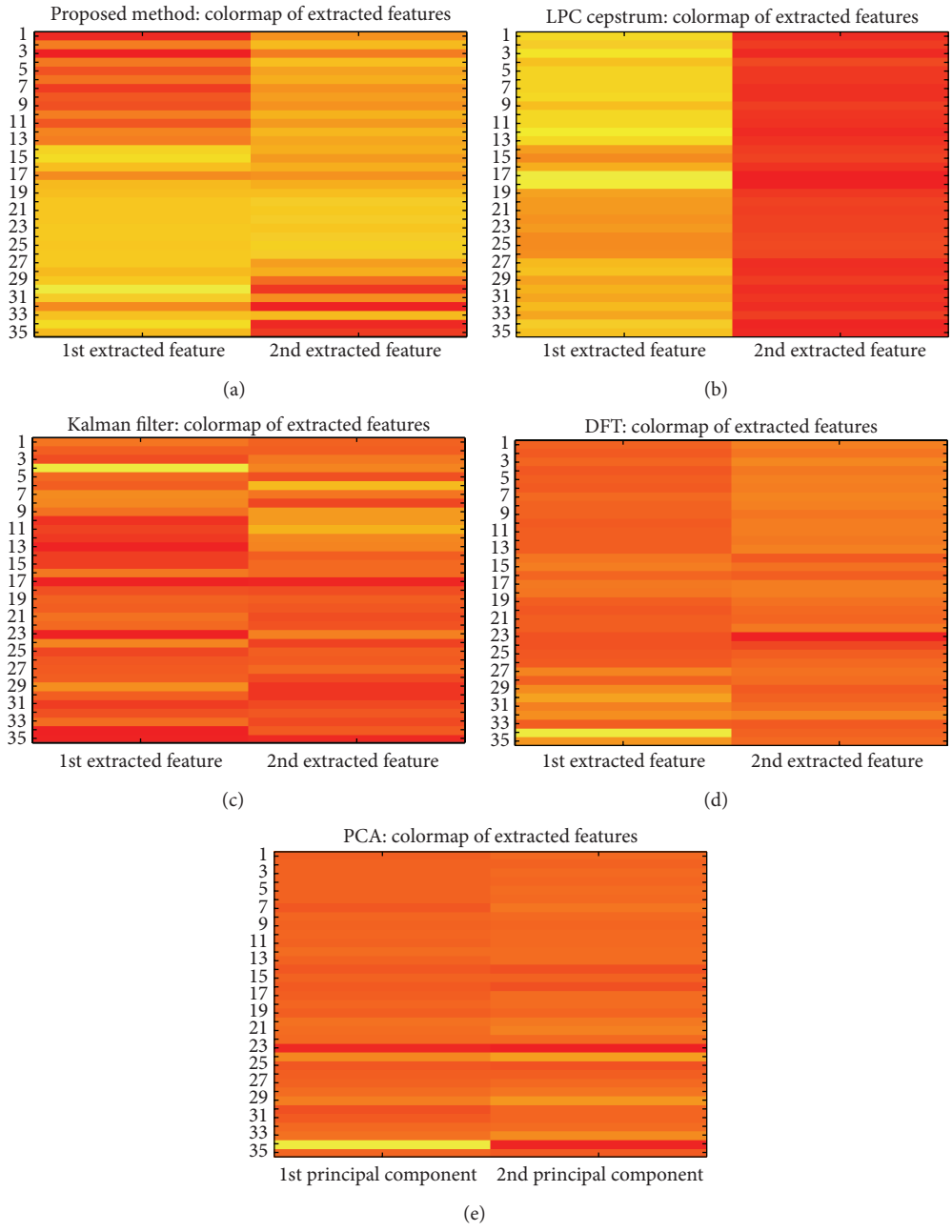

Figure 1: The first two extracted features of algorithms on EEG dataset.

SVD on the harmonic magnitude matrix, $\widetilde{C}_m \approx U_k \cdot S_k \cdot V_k^T$, where $\widetilde{C}_m$ is the column centered from C_m, U_k and V_k are orthogonal matrices with k columns, and S_k is a diagonal matrix. The interpretability of the prominent features can be obtained as $U_k \cdot S_k$. For the proper number of hidden dimension h in our ECG application, we use Fukunaka's principle rule [15, 21]. We choose h as the one with the 98th percentile of the total sum of squared singular values with s_i's being the singular values of Y in descending order. The formula is as follows:

$$h \longleftarrow \arg_h \frac{\sum_{j=1}^{h} s_j^2}{\sum_{i=1}^{m} s_i^2}. \quad (9)$$

In summary, HLDS includes four steps: (1) learning hidden variables using LDS, (2) taking eigendecomposition on transition matrix A to find the canonical form of hidden variables, which helps to find harmonics and mixing weight of harmonics, (3) taking the magnitude of the harmonic mixing matrix to eliminate phase shift, and (4) using SVD to combine harmonics.

3. Experimental Results and Discussion

In order to show the validation of the clustering by HLDS, we carry out experiments on real ECG dataset taken from

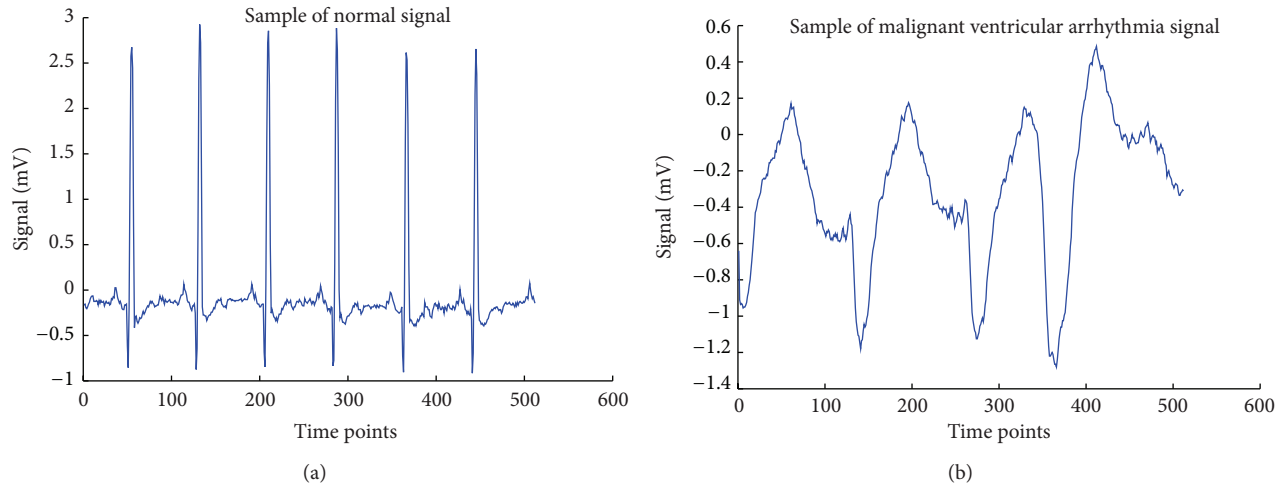

Figure 2: Original samples of normal and malignant ventricular arrhythmia time series, respectively.

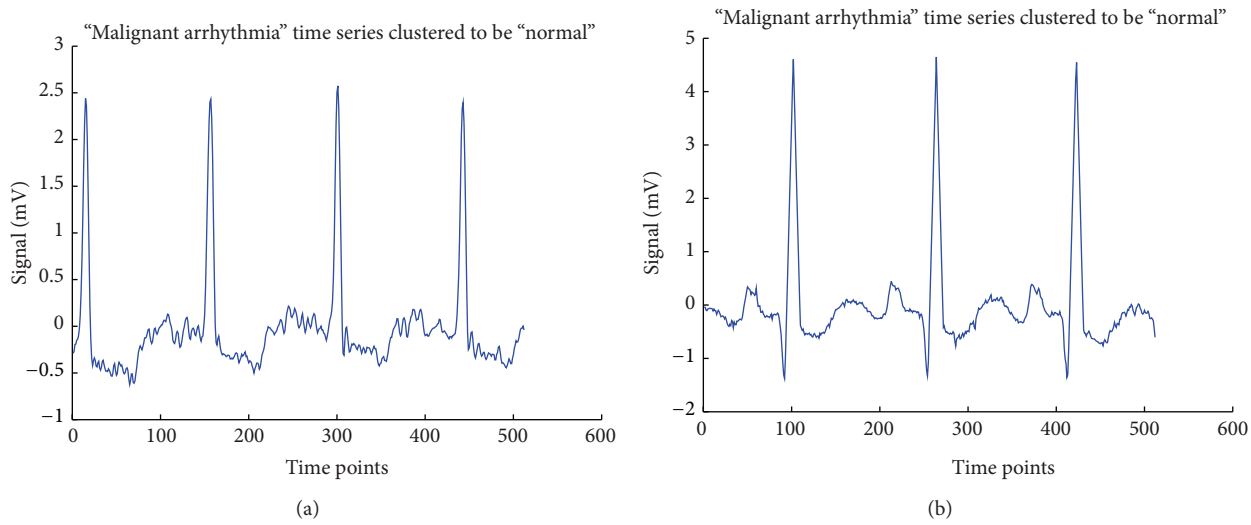

Figure 3: The 17th and 32nd malignant ventricular arrhythmia patterns clustered to be wrong cluster.

PhysioNet http://www.physionet.org/physiobank/database/ [31, 32]. A Harmonic Linear Dynamical System for the prominent feature extraction of ECG application is investigated successfully since the applications have the characteristics of lag correlations and temporal dynamics. These extracted features can group time series patterns in the same period with different lags and light amplitudes. Moreover, the applied method is expected to identify periodic patterns and group them into one cluster. ECG dataset contains three different groups of ECG time series: 13 time series of ECG recordings of healthy people, 22 time series of people having malignant ventricular arrhythmia, and 30 time series of people having supraventricular arrhythmia, taken from the following specific links:

(i) MIT-BIH Healthy/Normal Sinus Rhythm Database http://www.physionet.org/physiobank/database/nsrdb/;

(ii) MIT-BIH Malignant Ventricular Arrhythmia Database http://www.physionet.org/physiobank/database/vfdb/;

(iii) MIT-BIH Supraventricular Arrhythmia Database http://www.physionet.org/physiobank/database/svdb/.

There are two collections which are investigated. Collection 1 contains a group of healthy people and malignant ventricular arrhythmia while collection 2 is obtained by the group of healthy and supraventricular arrhythmia people. To evaluate the effectiveness of the feature extraction for the clustering, both the quality and scalability of normalized time series are considered against previous feature extraction approaches such as LPCC, PCA, DFT, and original Kalman filter. Normalization is carried out to compensate the differences in level and scale of dataset to a zero-mean and unit variance. In the experiment, we use the first two coefficients and cluster them by k-means algorithm with

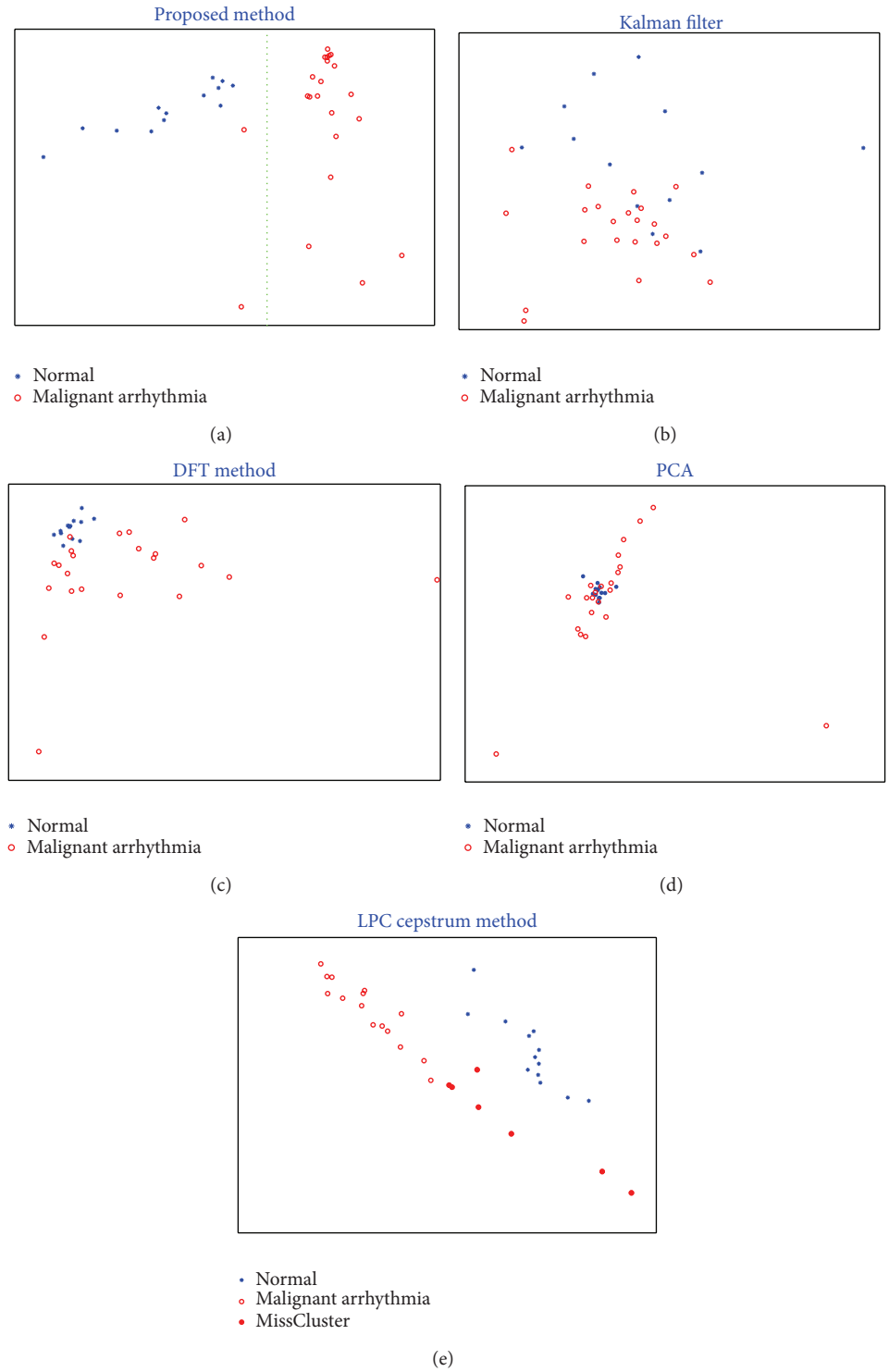

Figure 4: Scatter plot of clustering visualization.

Euclidean distance. For choosing the proper number of hidden variables, we set 98% of energy in each original data which is corresponding to the hidden dimension of 20 and 35 for collection 1 and collection 2, respectively.

To evaluate the quality of the clustering results, we use the confusion matrix since we know the ground truth labels of each sequence. The clustering performance of different methods on collection 1 of real ECG time series is recorded as follows: the proposed method (94.29%), LPCC (85.71%), KF (42.9%), DFT (57.14%), and PCA (40%). Compared to the previous feature extraction methods, the average performance of applied HLDS on real ECG datasets demonstrates

significant performances, that is, 9.1%, 54.5%, 39.39%, and 57.57% clustering improvement against the LPCC, original Kalman filter, DFT, and PCA, respectively.

Since this method can discover deeper hidden patterns which can capture correlation and temporal dynamics successfully, it provides the group of distinct harmonics that helps to handle the presence of the time shift effect with small shifts in frequency. These harmonic groups represent good resulting features which lead to good clustering as well as visualization.

In more detail, Figure 1 shows the comparison of the first two extracted features of ECG dataset by the proposed method, LPCC, original Kalman filter, DFT, and PCA. In each heat map of Figure 1, the rows represent the number of sequences of dataset and the columns show the first two features extracted from each method. Only the proposed method clearly illustrates the characteristic of the two clusters, normal and malignant ventricular arrhythmia especially in the 1st extracted features in Figure 1(a), where the rows have similar feature values colored in orange and yellow, so that they are grouped in the same cluster. On the other hand, the four remaining methods, Figures 1(b), 1(c), 1(d), and 1(e), do not show meaningful interpreted features.

The proposed method gives wrong clustering results for the 17th and 32nd signals. Even though the 17th and 32nd signals are malignant ventricular arrhythmia signals actually, the shapes of these signals are very similar to the normal case. Therefore, when applying method, they discover similar features as the normal cases; consequently, they are clustered to the normal cluster.

To verify them, the 17th and 32nd time sequences of Figure 1(a) are plotted in Figure 2 where the patterns of 17th and 32nd from Figure 1 are in very similar shape compared to the normal signal shown in Figure 3(a) where Figure 3(b) is a sample signal of malignant ventricular arrhythmia case.

Figure 4 shows the scatter plots of the first feature and the second feature from different methods for ECG clustering. On the other hand, the first two of extracted features are plotted to evaluate how much these features contribute to ECG recognition. It is observed that the HLDS shows clear separation of dots compared to the other approaches.

The proposed method again performs the best clustering accuracy for collection 2 which consists of healthy and supraventricular arrhythmia persons. The error rates for all of experimental methods are shown as follows: proposed method (0.139), LPCC (0.2326), KF (0.4419), PCA (0.3256), and DFT (0.3953).

The computational complexity of the HLDS is shown in Figure 5, executed on collection 1. It can be observed that wall clock times lie on almost a straight line over the duration of sequences since it would improve the scalability in ECG dataset. The computation time of HLDS is satisfied when the time duration T of the time sequences is increased.

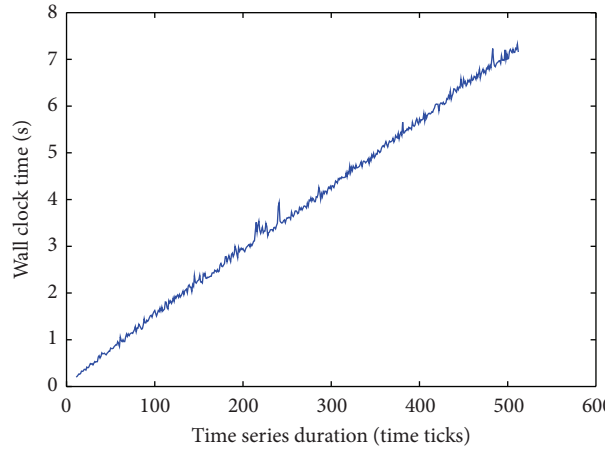

Figure 5: Linear execution time with respect to the length of sequences.

4. Conclusions

The proposed method, HLDS, considers the problem of handling the challenges of time series, namely, time shift, nearby frequencies, and harmonics. The applied method demonstrates the efficiency for solving these challenges in real applications of ECG time series domain. Interpretability of prominent features was discovered for the clustering as well as visualization. In most cases, HLDS gives the best result compared to the other feature extraction techniques such as Kalman filter, LPC cepstrum, DFT, and PCA. Moreover, the performance results show almost a linear speedup as we increase the input of the dataset.

For further study, we will investigate the harmonic linear dynamical system over much longer time series with missing values in various applications.

Conflict of Interests

The authors declare that there is no conflict of interests regarding the publication of this paper.

Acknowledgments

This research was supported by the MKE (The Ministry of Knowledge Economy), Korea, under the ITRC (Information Technology Research Center) support program supervised by the NIPA (National IT Industry Promotion Agency) (NIPA-2013-H0301-13-3005). This research was supported by Basic Science Research Program through the National Research Foundation of Korea (NRF) funded by the Ministry of Education, Science and Technology (2013-052849).

References

[1] R. T. Olszewski, *Generalized feature extraction for structural pattern recognition in time series data [Ph.D. thesis]*, School of Computer Science, Carnegie Mellon University, 2001.

[2] S. Papadimitriou and M. Vlachos, *Hand on Time Series Analysis with Matlab*, ICDM, Hong Kong, 2006.

[3] H. S. Guan and Q. S. Jiang, "Cluster financial time series for portfolio," in *Proceedings of the International Conference on*

Wavelet Analysis and Pattern Recognition (ICWAPR '07), pp. 851–856, November 2007.

[4] R. Krishnapuram, A. Joshi, O. Nasraoui, and L. Yi, "Low-complexity fuzzy relational clustering algorithms for web mining," *IEEE Transactions on Fuzzy Systems*, vol. 9, no. 4, pp. 595–607, 2001.

[5] X. Zhang, J. Liu, Y. Du, and T. Lv, "A novel clustering method on time series data," *Expert Systems with Applications*, vol. 38, no. 9, pp. 11891–11900, 2011.

[6] C. S. Möller-Levet, F. Klawonn, K. H. Cho, and O. Wolkenhauer, "Fuzzy clustering of short time-series and unevenly distributed sampling points," in *Advances in Intelligent Data Analysis V*, vol. 2810 of *Lecture Notes in Computer Science*, pp. 330–340, 2003.

[7] C. Goutte, L. K. Hansen, M. G. Liptrot, and E. Rostrup, "Feature-space clustering for fMRI meta-analysis," *Human Brain Mapping*, vol. 13, no. 3, pp. 165–183, 2001.

[8] K. Kalpakis, D. Gada, and V. Puttagunta, "Distance measures for effective clustering of ARIMA time-series," in *Proceedings of the 1st IEEE International Conference on Data Mining (ICDM '01)*, pp. 273–280, San Jose, Calif, USA, November-December 2001.

[9] Y. Xiong and D. Y. Yeung, "Time series clustering with ARMA mixtures," *Pattern Recognition*, vol. 37, no. 8, pp. 1675–1689, 2004.

[10] T. Warren Liao, "Clustering of time series data—a survey," *Pattern Recognition*, vol. 38, no. 11, pp. 1857–1874, 2005.

[11] I. T. Jolliffe, *Principal Component Analysis*, Springer, 2002.

[12] C. Ding and X. He, "K-means clustering via principal component analysis," in *Proceedings of the 21st International Conference on Machine Learning (ICML '04)*, pp. 29–32, July 2004.

[13] L. Li, J. McCann, N. Pollard, and C. Faloutsos, "DynaMMo: mining and summarization of coevolving sequences with missing values," in *Proceedings of the 15th ACM SIGKDD International Conference on Knowledge Discovery and Data Mining (KDD '09)*, pp. 507–515, New York, NY, USA, July 2009.

[14] L. Li and B. A. Prakash, "Time series clustering: complex is simpler!," in *Proceedings of the 28th International Conference on Machine Learning (ICML '11)*, pp. 185–192, July 2011.

[15] K. Fukunaga, *Introduction to Statistical Pattern Recognition*, Academic Press, San Diego, Calif, USA, 1990.

[16] Y. Wu, D. Agrawal, and A. E. Abbadi, "A comparison of DTF and DWT based similarity search in time series databases," in *Proceeding of the 9th ACM International Conference on Information and Knowledge Management (CIKM '00)*, pp. 488–495, 2000.

[17] M. Jahangiri, D. Sacharidis, and C. Shahabi, "Shift-split: I/O efficient maintenance of wavelet-transformed multidimensional data," in *Proceedings of the ACM SIGMOD International Conference on Management of Data (SIGMOD '05)*, pp. 275–286, June 2005.

[18] F. Morchen, "Time series feature extraction for data mining using dwt and dft," Tech. Rep. 33, Philipps-University Marburg, 2003.

[19] L. Rabiner and B. H. Juang, *Fundamentals of Speech Recognition*, Prentice-Hall, Englewood Cliffs, NJ, USA, 1993.

[20] S. N. Navnath and S. H. Raghunath, "DWT and LPC based feature extraction methods for isolated word recognition," *EURASIP Journal on Audio, Speech, and Music Processing*, vol. 2012, article 7, 2012.

[21] L. Li, B. Aditya Prakash, and C. Faloutsos, "Parsimonious linear fingerprint for time series," *Proceedings of the VLDB Endowment*, vol. 3, pp. 385–396, 2010.

[22] L. Ralaivola and F. D'Alché-Buc, "Time series filtering, smoothing and learning using the kernel Kalman filter," in *Proceedings of the International Joint Conference on Neural Networks (IJCNN '05)*, pp. 1449–1454, Montreal, Canada, August 2005.

[23] A. Jain, E. Y. Chang, and Y. F. Wang, "Adaptive stream resource management using Kalman Filters," in *Proceedings of the ACM SIGMOD International Conference on Management of Data (SIGMOD '04)*, pp. 11–22, June 2004.

[24] D. Gunopulos and G. Das, "Time series similarity measures and time series indexing," in *Proceedings of the ACM SIGMOD International Conference on Management of Data (SIGMOD '01)*, Santa Barbara, Calif, USA, May 2001.

[25] K. Deng, A. W. Moore, and M. C. Nechyba, "Learning to recognize time series: combining ARMA models with memory-based learning," in *Proceedings of the 1997 IEEE International Symposium on Computational Intelligence in Robotics and Automation (CIRA '97)*, pp. 246–251, July 1997.

[26] X. Wang, K. Smith, and R. Hyndman, "Characteristic-based clustering for time series data," *Data Mining and Knowledge Discovery*, vol. 13, no. 3, pp. 335–364, 2006.

[27] E. J. Keogh, T. Palpanas, V. B. Zordan, D. Gunopulos, and M. Cardle, "Indexing large human-motion databases," in *Proceedings of the 13th International Conference on Very Large Data Bases (VLDB '04)*, pp. 780–791, 2004.

[28] N. T. N. Anh, S. H. Kim, H. J. Yang, and S. H. Kim, "Hidden dynamic learning for long-interval consecutive missing values reconstruction in EEG time series," in *Proceedings of the IEEE International Conference on Granular Computing (GrC '11)*, pp. 653–658, Kaohsiung, Taiwan, November 2011.

[29] R. E. Kalman, "A new approach to linear filtering and prediction problems," *Transactions of the ASME Journal of Basic Engineering*, vol. 82, no. 1, pp. 35–45, 1960.

[30] R. H. Shumway and D. S. Stoffer, "An approach to time series smoothing and forecasting using the EM algorithm," *Journal of Time Series Analysis*, vol. 3, pp. 253–264, 1982.

[31] K. Kalpakis, D. Gada, and V. Puttagunta, "Distance measures for effective clustering of ARIMA time-series," in *Proceedings of the 1st IEEE International Conference on Data Mining (ICDM '01)*, pp. 273–280, San Jose, Calif, USA, December 2001.

[32] H. Zhang, T. B. Ho, Y. Zhang, and M. S. Lin, "Unsupervised feature extraction for time series clustering using orthogonal wavelet transform," *Informatica*, vol. 30, no. 3, pp. 305–319, 2006.

Hindawi Publishing Corporation
Computational and Mathematical Methods in Medicine
Volume 2014, Article ID 120357, 13 pages
http://dx.doi.org/10.1155/2014/120357

Research Article

Virtual Grasping: Closed-Loop Force Control Using Electrotactile Feedback

Nikola Jorgovanovic,[1] Strahinja Dosen,[2] Damir J. Djozic,[1] Goran Krajoski,[1] and Dario Farina[2]

[1] *Department for Systems, Signals and Control, Faculty of Technical Sciences, University of Novi Sad, Novi Sad, Serbia*
[2] *Department of Neurorehabilitation Engineering, University Medical Center Göttingen, Georg-August University, Göttingen, Germany*

Correspondence should be addressed to Nikola Jorgovanovic; nikolaj@uns.ac.rs

Received 27 September 2013; Accepted 20 November 2013; Published 2 January 2014

Academic Editor: Imre Cikajlo

Closing the control loop by providing somatosensory feedback to the user of a prosthesis is a well-known, long standing challenge in the field of prosthetics. Various approaches have been investigated for feedback restoration, ranging from direct neural stimulation to noninvasive sensory substitution methods. Although there are many studies presenting closed-loop systems, only a few of them objectively evaluated the closed-loop performance, mostly using vibrotactile stimulation. Importantly, the conclusions about the utility of the feedback were partly contradictory. The goal of the current study was to systematically investigate the capability of human subjects to control grasping force in closed loop using electrotactile feedback. We have developed a realistic experimental setup for virtual grasping, which operated in real time, included a set of real life objects, as well as a graphical and dynamical model of the prosthesis. We have used the setup to test 10 healthy, able bodied subjects to investigate the role of training, feedback and feedforward control, robustness of the closed loop, and the ability of the human subjects to generalize the control to previously "unseen" objects. Overall, the outcomes of this study are very optimistic with regard to the benefits of feedback and reveal various, practically relevant, aspects of closed-loop control.

1. Introduction

Human grasping is characterized by a remarkable flexibility. Humans can easily grasp, lift, and manipulate objects of very different properties (e.g., texture, weight, and stiffness). Obviously, this process requires an advanced control of grasping forces, which is in human motor control implemented through a blend of feedforward and feedback mechanisms [1]. The former is well reflected in the paradigm of economical grasping: humans use previous sensory-motor experience to scale appropriately the grasping forces according to the expected (estimated) weight of the target object. The goal is to minimize the forces and thereby energy expenditure, and yet avoid slipping. However, this specific mechanism and also grasping as a whole can be significantly impaired when somatosensory feedback pathways are not fully functional due to a disease of the nervous system (e.g., multiple sclerosis [2], deafferented patients [3]).

After an amputation of the hand, a prosthetic device can be used as a functional and morphological replacement of the lost limb. To control the artificial limb, the intention of the user can be inferred from the recorded activity of the user's muscles (myoelectric control). This method, which essentially implements the feedforward pathway between the brain and artificial limb, has been in routine use in commercially available prostheses for decades [4, 5]. However, none of the commercial systems provides any deliberate somatosensory feedback to the user to close the control loop.

Providing somatosensory feedback is a well-known, long standing challenge in the field of prosthetics. The researchers have been investigating various approaches to provide feedback artificially, ranging from direct neural stimulation [6] to noninvasive sensory substitution methods [7, 8]. In the latter, the state of the prosthesis (e.g., joint angles or grasping forces) is communicated to the user by stimulating the skin

of the residual limb using mechanical (e.g., vibration motors [9–11], pressure cuffs [12], and motor driven pushers [13]) or electrical stimulation [14]. Closed-loop control of grasping force was most commonly tested. This is not surprising since an appropriate grasping force is necessary for safe lifting and object handling and since this variable cannot be assessed directly using vision (contrary to, for example, hand joint angles).

Although there are many studies presenting closed-loop systems, only a few of them objectively evaluated the closed-loop performance, mostly using vibrotactile stimulation. The conclusions of earlier studies are however partly contradictory. Some found that the feedback improved the performance [12, 13, 15], while others did not find a clear advantage of the closed-loop control [11]. In some studies, the feedback was beneficial only under certain conditions (e.g., feedforward uncertainty [16] and experienced subjects [17]).

In the case of electrical stimulation, systematic evaluation is very scarce. Scott et al. [18] reported subject satisfaction with the provided electrotactile feedback while Wang et al. [19] stated that the users could differentiate appropriate gripping force for a wide variety of different activities, but in both cases the claims were not backed up with the actual results. Lundborg et al. [20] evaluated two-channel electrical stimulation feedback in four patients with sensory impairments (recent median nerve repair) and a single user of a myoelectric prosthesis. In all subjects, the performance in force control during a force matching task was better when using electrical stimulation with respect to the condition with no tactile feedback. Only one level of force, selected as comfortable by the subject before the test, was used during the task. Zafar and Van Doren [21] tested a single channel electrical stimulation feedback using a specialized setup simulating grasping of a compliant object, thereby allowing the subject to exploit visual cues for the force control in parallel to the tactile feedback. It was found that the supplemental feedback slightly improved the force control even when additional visual cues were provided.

The goal of the current study was to systematically and objectively investigate the capability of human subjects to control grasping force in closed loop using electrotactile feedback. We have developed a virtual setup that allowed us to investigate different aspects of the closed-loop control. The setup is also realistic in the sense that it operates in real time and includes a set of real life objects, as well as a graphical and dynamical model of the prosthesis. We have used the setup to investigate the role of training, feedback and feedforward control, robustness of the closed loop, and the ability of the human subjects to generalize the control to previously "unseen" objects.

2. Methods

2.1. Subjects. The experiment was carried out in the Biomedical Engineering Lab at the Department for Systems, Signals and Control, Faculty of Technical Sciences, University of Novi Sad, Serbia. Ten healthy, able bodied volunteer subjects (5 males and 5 females, 28 ± 3 years old) participated in the experiment after signing the consent form which was approved by the local ethical committee.

2.2. Experimental Setup. The experimental setup (see Figure 1) comprised the following components: (1) single-axis contactless joystick (CH Products, USA), (2) mechanical pushbutton, (3) current-controlled multichannel stimulator TremUNA (UNA systems, SRB), and (4) a standard desktop computer (host PC) equipped with a data acquisition card (PCI 6024, National Instruments, USA). The control program for virtual grasping experiments was implemented using Matlab 2012b and Simulink, Simulink 3D Animation, and Real Time Windows Target toolboxes. The signals from the joystick and the mechanical pushbutton were acquired by the DAQ card and supplied as the control inputs to the model of the prosthesis. The control loop operated in real time at the sampling frequency of 100 Hz. Based on the grasping force generated by the prosthesis, the stimulation unit provided the electrotactile feedback to the user. The unit included eight stimulation channels in total but only two were actually used in the current experiment. The stimulation parameters were controlled in real time from the host PC via a USB port, and the current pulses were delivered by using self-adhesive concentric electrodes (CoDe 501500, 4 cm diameter, SpesMedica, IT).

The graphical user interface depicted a model of a simple, single degree of freedom prosthetic hand (gripper) and the object that was the target for grasping. The object was positioned between the fingers of the prosthesis so that when the hand closed, it grasped the object. In some experimental conditions, visual force feedback was also provided to the subject in the form of a bar graph (see Figure 1 and Section 2.5). The virtual hand was controlled by the joystick and it operated as a first order, velocity-controlled system (i.e., transfer function $G(s) = 0.5/s$). Before the hand contacted the object, the joystick inclination was proportional to the speed of hand closing, whereas after the contact has been made, the joystick inclination was proportional to the buildup rate of the grasping force. This was similar to the "gated ramp controller" that was also used in [16, 22]. The pushbutton indicated the end of force control phase and the start of the object lift-off phase (see Section 2.4).

Joystick was selected since it provided a stable feedforward interface. Using myoelectric control would have been possible as well; however, in the current study the focus was on the feedback interface and therefore the influence of the other system components was minimized by assuming ideal behaviors. The gated ramp controller was adopted since it is similar to the control method actually used in one of the commercially available hands (i-Limb from Touch Bionics [4]) and also since this approach effectively "decoupled" the position of the joystick from the amplitude of the grasping force; if the force would be controlled proportionally as in some other prosthesis (Sensor Hand Speed and Michelangelo Hand from Otto Bock [5]), the subjects could easily estimate the current force level directly from the joystick inclination and without using electrotactile feedback information. In addition to the possibility to "safely" conduct tests which could be difficult to realize in real life (i.e., breaking objects),

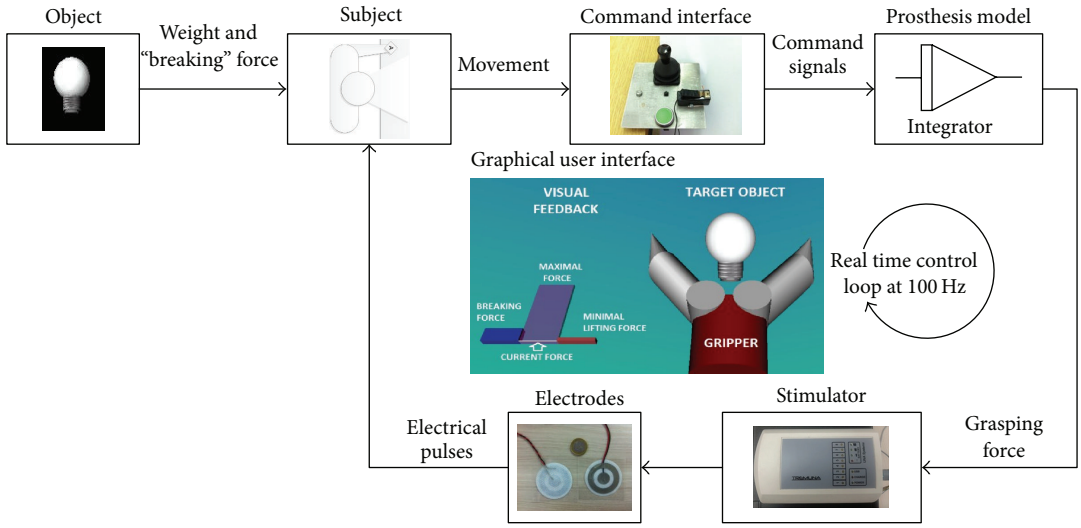

Figure 1: Experimental setup for closed-loop force control using electrotactile stimulation. The task for the subject was to generate an appropriate force to lift the target object without breaking it. The command interface was joystick and a push button. The electrotactile feedback was provided using a stimulation unit and concentric electrodes placed on the forearm of the subject. The control loop operated in real time at the sampling frequency of 100 Hz. The graphical interface for the subject included a model of the prosthesis, target object, and a force bar showing the minimal, current, maximal and breaking force. The bar plot was used at the beginning of the training to teach the subjects the task they should perform as well as the meaning of the electrotactile feedback. Otherwise, the visual force feedback was not shown on the screen. For detailed explanation see Section 2.4.

an advantage of the virtual setup was that it provided very controlled feedback and prevented incidental sources of information which would be available if the users controlled a real prosthesis (e.g., motor sound and vibrations).

2.3. Electrotactile Feedback. Electrotactile feedback was provided using two bipolar concentric electrodes placed on the dorsal side of the subject forearm, approximately midway between the elbow and wrist. The stimulation was delivered in monopolar configuration: the inner fields were used as the cathodes and the outer rings were connected together as a common anode. The stimulation was monophasic compensated; rectangular depolarizing pulse injecting charge to activate cutaneous afferents and elicit tactile sensation was followed by an exponential discharge waveform of opposite polarity to remove the charge out of the tissue. The rate of pulse delivery was constant and set to 100 Hz. This frequency was selected since pilot tests demonstrated that it elicited a well-localized, continuous sensation (i.e., responses to individual pulses fused together) resembling constant pressure on the surface of the skin. The current amplitude was also constant and set to 3 mA, and the pulse width was modulated within the dynamic range of the stimulation. The latter was determined for each subject individually as the interval between $1.2 * \mathrm{ST}$ and $0.8 * \mathrm{PT}$, where ST and PT are sensation and pain thresholds tested before the start of the experiment. The thresholds were detected using the method of limits [23]; that is, the pulse width was set to minimal value (50 μs) and then successively increased in steps of 50 μs until the subject indicated that he/she felt the stimulation (SP) or that the stimulation became painful (PT). This procedure was repeated three times in succession, and the average was used as the final value. The scaling factors for ST and PT defining the dynamic range [$1.2 * \mathrm{ST}$, $0.8 * \mathrm{PT}$] were adopted heuristically to assure that the minimal stimulation within the dynamic range can be perceived by the subject (pulse width > ST) while maximal stimulation is still nonpainful (pulse width < PT). The stimulation was proportional to the force; that is, normalized force (0-1) was linearly mapped to the dynamic range. Stimulation intensity was modulated by adjusting the pulse width since this allowed a finer control of elicited sensations compared to changing the current intensity (pilot tests). The two electrodes delivered the same information, that is, the same force scaled between the respective electrode thresholds as explained above. This configuration was selected since the pilot tests demonstrated that two electrodes provided better quality and discriminability of sensation compared to the use of a single electrode.

2.4. Virtual Grasping Task. At the beginning of the trial, a graphical model of the object that was the target for grasping was shown, positioned directly in front of the gripper and in-between the fingers, as explained before. Each object was characterized by two parameters: minimal grasping force needed to successfully lift the object and maximal allowed grasping force ("breaking" threshold). In total, 19 different objects were used for the experiment (see Table 1). The limits for each object (min/max force in Table 1) are expressed as normalized force, where 1 corresponds to the maximal force that the virtual prosthesis could produce. The force limits were selected heuristically but the goal was to reflect the reality as much as possible. The minimal force was proportional to the weight of the object, and the maximal

Table 1: Objects used in the tests.

Object number	Object	Normalized min/max force	Object number	Object	Normalized min/max force
1	Egg	0.05/0.2	12	Wine glass empty	0.15/0.3
2	CD	0.05/0.2	13	Wine glass half full	0.28/0.4
3	Orange	0.2/0.4	14	Light bulb	0.05/0.2
4	Wine glass full	0.35/0.5	15	Brick small	0.45/0.6
5	Bottle half full	0.5/0.7	16	Hammer small	0.6/0.8
6	Hammer	0.75/0.97	17	Lighter	0.05/0.2
7	Stack of cards	0.08/0.25	18	Lemon	0.2/0.4
8	Cereal box small	0.15/0.3	19	Apple	0.2/0.4
9	Cereal box	0.3/0.5			
10	Book thin	0.3/0.5			
11	Brick	0.75/0.9			

force was set to about 130% of the minimal force. The role of the maximal force was to prohibit the subjects from using excessively high forces to lift the objects, enforcing the paradigm of economical grasping (i.e., minimizing grasp forces while avoiding object slip [16]). Without this constraint, each object could have been securely grasped simply by generating the maximum force. However, generating too high grasping forces during the real life not only would mean excessive energy expenditure and lower battery life (i.e., noneconomical prosthesis use) but could also damage or even break the objects (e.g., a light bulb or an egg). Note that it was not important for the force limits to strictly reflect the reality, since the subjects anyway got the opportunity to "learn" the objects before the performance was evaluated (see Section 2.5). The goal was to give more general, absolute (e.g., heavy or light) or relative (i.e., heavier/lighter than the previous object), visual cues about the object weight.

The task for the subject was to grasp and lift the object by generating force that was within the predefined limits (target window), that is, enough to lift the object and yet lower than the "breaking" force. The hand was initially fully opened. The subject started hand closing by pushing on the joystick. After the contact was detected, the joystick controlled the grasping force, as explained before. At the same time, the electrotactile feedback was activated. All the objects were absolutely stiff (no deformation, i.e., static grasp) and therefore the visual cues about the developed force were not available. When the subject judged that the grip strength was appropriate, he/she pressed the button to signal that the hand should lift the object. If the force was above the lower limit, the hand would successfully lift the object (task successfully accomplished). Otherwise, if the force became less than the lower limit anytime during the object lift-off, the object would slip from the hand (task failed). Similarly, if the grasping force went above the higher limit for the given object anytime during the trial, the gripper would immediately "fall through," signaling that the object has been broken (task failed). The steps within the trial are shown in Figure 2, while Figure 3 depicts the relevant signals and prosthesis behavior.

2.5. Experimental Protocol. The subjects were comfortably seated in a chair in front of the table so that he/she was able to operate the joystick and a pushbutton. The experimental session comprised training and evaluation, and each phase included several conditions which are described in sequel. In total, the experiment lasted approximately 2.5 h. Before starting, the experiment was explained to the subject, the stimulation thresholds were determined, and the subject was allowed to practice virtual grasping with one object for approximately 5 min (simultaneous electrotactile and visual feedback). The goal was for the subject to familiarize with the setup and the task, to accommodate to the sensation of continuous stimulation, and also to learn the force coding through electrotactile stimulation.

The training phase comprised the following conditions.

(i) TR-VIS-ELE: Training with Visual and Electrotactile Feedback. The subject performed virtual grasping trials with five different target objects, while visual (force bar) and electrotactile force feedback were simultaneously provided. Due to visual feedback (see Figure 1), this was an easy task and each object was grasped two times. The objects were selected to span the full range of normalized weights (0-1), and they were ordered and presented to the subjects according to their weight, from light to heavy (i.e., see Table 1, objects 1, 2, 3, 4, and 11). The goal of this step was for the subjects to become familiar with a set of objects by learning their weights and corresponding electrotactile sensations assisted by the full visual feedback about force (force bar).

(ii) TR-ELE-1: Training with Electrotactile Feedback and Known Objects. The same five objects as in TR-VIS-ELE were presented again and in the same order, but this time only the electrotactile force feedback was given. Each object was presented repeatedly, until the subject accomplished the grasping task successfully two times in a row or until the maximum number of trials was exceeded (15 trials). After grasping and lifting the object two times in succession, we assumed that the subject learned to adjust the correct force for that particular object by relying on the electrotactile feedback.

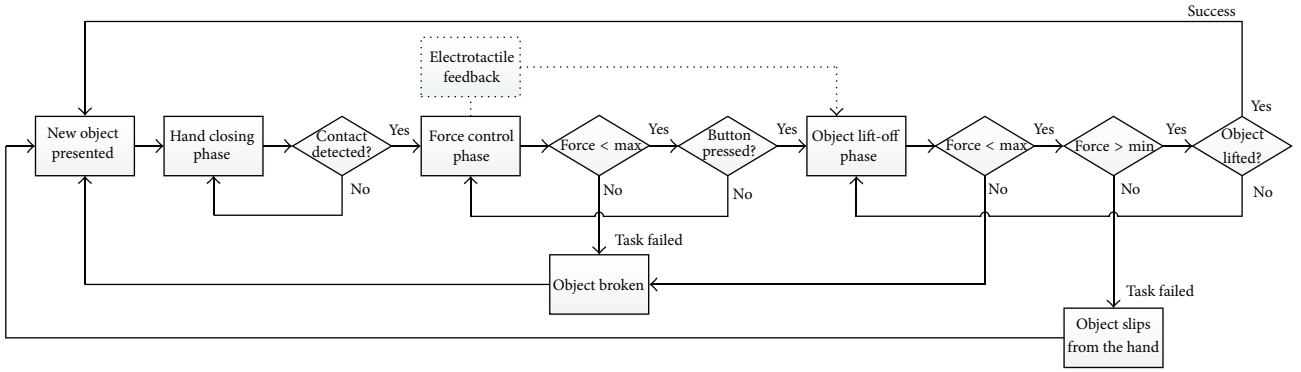

Figure 2: The steps comprising a single trial of a virtual grasping. There were three phases: (1) hand closing, (2) force control, and (3) object lift-off. The trial was deemed successful if the object was successfully lifted, while keeping the grasping force within the predefined limits (target window) for the given object.

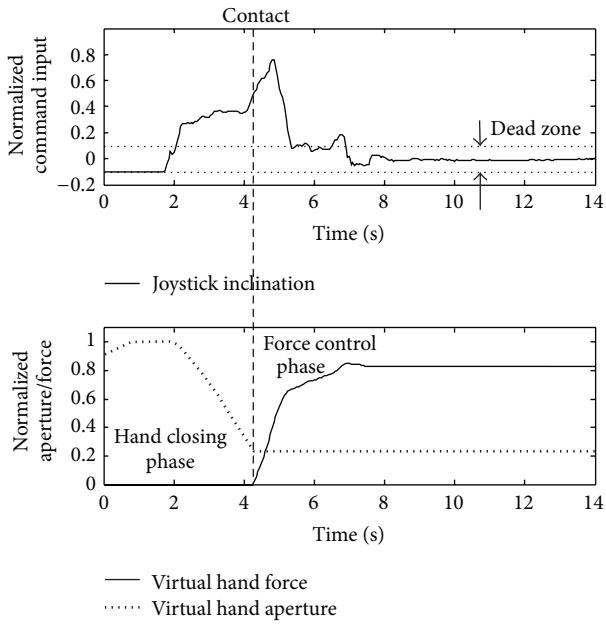

Figure 3: Control signals and prosthesis state variables recorded during a representative trial. In the hand closing phase, the joystick controls the hand aperture and after contacting the object, it controls the grasping force. Initially the subject increased the force faster to bring the signal in the vicinity of the target window. Afterwards, the subject becomes more careful, slowing down the force increase and performing fine corrections. To achieve stable control, a dead zone for the joystick signal was adopted.

(iii) TR-ELE-2: Training with Electrotactile Feedback and "Unseen" Objects. The procedure was the same as in TR-ELE-1 but this time a new set of five objects was used. Again, the objects were selected to sample the full range of weights, and they were presented to the subjects ordered according to their weights (i.e., see Table 1, objects 7, 8, 10, 5, and 6). This condition was compared to the previous one. The goal was to evaluate if the subjects could generalize the principles learned in TR-VIS-ELE and TR-ELE-1 to grasp a set of novel objects in this condition using only electrotactile feedback (i.e., without previously revealing the object weight through simultaneous electrotactile and visual feedback).

The evaluation phase comprised the following conditions.

(i) TE-FDB: Closed-Loop Performance Test. Ten objects used in TR-ELE-1 and TR-ELE-2 were presented to the subject, each object twice in succession (20 trials in total). The goal of this test was to determine the baseline closed-loop control performance, that is, the performance of grasping ten objects which were used during the training. This was the control condition for all the other tests to follow.

(ii) TE-FWD: Feedforward Test (No Feedback). The procedure was the same as in the previous test, but this time no force feedback was provided. This condition was compared to TE-FDB to test to what extent the subjects relied on the feedback for the task accomplishment. Since the prosthesis was modeled as an ideal integrator, the grasping task could be accomplished without using the feedback. Instead, the subjects could set the joystick in a certain position and count the time needed for the force to increase to a desired value (pure feedforward control). To further simplify the task for the subjects, the hand was already in contact with the object at the beginning of the trials in this condition (i.e., no need to close the hand and visually confirm that the contact has been made).

(iii) TE-FWD-ALT: Feedforward Test (No Feedback) with Altered System Parameters. The procedure was as in the previous condition, but the prosthesis model $G(s)$ was changed (i.e., integrator gain doubled, $G(s) = 1/s$), making the force responding two times faster to the joystick command. The goal was to test how robust was the feedforward control to the change of the model parameters. Since there were two trials per object and the set of objects was known, the assumption was that the subjects could implicitly discover that the system behavior has been changed, for example, by using the task accomplishment or failure as the feedback to update the control in the subsequent trials.

Table 2: Objects used in TE-FDB-GEN.

Reference object	Test object
Egg	Light bulb
Egg	Lighter
Orange	Apple
Orange	Lemon
Stack of cards	Stack of cards × 2
Cereal box	Cereal box small
Cereal box small	Cereal box small × 2
CD	CD × 5
CD	CD × 4
Thin book	Thin book × 3
Thin book	Thin book × 2
Small hammer	Small brick

(iv) TE-FDB-ALT: Closed-Loop Performance Test with Altered System Parameters. The procedure was the same as in the previous condition, but with the electrotactile feedback provided. If the subject used the feedback with the original system, this test would show how robust closed-loop control was with respect to a significant change in the system behavior. If the subjects used feedforward control with the original system, this test would show if closing the loop was useful at least when there was a change in the system behavior (uncertainty).

(v) TE-FDB-GEN: Closed-Loop Performance Test for Generalization. In this test, objects were presented in pairs (see Table 2). First, one object used in the previous conditions was presented as a reference, and the grasping trials were repeated with the same object until the task was accomplished successfully. Then, a novel, test object was presented, where this object was "derived" from the reference in several ways: (1) similar weight as the reference, (2) a composite comprising a stack of the reference objects (e.g., two reference objects packed together), and (3) scaled version of the reference (i.e., scaled up or down in volume with respect to the reference). The first case was essentially a classical force matching task [17] while in the two other cases the subjects had to accomplish a "multiplication"/"division" in the space of force/electrotactile sensations. The goal of this step was to test the ability of the subject to solve the type of tasks that we envision the users of the prosthesis could face during the real life application of the device (i.e., grasping a novel object that can be related through the user's experience to a similar object that was handled in the past).

Contrary to training conditions in which the objects were presented ordered according to their weight (from lighter to heavier), during all the evaluations the objects were presented in the random order.

2.6. Data Analysis. The performance was measured using the following outcome measures.

(i) *Average number of attempts (ANA):* This performance index was used to evaluate the training and it was defined as the average number of grasping trials per object before the subject "learned" to grasp the object, that is, before the object was grasped successfully two times in succession.

(ii) *Success rate in task accomplishment (SR):* As explained before, if the subject successfully lifted the object without object slipping or breaking, the trial was deemed successful. Success rate was expressed in percent.

(iii) *Force error (FE):* FE was calculated as the difference between the minimal force to lift the given object and the applied grasping force, but only considering those trials in which the grasping force was not high enough and the object thereby slipped from the grasp. FE evaluated the average level of undershooting and it was adopted as a more sensitive, continuous measure of performance compared to SR, which had only a binary outcome (success or failure).

(iv) *Time to accomplish the task (TAT):* This was the time from the beginning and until the end of the trial (success, slip, and break).

Data analysis was performed using custom functions written in MATLAB 2012b (MathWorks, US). Statistical tests were performed using STATISTICA 10 (StatSoft, US). Repeated measures ANOVA with the experimental condition as the within-subject factor was used for the group comparison and Tukey's honestly significant difference criterion for the post hoc pairwise tests. The data were tested for sphericity (Mauchly's sphericity test). The threshold for the statistical significance was set to $P < 0.05$.

3. Results

The average sensation and pain thresholds were $120 \pm 50\ \mu$s and $500 \pm 50\ \mu$s, respectively. Figure 4 shows a representative result from the second and third training condition (TR-ELE-1 and TR-ELE-2). It can be seen (Figure 4(a), third object) that the subject was adjusting the force in the next trial based on the outcome of the previous one, reaching the target window in a few steps. In the case of light and medium objects (e.g., object 3 in TR-ELE-1), these steps were rather small, suggesting fine control, whereas for the heavy object (e.g., object 5 in TR-ELE-1), the adjustments were more crude, producing trial by trial oscillations above and below the target window. Fewer trials were needed to complete the training in TR-ELE-2. The summary results of the training are given in Figure 5. The average number of attempts (ANA) per object was similar in TR-ELE-2 and TR-ELE-1 condition (Figure 5(a)), despite the fact that in TR-ELE-2 the subjects faced a set of objects that were not handled before using visual force feedback (as in TR-VIS-ELE and TR-ELE-1). In addition, it seems that heavier objects posed a challenge for the subjects in TR-ELE-1, while in TR-ELE-2 the performance was similar across all objects (i.e., no statistically significant differences between light and heavy objects). The data for individual objects (Figure 5(b)) did not pass the sphericity test, and therefore ANOVA with

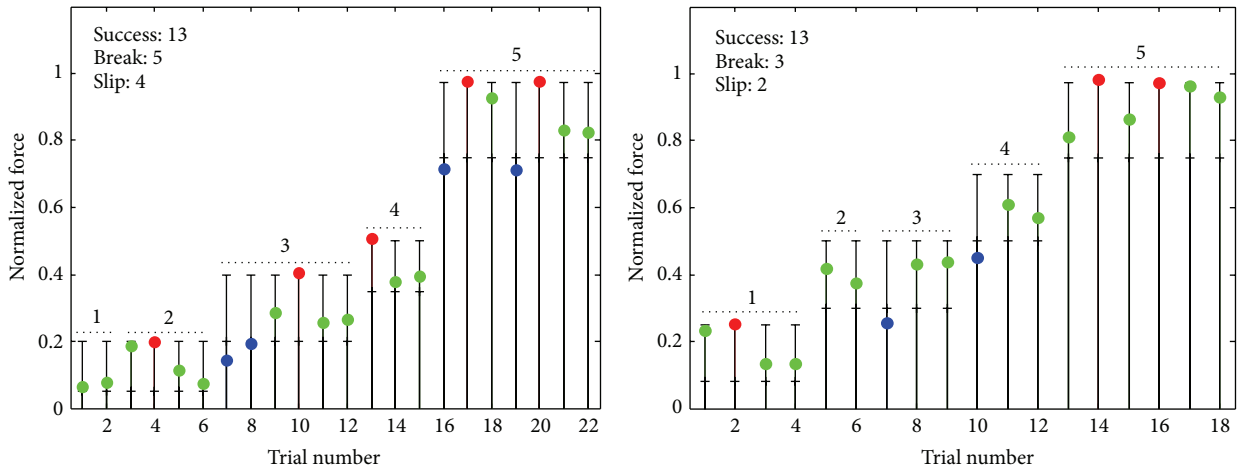

(a) TR-ELE-1 (b) TR-ELE-2

Figure 4: Representative results of the training: (a) TR-ELE-1 and (b) TR-ELE-2. The horizontal lines are force limits, green circle is a successful grasp and lift, blue circle denotes the trial in which the object slipped from the grasp (i.e., grasping force lower than the minimal necessary force), and the red circle represents the trials in which the object was broken (i.e., grasping force crossed the upper limit). The trials with the same object are grouped by a dashed line. From trial to trial, the subject adjusted the grasping force, eventually reaching the target force window. The training was faster in TR-ELE-2.

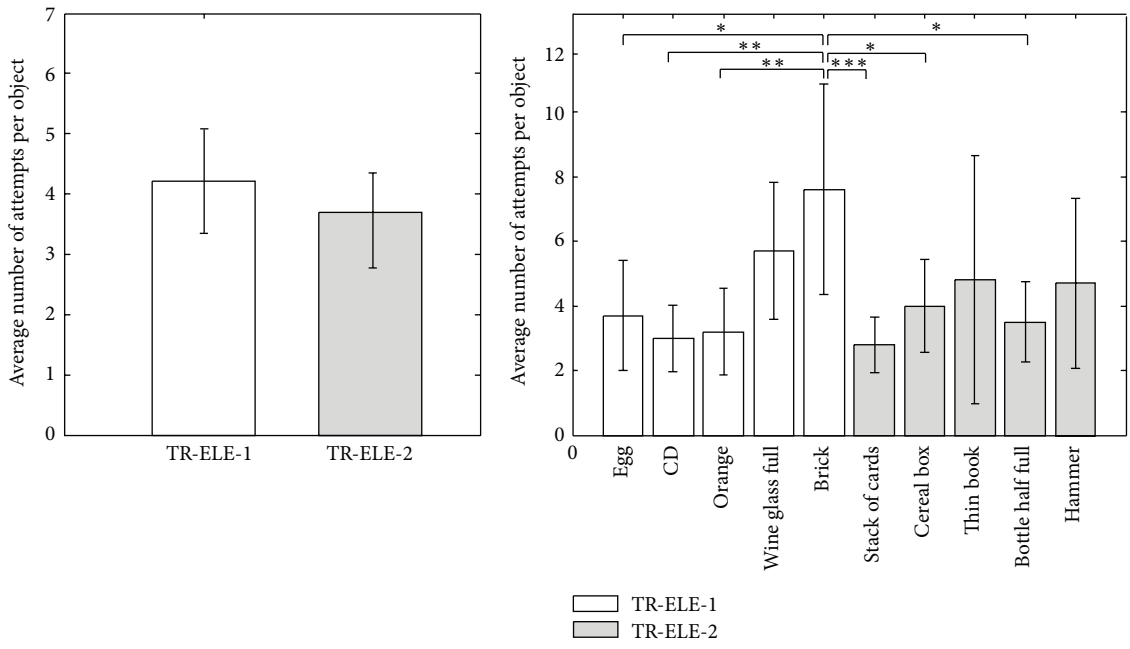

(a) (b)

Figure 5: Overall training results (i.e., average number of attempts per object ± standard deviation): (a) across conditions and (b) across objects. The training took similar number of trials in TR-ELE-2 ("unseen" objects) and TR-ELE-1 (previously "seen" objects). In addition, in TR-ELE-2 the subjects learned how to handle heavy objects, which were particularly challenging in TR-ELE-1. Within each condition, the objects in (b) are arranged by their weight ($^{*}P < 0.05$; $^{**}P < 0.01$; $^{***}P < 0.001$).

Greenhouse-Geisser correction was used in this case, and it showed that there was a significant difference between the objects (adjusted $P < 0.05$).

Figure 6 illustrates the results from the four testing conditions. For this particular subject, the success rate during the closed-loop control was 70% (TE-FDB) and the performance was similar even after the system behavior was significantly changed (SR of 60% in TE-FDB-ALT). Without feedback, the performance was low (20% in TE-FWD and 15% in TE-FWD-ALT). In the conditions with feedback, the subject was more successful in hitting the target force window already in the first trial (i.e., 7 out of 10 in TE-FDB versus 1 out of 10 in

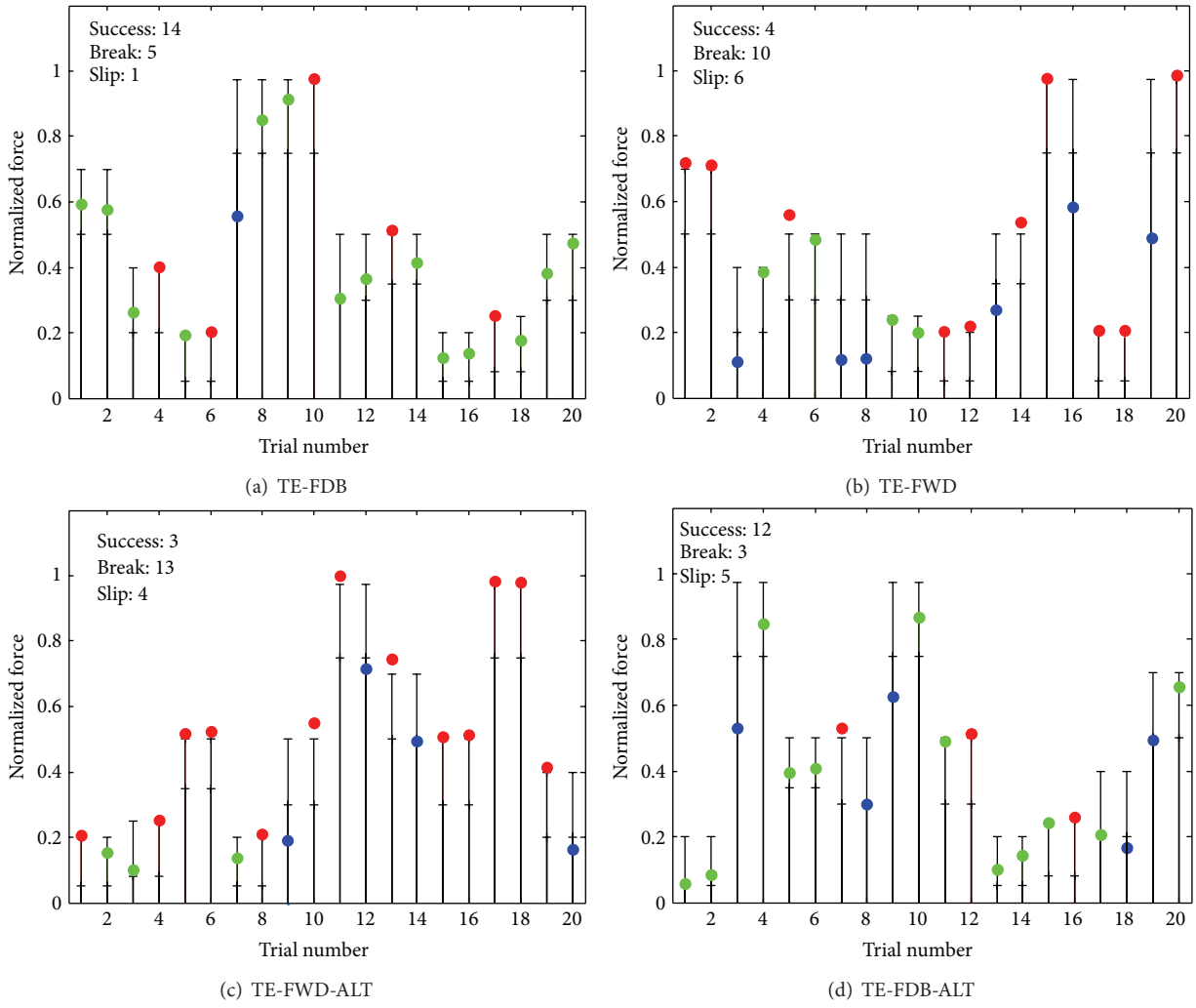

FIGURE 6: Representative results for the testing conditions: (a) TE-FDB, (b) TE-FWD, (c) TE-FWD-ALT, and (d) TE-FDB-ALT. The horizontal lines are force limits, green circle is a successful grasp and lift, blue circle denotes the trial in which the object has slipped from the grasp (i.e., grasping force lower than the minimal necessary force), and the red circle represents the trials in which the object was broken (i.e., grasping force crossed the upper limit). For each of the ten objects, there were two grasping trials in succession. The performance was much better when the feedback was provided.

TE-FWD). Furthermore, if the first trial was unsuccessful, the subject was better in correcting the mistake in the second trial. Without feedback, the subject tried to correct as well, but he/she was not very precise, often first overshooting (break) and then in the very next trial undershooting (slip) or vice versa (e.g., see trials 13-14 and 15-16 in TE-FWD; Figure 6).

The characteristics of the human control in different conditions can be seen from the force traces depicted in Figure 7. Different subjects exhibited similar control strategies in the same condition. When the subjects were provided with electrotactile feedback, they would steadily increase the force, but they would also modulate the rate of force increase many times during the trial (several joystick adjustments). Without feedback, the subjects would simply increase the force at a constant rate by always keeping the joystick at one selected inclination.

The overall results from the testing phase are given in Figure 8. The average performance during closed-loop control (Figures 8(a) and 8(b)) was 64 ± 18% for first trials only and 72 ± 10% for first and second (correction) trials together. During feedforward control, the success rate dropped significantly: 30±15% and 41±13% in TE-FWD and 36 ± 21% and 36 ± 18% in TE-FWD-ALT, for the first trials only and first and second trials together, respectively. When the feedback was reactivated, the performance recovered to a similar level as before, that is, 57 ± 13% (first trials) and 63 ± 11% (first and second trials) in TE-FDB-ALT, despite the fact that the system behavior was in this case significantly changed (Figures 8(a) and 8(b)). There is an indication that during the closed-loop control the subjects tended to make smaller force errors in the unsuccessful trials (Figure 8(c)); that is, in the failed trials in which object slipped from the grasp, the generated forces were closer to the target window if the subjects were provided with the electrotactile force feedback. However, the differences were statistically significant only between TE-FWD and TE-FDB-ALT. Finally,

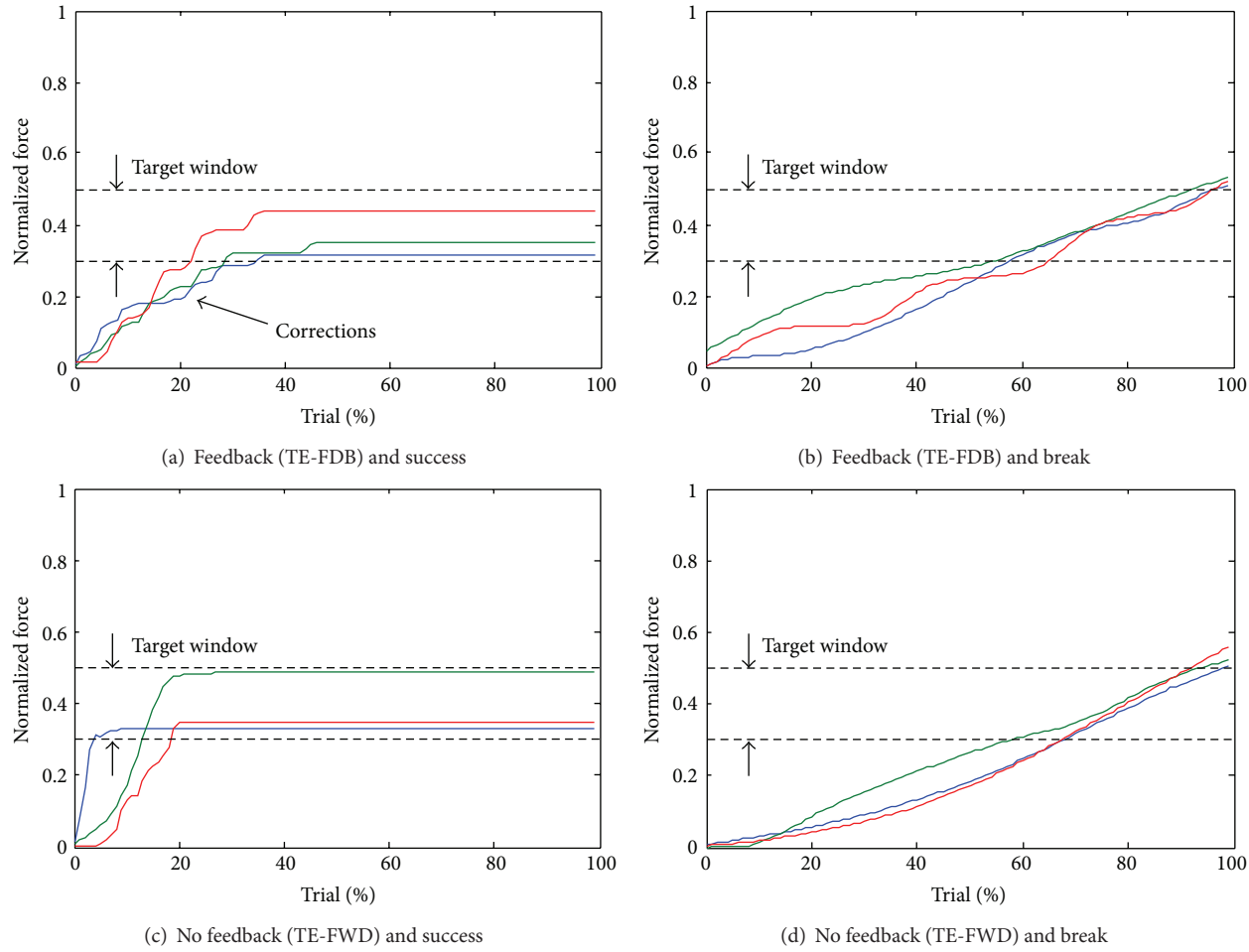

FIGURE 7: Representative examples of forces generated by different subjects (color profiles) grasping the same object in different testing conditions: (a) and (b) for successful grasping and breaking during TE-FDB, respectively, and (c) and (d) for successful grasping and breaking during TE-FWD, respectively. In both conditions, the subjects would steadily increase the force, but when the feedback was provided, they would also adjust the rate of force increase many times during the trial (e.g., see corrections in (a)). The time is normalized to the duration of the trial in order to emphasize the similarity in the shape of the force profiles for different subjects in the same condition.

when the feedback was delivered, the subjects were more successful in using the outcome of the previous trial (slip or break) to modify the force and correctly grasp the same object from the second chance (83% and 64% versus 43% and 27% for the SR in corrections in Figure 8(d)). It can be noted from the standard deviations that the results were variable between the subjects. For example, the subject success rates (Figure 8(b)) in the two conditions with feedback (TE-FDB and TE-FDB-ALT) were in the ranges 55–90% and 55–85%, respectively. Without feedback, the performance could be as low as 20% in TE-FWD and 10% in TE-FWD-ALT, but it could also reach up to 60 and 65% (best results), respectively.

The average time to accomplish the task (Figure 9) was significantly longer during closed-loop control conditions, that is, 16 ± 8 s and 14 ± 9 s for TE-FDB and TE-FDB-ALT versus 12 ± 7 s and 7 ± 7 s for TE-FWD and TE-FWD-ALT. There was a statistically significant difference also between the two conditions in which the feedback was provided (TE-FDB versus TE-FBD-ALT). This can be due to the fact that the altered system responded faster, resulting in shorter trials. Also with this system, the subjects were almost two times faster without feedback than with feedback, suggesting the lack of meaningful control in TE-FWD-ALT. Similar to the success rates, note that there was a large variability between the subjects also in the time that they used to accomplish the task.

The results of TE-FDB-GEN test are given in Figure 10. The test evaluated the ability of the human subjects to generalize the closed-loop control to an object that was similar to a reference one (force matching task) or represented a stacked/scaled version of the reference (see Table 2). In the case of lighter objects, the subjects were very good in generating grasping forces for the similar test and reference objects and also in up-/downscaling of the force to reflect the up-/downscaling of the reference object (success rate > 80%, except for one outlier). However, when the force that the subjects had to generate increased (heavier objects), the success rate decreased to around 50% for the normalized forces of approximately 0.5 and to only 9% for the normalized forces of 0.8.

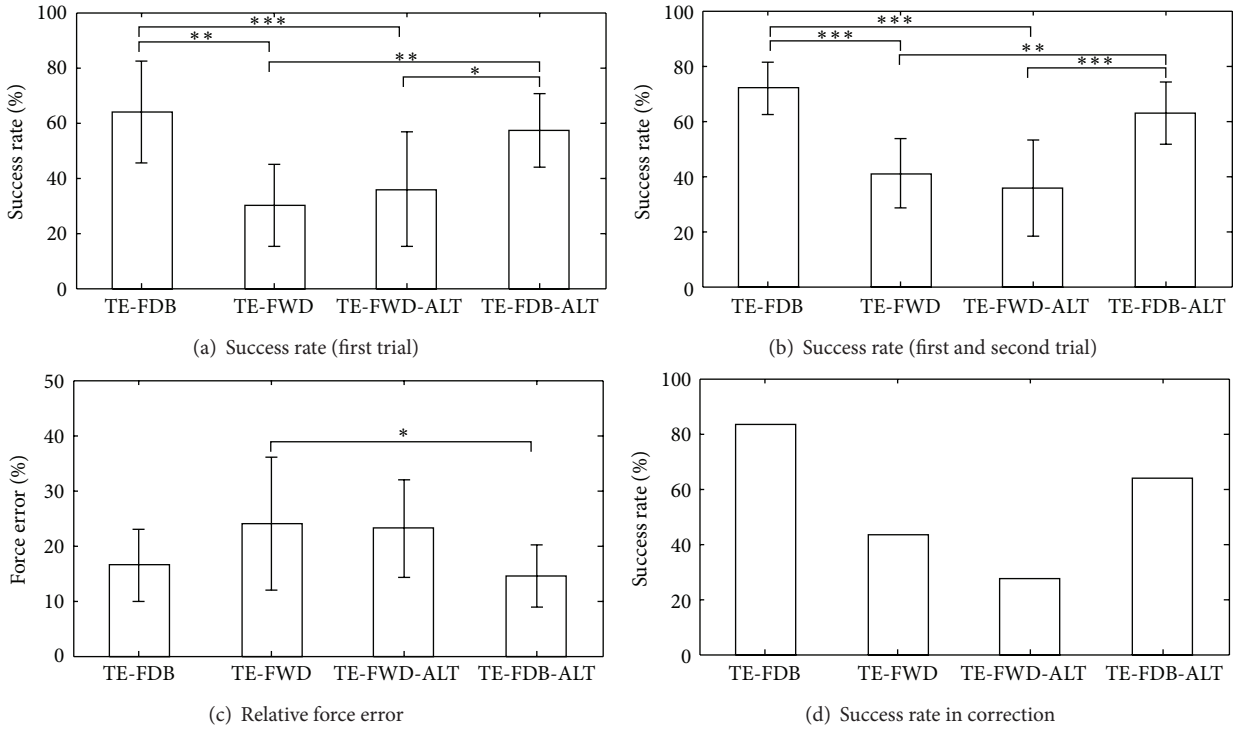

(a) Success rate (first trial)

(b) Success rate (first and second trial)

(c) Relative force error

(d) Success rate in correction

Figure 8: Overall results (mean ± standard deviation) in different testing conditions: (a) success rates (SR) from the first trials only, (b) SR from the first and second (correction) trials together, (c) force errors (FE) in the trials in which the object slipped from the grasp, and (d) SR in corrections (second trial was successful after the first had failed). In (d), only a grand average is reported, since the number of failed first trials was very different between subjects and conditions (30/36, 29/67, 12/44, and 28/44 for overall corrected/failed, left to right). The subjects were more successful in grasping the objects, made smaller errors in the failed trials, and better corrected the unsuccessful trials when the feedback was provided ($^{*}P < 0.05$; $^{**}P < 0.01$; $^{***}P < 0.001$).

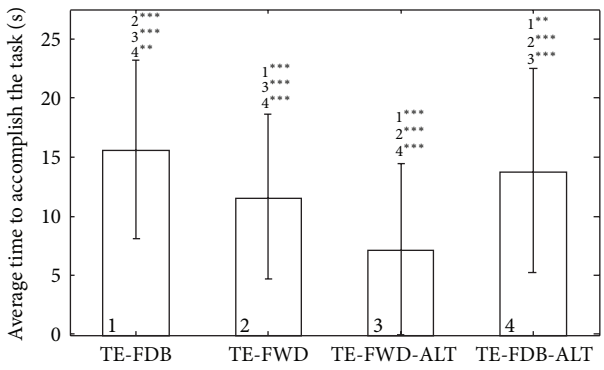

Figure 9: Average time to accomplish the task (ATA) (mean ± standard deviation) in different testing conditions. Providing feedback increased the time to accomplish the task.

4. Discussion and Conclusions

In this study, we have developed a test system for the closed-loop control of force based on electrotactile feedback. The system operates in real time and integrates a setup for virtual grasping using a dynamic model of a single degree of freedom prosthetic hand. We have used this tool to investigate different properties of closed-loop force control during grasping of a set of daily life objects spanning a full range of normalized weights (0-1).

There are only a limited number of studies evaluating objectively the role and utility of closed-loop control in prosthetics, especially regarding the electrotactile feedback. Contrary to some other studies which showed no or limited improvement during closed-loop force control [11, 16, 17], the results in the current study are very optimistic with respect to the benefits of feedback.

After training shortly with only 5 objects (TR-ELE-VIS and TR-ELE-1) sampling the range of weights (from light to heavy), the subjects understood the "meaning" of electrotactile feedback and learned how to scale the force (tactile sensation) with the expected weight of the object. This first step (i.e., a basic introduction) facilitated the future training so that the subjects "learned" novel objects (TR-ELE-2, Figure 5) using only electrotactile feedback at the same pace as when they were learning objects assisted by both visual and electrotactile force feedback (TR-VIS-ELE and TR-ELE-1). Finally, after a short training which lasted less than 30 min in total, the subjects were able to grasp 10 objects of very different weights (from an egg to a hammer) with a success rate of 72% in total. As one of the future steps, it would be interesting to evaluate the effect of a more extensive training (longer time and/or more objects to grasp). As demonstrated in different context (i.e., object manipulation rather than grasping) and for vibrotactile feedback [24], the training is very important for performance, even more than the actual stimulation setup [25].

We have also shown that in this particular task the feedback was truly instrumental for good performance. The success rates dropped significantly with purely feedforward control (Figure 8), and also as demonstrated by the force profiles (Figure 7), the subjects used very different control strategies with and without the feedback. The subjects relied on the feedback both to adjust the force while grasping an object and also to correct the control based on the outcome of the previous trial. Both of these mechanisms were significantly less effective in the feedforward control. Finally, the closed-loop control showed to be very robust with respect to the change of system parameters. When the rate of change of force was doubled, the performance did not significantly change. There were no statistically significant differences in any of the outcome measures between TE-FDB and TE-FDB-ALT (Figure 8), except for the time to accomplish the task (Figure 9). The feedback improved the performance but at the expense of the longer time to accomplish the task due to a more complex processing that had to be accomplished by the subject. We have also demonstrated (Figure 10) that closed-loop control could be successfully used to grasp not only objects that were trained, but also novel objects that were "derived" from the latter ones in nontrivial ways (stacking up and scaling).

In some of the previous studies investigating the closed-loop control using vibrotactile stimulation, the ineffectiveness of the closed-loop control might be due to the actual experimental task. In some studies, only two [16] or three [10, 17] target force levels have been used. In Cipriani et al. [11], many objects were tested but the subjects were not instructed explicitly to follow the economical grasping paradigm. Saunders and Vijayakumar [16] used a binary switch as the controller and a single, constant rate of force increase/decrease. It might be that in these cases it was easier for the subjects to learn the task and system dynamics, after which they could "switch" to mostly feedforward control. In the current study, we have used more force levels and also an analog control interface (joystick) with continuous system dynamics (integrator). A greater variety and a relatively brief training could have made the feedback information essential for accomplishing the task. Note that this context is similar to the one that a user of a prosthesis will face in the real life (e.g., many different objects to handle). However, the reliance on feedback likely depends strongly on the provided training; it might be that, with a longer training, the subjects would eventually switch to feedforward control. An interesting outcome was that also in this study the subjects could reach a success rate of around 40% by relying purely on the feedforward control.

In the study by Meek et al. [13], the object to be grasped had a constant weight and the breaking force has been modified in different conditions. Similarly, Zafar and Van Doren [21] used a single target force level and several values for the width of the target force window. These studies have therefore shown that feedback improves the precision when reaching a single level of target force. In the current study, however, we have demonstrated that the feedback improved the performance when reaching a broad range of target force levels. In a recent conference paper by Witteveen et al. [15] a somewhat similar setup was used. However, vibrotactile stimulation was investigated and dynamic behavior of the prosthesis was not considered.

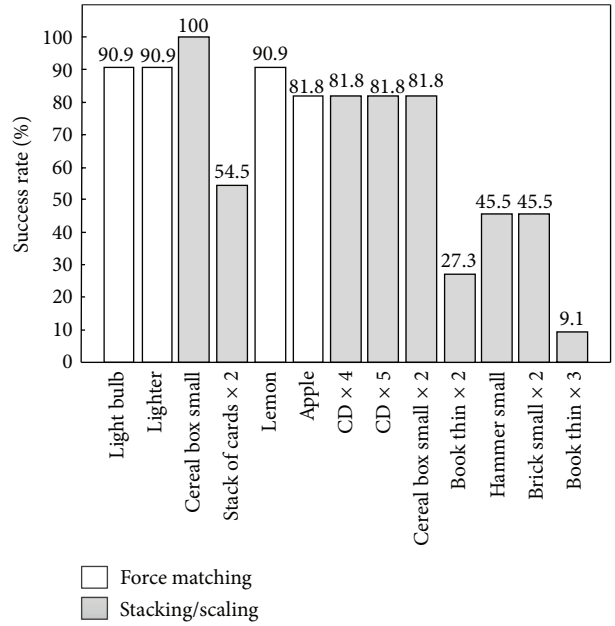

Figure 10: Success rates in generalizing closed-loop control from a reference object to a test object (see Table 2). The task was to grasp an object that was similar to the reference (white bars) or represented a stacked/scaled version of the reference (gray bars). The objects are ordered according to the weight (from lighter to heavier). For the small forces (lighter objects), the subjects were very successful in both tasks.

In general, the subjects were more successful when controlling lower forces, that is, when handling lighter objects. There might be two reasons for this. The first one is the linear scaling of the pulse width that we have used for information coding. It is well known that in general the intensity of the sensory stimulus does not map linearly to the intensity of perceived sensation [23]. For the higher pulses widths, larger absolute steps have to be made in the pulse width to produce a just noticeable difference in the elicited sensation [26]. We could have used a different scaling (e.g., power law or exponential function [27]). However, there is no agreement in the literature about the exact parameters of this mapping [8, 28], and the goal in this initial study was to test what can be done using the simplest approach. The second reason for the difficulties in handling heavy objects could be the habituation, which is more pronounced at higher intensities [7, 8]. While adjusting the force around the target window, the subjects might have lost the basic sensitivity in discriminating the changes in the intensity of the electrotactile stimulation. Importantly, most of the grasps in daily life are performed with light to medium objects, and also fine force control is mostly needed in the low to medium ranges, since the heavier objects are usually more robust. Nevertheless, the possibility of losing the basic sensitivity in the perception of electrotactile stimulation due to nonlinear psychometric function and/or habituation is an important problem. It affected

the results in this study as described above and it therefore needs to be resolved for the future experiments, especially when considering the intended practical application. One possible approach could be to use the intermittent stimulation to decrease the habituation as successfully demonstrated in [29]. Moreover, in addition to the aforementioned scaling laws, different modulation schemes (e.g., simultaneous intensity and frequency modulation) could be tested to increase the discriminability of the stimulation [30].

Finally, in the next paragraphs, we point out certain limitations of the current study. It was not our goal to capture the full intricate complexity of the real life grasping task in which there are numerous factors affecting the selected grasping strategy, control, and progression. For example, grasping strongly depends on the object properties (e.g., texture and stiffness) and geometry, hand-object interaction (contact points), prosthesis features (e.g., nonideal dynamic response), and the functional goals (e.g., strong, stable grip versus fine manipulation). We implemented a virtual setup including certain realistic features (e.g., real time operation and set of real life objects) but we also assumed an ideal feedforward interface (joystick), prosthesis dynamic response (pure integrator), and contact dynamics (contact stability depended only on the grasping force). These simplifications were however intentional since the goal was to isolate a specific aspect that was of most interest in the current study: the general utility and characteristics of the electrotactile feedback during closed-loop control of grasping force. Importantly, some of the aforementioned, presently disregarded factors can be accommodated by our virtual grasping setup and investigated in the future experiments, as explained later.

The experimental protocol and the results of the current study can be discussed from the viewpoint of the common mechanisms of human perceptual and motor learning [31]. Namely, the research in this field has demonstrated that a rapid improvement in performance when an individual is first exposed to a novel task is a general characteristic of human learning both in motor and sensory domains. In the context of the current study, the success that the subjects have demonstrated during the tests evaluating the closed-loop control (TE-FDB, TE-FDB-ALT, and TE-FDB-GEN) could reflect this fast learning paradigm. Importantly, since the task at hand was closed-loop control, the learning took place in both domains simultaneously, integrating tactile feedback with motor commands (sensory-motor integration learning). However, it is still unclear if the achieved performance is just due to a normal, short term adaptation to the given sequence of motor tasks, or it reflects a more robust sensory-motor representation which could be stable over time (consolidated memory) or in different scenarios (randomized tests). This is an important question that needs to be addressed in the future studies by, for example, repeating the tests in several sessions over different days to assess the relevant mechanisms (e.g., stabilization, between-session and generalization of learning).

It is well known from the general psychometry [23] that sensory perception is affected by many internal and external factors (e.g., subject concentration) and that it can be therefore very variable both within session and between subjects. Since the performance in sensory processing is instrumental for the execution of the closed-loop control task, this could be a possible explanation for the variability of the results (i.e., large standard deviations in Figures 8 and 9). Also related to this, the number of subjects in this study was limited but sufficient to reach general conclusions (e.g., feedback versus feedforward) with statistical significance. However, a larger pool of subjects needs to be tested in order to assess with more confidence the actual baseline performance values in each of the tested conditions.

The setup developed in this study is very general and can be used to implement many different experimental scenarios for testing of the closed-loop control. It relies on modelling and virtual objects, which make it flexible, while at the same time it provides a realistic behaviour through real time performance. A more sophisticated and realistic model of a prosthesis can be easily implemented by changing few parameters of a Matlab Simulink block (e.g., using an integrator with a lag element and a pure time delay). Also, this is an ideal environment for testing how different feedback variables (position, velocity, force, and jerk) or modes of control (position or force control) affect the closed-loop performance. The developed test bench therefore provides a high flexibility in implementing real time closed-loop control scenarios that could generate important insights about the various aspects of artificial sensory feedback in prosthetics. Importantly, one should keep in mind that these experiments are still conducted in well-controlled conditions and by using an abstraction (model) of reality and that therefore the ultimate test of these results is an actual real life assessment. We intend to use the insights from this and similar virtual reality experiments as general guidelines for designing prototype systems, which will then be evaluated in subjects (healthy and amputees) operating real prosthesis to accomplish practical tasks (e.g., grasping real life objects).

Conflict of Interests

The authors declare that there is no conflict of interests regarding the publication of this paper.

Acknowledgments

This research was supported by the Ministry of Education and Science of the Republic of Serbia (Project no. III-41007), by the European Commission under the MYOSENS (FP7-PEOPLE-2011-IAPP-286208) projects, and by the German Ministry for Education and Research (BMBF) via the Bernstein Focus Neurotechnology (BFNT), Göttingen, under Grant no. 01GQ0810.

References

[1] R. S. Johansson and K. J. Cole, "Sensory-motor coordination during grasping and manipulative actions," *Current Opinion in Neurobiology*, vol. 2, no. 6, pp. 815–823, 1992.

[2] V. Iyengar, M. J. Santos, M. Ko, and A. S. Aruin, "Grip force control in individuals with multiple sclerosis," *Neurorehabilitation and Neural Repair*, vol. 23, no. 8, pp. 855–861, 2009.

[3] J. C. Rothwell, M. M. Traub, and B. L. Day, "Manual motor performance in a deafferented man," *Brain*, vol. 105, no. 3, pp. 515–542, 1982.

[4] "Touch Bionics iLimb," 2013, http://www.touchbionics.com/.

[5] "Otto Bock Sensor Hand Speed," 2013, http://www.ottobock.de/cps/rde/xchg/ob_com_en/hs.xsl/3652.html.

[6] G. S. Dhillon and K. W. Horch, "Direct neural sensory feedback and control of a prosthetic arm," *IEEE Transactions on Neural Systems and Rehabilitation Engineering*, vol. 13, no. 4, pp. 468–472, 2005.

[7] A. Szeto and F. A. Saunders, "Electrocutaneous stimulation for sensory communication in rehabilitation engineering," *IEEE Transactions on Biomedical Engineering*, vol. 29, no. 4, pp. 300–308, 1982.

[8] K. A. Kaczmarek, J. G. Webster, P. Bach-y-Rita, and W. J. Tompkins, "Electrotactile and vibrotactile displays for sensory substitution systems," *IEEE Transactions on Biomedical Engineering*, vol. 38, no. 1, pp. 1–16, 1991.

[9] C. Pylatiuk, A. Kargov, and S. Schulz, "Design and evaluation of a low-cost force feedback system for myoelectric prosthetic hands," *Journal of Prosthetics and Orthotics*, vol. 18, no. 2, pp. 57–61, 2006.

[10] A. Chatterjee, P. Chaubey, J. Martin, and N. Thakor, "Testing a prosthetic haptic feedback simulator with an interactive force matching task," *Journal of Prosthetics and Orthotics*, vol. 20, no. 2, pp. 27–34, 2008.

[11] C. Cipriani, F. Zaccone, S. Micera, and M. C. Carrozza, "On the shared control of an EMG-controlled prosthetic hand: analysis of user-prosthesis interaction," *IEEE Transactions on Robotics*, vol. 24, no. 1, pp. 170–184, 2008.

[12] P. E. Patterson and J. A. Katz, "Design and evaluation of a sensory feedback system that provides grasping pressure in a myoelectric hand," *Journal of Rehabilitation Research and Development*, vol. 29, no. 1, pp. 1–8, 1992.

[13] S. G. Meek, S. C. Jacobsen, and P. P. Goulding, "Extended physiologic taction: design and evaluation of a proportional force feedback system," *Journal of Rehabilitation Research and Development*, vol. 26, no. 3, pp. 53–62, 1989.

[14] G. F. Shannon, "Sensory feedback for artificial limbs," *Medical Progress through Technology*, vol. 6, no. 2, pp. 73–79, 1979.

[15] H. J. B. Witteveen, J. S. Rietman, and P. H. Veltink, "Grasping force and slip feedback through vibrotactile stimulation to be used in myoelectric forearm prostheses," in *Proceedings of the Annual International Conference of the IEEE Engineering in Medicine and Biology Society*, vol. 2012, pp. 2969–2972, January 2012.

[16] I. Saunders and S. Vijayakumar, "The role of feed-forward and feedback processes for closed-loop prosthesis control," *Journal of NeuroEngineering and Rehabilitation*, vol. 8, article 60, 2011.

[17] A. Chatterjee, P. Chaubey, J. Martin, and N. V. Thakor, "Quantifying prosthesis control improvements using a vibrotactile representation of grip force," in *Proceedings of the IEEE Region 5 Conference*, pp. 1–5, Kansas City, Mo, USA, April 2008.

[18] R. N. Scott, R. R. Caldwell, and R. H. Brittain, "Sensory-feedback system compatible with myoelectric control," *Medical and Biological Engineering and Computing*, vol. 18, no. 1, pp. 65–69, 1980.

[19] G. Wang, X. Zhang, J. Zhang, and W. A. Gruver, "Gripping force sensory feedback for a myoelectrically controlled forearm prosthesis," in *Proceedings of the IEEE International Conference on Systems, Man and Cybernetics*, pp. 501–504, October 1995.

[20] G. Lundborg, B. Rośn, K. Lindström, and S. Lindberg, "Artificial sensibility based on the use of piezoresistive sensors: preliminary observations," *Journal of Hand Surgery*, vol. 23, no. 5, pp. 620–626, 1998.

[21] M. Zafar and C. L. Van Doren, "Effectiveness of supplemental grasp-force feedback in the presence of vision," *Medical and Biological Engineering and Computing*, vol. 38, no. 3, pp. 267–274, 2000.

[22] S. D. Humbert, S. A. Snyder, and W. M. Grill Jr., "Evaluation of command algorithms for control of upper-extremity neural prostheses," *IEEE Transactions on Neural Systems and Rehabilitation Engineering*, vol. 10, no. 2, pp. 94–101, 2002.

[23] F. A. A. Kingdom and N. Prins, *Psychophysics: A Practical Introduction*, Academic Press, 2009.

[24] C. E. Stepp, Q. An, and Y. Matsuoka, "Repeated training with augmentative vibrotactile feedback increases object manipulation performance," *PLoS ONE*, vol. 7, no. 2, Article ID e32743, 2012.

[25] C. E. Stepp and Y. Matsuoka, "Object manipulation improvements due to single session training outweigh the differences among stimulation sites during vibrotactile feedback," *IEEE Transactions on Neural Systems and Rehabilitation Engineering*, vol. 19, no. 6, pp. 677–685, 2011.

[26] A. Y. J. Szeto, J. Lyman, and R. E. Prior, "Electrocutaneous pulse rate and pulse width psychometric functions for sensory communications," *Human Factors*, vol. 21, no. 2, pp. 241–249, 1979.

[27] P. McCallum and H. Goldberg, "Magnitude scales for electrocutaneous stimulation," *Perception and Psychophysics*, vol. 17, no. 1, pp. 75–78, 1975.

[28] P. L. Marcus and A. J. Fuglevand, "Perception of electrical and mechanical stimulation of the skin: implications for electrotactile feedback," *Journal of Neural Engineering*, vol. 6, no. 6, Article ID 66008, 2009.

[29] D. G. Buma, J. R. Buitenweg, and P. H. Veltink, "Intermittent stimulation delays adaptation to electrocutaneous sensory feedback," *IEEE Transactions on Neural Systems and Rehabilitation Engineering*, vol. 15, no. 3, pp. 435–441, 2007.

[30] A. Y. J. Szeto and G. R. Farrenkopf, "Optimization of single electrode tactile codes," *Annals of Biomedical Engineering*, vol. 20, no. 6, pp. 647–665, 1992.

[31] N. Censor, D. Sagi, and L. G. Cohen, "Common mechanisms of human perceptual and motor learning," *Nature Reviews Neuroscience*, vol. 13, no. 9, pp. 658–664, 2012.

Hindawi Publishing Corporation
Computational and Mathematical Methods in Medicine
Volume 2013, Article ID 343084, 7 pages
http://dx.doi.org/10.1155/2013/343084

Research Article

SVM versus MAP on Accelerometer Data to Distinguish among Locomotor Activities Executed at Different Speeds

Maurizio Schmid, Francesco Riganti-Fulginei, Ivan Bernabucci, Antonino Laudani, Daniele Bibbo, Rossana Muscillo, Alessandro Salvini, and Silvia Conforto

Department of Engineering, Roma Tre University, Via Vito Volterra 62, 00146 Rome, Italy

Correspondence should be addressed to Maurizio Schmid; maurizio.schmid@uniroma3.it

Received 18 July 2013; Revised 7 October 2013; Accepted 18 October 2013

Academic Editor: Strahinja Dosen

Two approaches to the classification of different locomotor activities performed at various speeds are here presented and evaluated: a maximum a posteriori (MAP) Bayes' classification scheme and a Support Vector Machine (SVM) are applied on a 2D projection of 16 features extracted from accelerometer data. The locomotor activities (level walking, stair climbing, and stair descending) were recorded by an inertial sensor placed on the shank (preferred leg), performed in a natural indoor-outdoor scenario by 10 healthy young adults (age 25–35 yrs.). From each segmented activity epoch, sixteen features were chosen in the frequency and time domain. Dimension reduction was then performed through 2D Sammon's mapping. An Artificial Neural Network (ANN) was trained to mimic Sammon's mapping on the whole dataset. In the Bayes' approach, the two features were then fed to a Bayes' classifier that incorporates an update rule, while, in the SVM scheme, the ANN was considered as the kernel function of the classifier. Bayes' approach performed slightly better than SVM on both the training set (91.4% versus 90.7%) and the testing set (84.2% versus 76.0%), favoring the proposed Bayes' scheme as more suitable than the proposed SVM in distinguishing among the different monitored activities.

1. Introduction

With the evolution of wireless communication technology, it is now possible to use inertial sensors (Inertial Measurement Units (IMU)) to gather and transmit over the air patterns associated with different activities performed by people moving in unconstrained environments [1]. IMUs allow to collect kinematic data through miniaturized accelerometers [2], gyroscopes [3], and possibly magnetometers [4].

Restricting the analysis to accelerometers, they are popular as fall detectors [5], as means to monitor physical activity [6], and also as tools to classify among different motor activities [7, 8]. They have also been shown as good predictors of the functional capacity in healthy adults [9] and elderly people [10] and of the level of energy expenditure [11, 12]. In these specific regards, since the accuracy in the prediction strongly depends on the kind of activity [13], classification of activities is often necessary as a preliminary step for energy expenditure estimation [14].

The utility of distinguishing between activities is also apparent when, for long term monitoring, the wearable device needs to transmit data in a compact way. Following this perspective, the general communication model of having raw data to be sent continuously from the sensing devices over the air, and let the receiving unit extract relevant information from the data [15], may be a suboptimal solution. If, instead, on-board processing is available, the processing unit in each sensing unit may incorporate the function of feature extraction and subsequent activity classification [16]. In order to do this, each sensing unit will incorporate three successive functions: (1) the detection and windowing (or segmentation) of each activity epoch, (2) the extraction of the features from the windowed activity, and (3) the classification of that epoch based on a specific scheme.

As far as the classification stage is concerned, while the classification between postures is a relatively easy task [17], in the case of dynamic activities (such as different locomotion types), the classification task is more complex.

This task is usually accomplished by using a multiplicity of sensors, located in different body segments and able to record the 3D components of acceleration for each segment [18]. Once an activity epoch has been detected and segmented, features from different domains are then extracted from these windowed data [19], and the classification is then performed based on a combination or a subset of these features [20]. Simple features to be extracted from windowed data include energy or amplitude parameters [21], while more complex approaches are based, for example, on dynamic programming [22], wavelet coefficients [23], and decision trees [24]. Other approaches may include particle swarm optimization, a technique that has been successfully implemented for classification and prediction in different research areas [25, 26]. Multiple accelerometers are usually added in order to improve the classification accuracy [24], even if the burdensomeness associated with the increased setup time and computational complexity makes this approach to be sought only when the increase in accuracy is significant.

In the present paper, we will thus focus on the presentation of a technique able to incorporate the functions herein described, by specifically presenting two different schemes for classification, respectively, based on the use of the maximum a posteriori approach and on a Support Vector Machine. The general objective of this work is to evaluate these two schemes in terms of their ability to distinguish among locomotor activities by using a single sensor.

The paper is structured as follows: in the second section, the structure of the two different classification schemes is presented, after giving details on the experimental procedure and providing information on the performance analysis that has been set up for evaluation. Then, we will focus on the results obtained in the experimental section, and the final section draws the conclusions.

2. Methods

2.1. Experimental Setup and Data Collection. 10 healthy young adults (age 25–35 years, 4 females) volunteered in the study. They were requested to perform an 800 m path composed of different locomotor activities: walking level and incline at different slopes, stair climbing, and stair descending. They were allowed to choose their own preferred speed with which they could complete the path; in some randomly chosen sections of the path, they were requested to increase or decrease their speed, according to a command by the experimenter. In order to have the reference values, the experimenter manually noted the activity sequences.

Data were collected through a custom-made wireless inertial sensor unit placed on the shank of the subject's preferred leg (see Figure 1); the unit is able to collect acceleration and angular rate data, as it incorporates a triaxial accelerometer (ADXL345, from Analog Devices, Inc.) and a triaxial gyroscope (ITG-3200, from Invensense, Inc.), and it includes a microcontroller (Atmega328 from Atmel Corporation) to collect and sync data from the sensors, and then send them wirelessly to a portable unit through a bluetooth transceiver (WT12, from Bluegiga Technologies Ltd.). For the purposes of this study, just the proximal-to-distal component of the accelerometer sensor was used. Data were collected at a sampling rate of 100 samples/s.

The overall data processing structure will be then detailed in the following sections of the chapter. Figure 2 shows the overall structure of the classification schemes.

2.2. Activity Detection and Feature Extraction. Upon digital conversion, the acceleration data were first bandpass filtered (2–20 Hz, Butterworth 4th order), underwent the segmentation process, which consisted of an integration and threshold technique [8] with first-guess threshold set at 0.35 m/s, and then were on-line adapted at 0.75 times the maximum value of the detected activity integral (100 ms window) at the previous step. Once an activity is detected, a refractory period was used (i.e., a time range when no new activities were to be detected). The first-guess refractory period was set at 600 ms, and then updated on-line at 0.5 times the duration of the last detected activity epoch. From each of the segmented activities (a walking stride or an epoch corresponding to a descending or climbing step), the procedure for the extraction of features was performed.

Sixteen different features were extracted from each detected activity: in the time domain (see Figure 3), those were: the maximum value (and its relative timing with respect to the start of the activity epoch, resp., (b) and (a) in Figure 3), the minimum value (and its relative timing, (d) and (c) resp.), the temporal distance between the maximum and the minimum value (e), the number of zero-crossings (f), the distance between two consecutive peaks (g), and the distance between two consecutive valleys (h); the maximum value of the time derivative of the epoch, and its minimum value, the maximum value of its integral (as calculated along a 100 ms window), and its minimum value; in the frequency domain, for each activity epoch, the temporal variation of its mean frequency was calculated, according to [27], and its minimum and maximum values, both in linear and logarithmic scale.

These 16 features were chosen in this way, as they were able to represent data variability on a different population sample performing similar activities [28].

2.3. Feature Reduction and Training Data Use. In order to reduce the number of features (yet maintaining relevant information), Sammon's Mapping Function (SMF, [29]) was applied to the 16-dimensional feature set, that was mapped into a 2D output space. Nonlinear mapping was preferred to other linear factorization methods, as it qualitatively showed better results than PCA on a subsample of the training dataset. Since the mapping procedure is a recursive one, and the input-output relation cannot be determined analytically, an Artificial Neural Network (Multilayer Perceptron, one hidden layer with 40 neurons) was trained to mimic its nonlinear behavior. ANNs are one of the possible choices to solve MIMO problems that cannot be determined analytically [30, 31]. Out of the overall dataset that was used, 15% of its feature data points were used for the training of the ANN able to mimic the SMF behavior, with the same procedure that was used in [28] and in [32]. This 15% was randomly extracted from epochs of all the subjects, in order to maximize the generalization ability of the system.

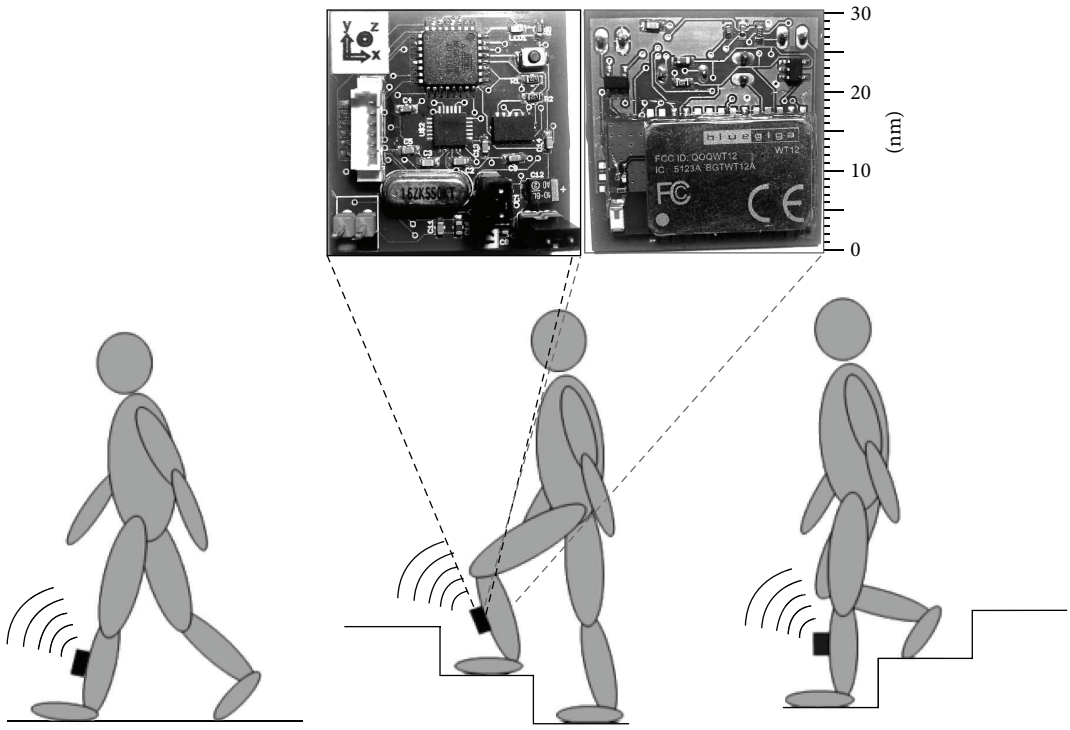

Figure 1: Sensor unit placement, and picture of the sensor unit: top side (left) and bottom side (right).

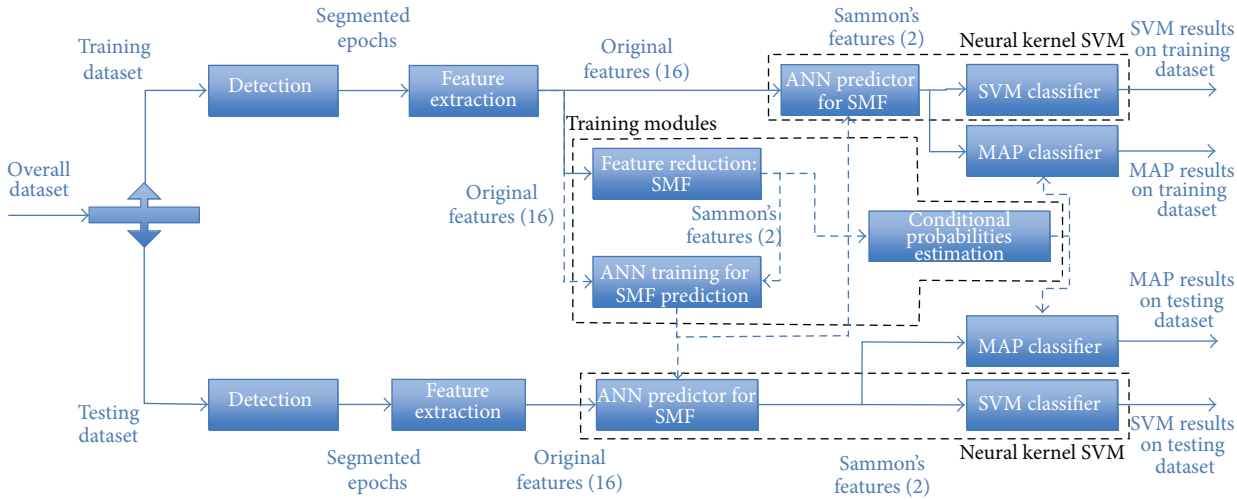

Figure 2: Structure of the classification schemes. Where not specifically denoted, same labels for each stage correspond to the same implementation.

The ANN was trained through Levenberg-Marquardt [33] backpropagation, following the same procedure proposed in [34], and the ANN was deemed as trained if the Mean Square Error fell below 0.1%. This actually happened with approximately 10000 iterations. Figure 4 shows the results of the mapping estimation through the ANN: as expected, ANN was able to accurately predict Sammon's features in the training dataset, thanks to its ability to adapt to different mapping and approximation [35] problems, as shown, for example, in [36, 37]. Cross correlation of the training set data, between features coming from SMF and the ones estimated through the ANN, resulted to be higher than 0.98.

2.4. Classifiers. Once the two features were estimated with the ANN, the following stage consisted of classifying among the different locomotor activities. In order to complete this, two different classifiers were implemented: the first relies on the representation of Bayes' Theorem and estimates the activity based on a maximum a posteriori (MAP) criterion, and it will be called as MAP in the following; the second makes use of the Support Vector Machines, and it will be denoted as SVM in the following. The structure of both the classifiers is detailed in the following subsections.

2.4.1. Maximum A Posteriori (MAP) Approach. According to Bayes' theorem, we will determine the estimated activity

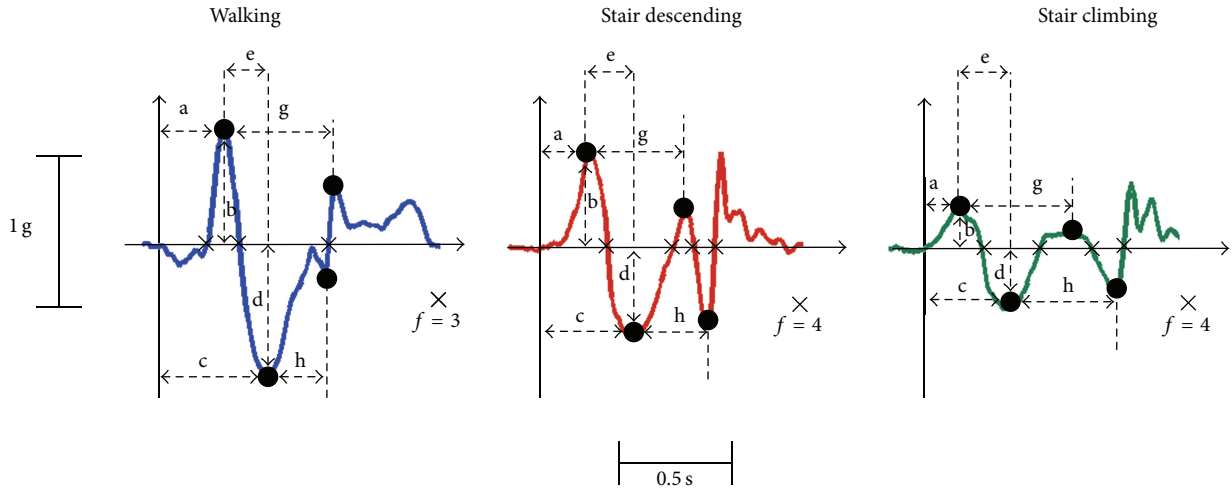

Figure 3: Samples of acceleration data for epochs of the three different activities performed by one participant. The corresponding features extracted from time domain ((a)–(h), please refer to text for the definition) are also shown. Four additional features extracted from the derivative in the time domain and four coming from the frequency domain are not shown here.

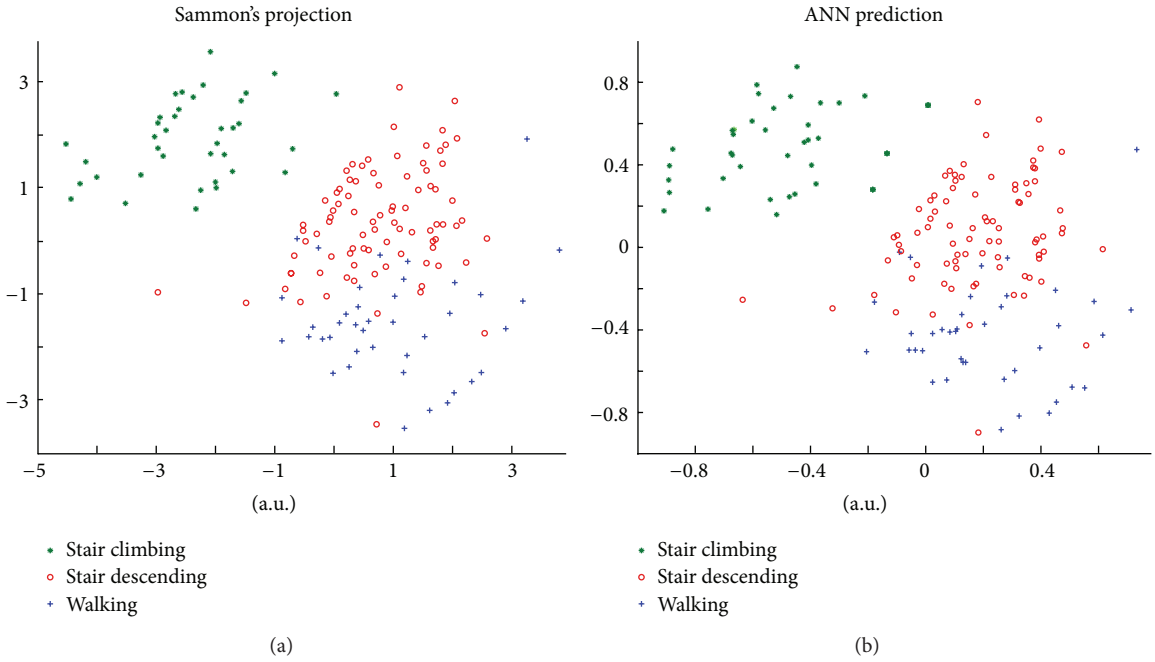

Figure 4: Excerpt of Sammon's features, as output from the SMF (left panel), and as estimated from the ANN (right panel), across three locomotor activities, coded by color and marker. Differences in scale were not detrimental to the successive processing phases.

$\widehat{\text{act}}$, based on the calculation of the conditional probabilities associated with the different locomotor activities act_i, and the current value of Sammon's feature vector (2D) s, according to the following equations:

$$P(\text{act}_i \mid s) = p(s \mid \text{act}_i) * \frac{P(\text{act}_i)}{p(s)},$$
$$\widehat{\text{act}} = \arg \max_{i \in I} P(\text{act}_i \mid s), \tag{1}$$

where I represents the domain of possible activities to be classified.

In order for the MAP criterion to be utilized, we thus need the conditional probabilities $p(s \mid \text{act}_i)$ and the prior probabilities $P(\text{act}_i)$. The first ones were hypothesized as coming from a 2D Gaussian probability density function, with first- and second-order moments equal to the values obtained from the training dataset. The prior probabilities were hypothesized as equally distributed. In the current case, this choice slightly underestimated the priors for walking activities in the used set, but we chose this criterion, in order for the classifier to be more general in classification capabilities. The MAP classifier also incorporated an update rule for the prior probabilities to be used in the current step,

Table 1: Activity epochs for the dataset.

Activity	Requested slow speed	Self-selected speed	Requested fast speed	Total
Walking	720	4265	463	5448
Stair climbing	322	2742	340	3404
Stair descending	296	2678	326	3300
Total	1338	9685	1129	12152

which was based on replacing, within a sample vector of 240 activity identifiers, the oldest sample for the classified activity with the one classified at the previous step.

2.4.2. Support Vector Machine. In the case of the Support Vector Machine, there was no kernel use, even if the transformation from the 16-dimensional space of the original features into the 2D predicted Sammon's features may be considered as a kernel *perse*, as it incorporated a nonlinear mapping to be considered as a kernel trick, with the major difference that, in this case, the new space is low-dimensional as compared to the original one.

With regard to the implementation, since we chose a low-dimensional space for the SVM to be used, linear classification was suboptimal, and we used a penalty coefficient to take into account misclassifications; concerning the optimization, we used the Mitchell-Demyanov-Malozemov (MDM) algorithm [38], with a regularization constant value of 5. Given that three classes were to be used, multiclass condition was solved by using the one versus one conditions, with max-wins voting criterion.

2.5. Performance Indicators. In order to evaluate the performance of both the classifying schemes, we calculated the classification rate for both the training set and the testing set. Confusion matrix and normalized mutual information [39] were also reported for the testing set. With ten subjects performing the requested walk path, a total of approximately 12000 activity epochs were collected. Table 1 shows the overall number of activities as split among the different kinds and speeds. It is here to be highlighted that speed was considered as a confounding factor and not as a variable on which classification was made. This is to mimic a natural scenario, where differences in energy associated with each epoch can be extracted directly on the data of each epoch, once the classification is made.

3. Results

Classification rates for the training set and the testing set are reported in Table 2. As expected, both classifiers perform quite accurately in the training set, while there is a marked difference between MAP and SVM in the case of the testing set that favored the first as compared to the second.

Performance in the training set is almost independent from the activity kind. Moreover, as reported in Table 3, misclassification in the testing set more frequently occurs between walking strides and strides of descending stairs.

Table 2: Classification results.

Training set	SVM	MAP
Walking (%)	90.4	91.8
Stair climbing (%)	91.3	90.9
Stair descending (%)	90.1	90.0
Testing set	SVM	MAP
Walking (%)	77.2	85.1
Stair climbing (%)	77.7	87.2
Stair descending (%)	74.2	81.3

4. Discussion and Conclusions

Classification rates for both schemes were, on average, good on the training dataset. Misclassifications, which occurred most frequently with walking and stair descending, may be associated with the fact that the features extracted from these two activities are on average more similar than the ones coming from stair climbing (see Figure 3); this similarity may be even more exacerbated in the transition activities (initiating a stair climbing or descending after walking or vice versa).

For the testing dataset, the maximum a posteriori approach performed better than the SVM. We speculate that, based on the results obtained in the training dataset, the structure of the MAP approach implemented in this paper has a higher generalization ability than the SVM in classifying these activities, since it includes an adaptation that updates the prior probabilities based on the history of the classification. This has not been implemented in the SVM approach, which may consequently have a decreased ability to track differences in the extracted features as a consequence of subjective and environmental factors (fatigue and variations in speed).

As far as the overall performance is concerned, classification rates are similar to those reported in [40] and in [18], where different accelerometer configurations and features were tested, with classification accuracies lying in the range 68%–97% for triaxial sensors. It is here to be highlighted that the obtained classification rates have been based on the use of just a single component of an accelerometer. This was done in order to check whether on-board processing might be considered as a viable alternative to continuous raw data communication. It is predicted that, if multiple instances of the same classification schemes may be adopted on multiple sensors placed on different body segments, the portable unit may produce better results, possibly based on a max-wins voting criterion.

As for the current implementation, the structure is relatively easy to be implemented on-board; the detection and feature extraction section is relatively light in terms of computational complexity (with only frequency features slightly weighing in), and, once the training modules are appropriately determined based on an adequate number of subjects, running the classifying modules and determining the decisions is a pretty straightforward step for both approaches: for MAP, it corresponds to running the ANN predictor and calculating the posterior probabilities and for

Table 3: Confusion matrix and Normalized Mutual Information (NMI) for the testing set.

		Predicted SVM		(NMI = 0.3550)
	Activity	Walking	Stair climbing	Stair descending
Actual	Walking (%)	77.2	8.1	14.6
	Stair climbing (%)	10.2	77.7	12.1
	Stair descending (%)	15.8	9.9	74.2
		Predicted MAP		(NMI = 0.5134)
	Activity	Walking	Stair climbing	Stair descending
Actual	Walking (%)	85.1	4.8	10.1
	Stair climbing (%)	6.6	87.2	6.3
	Stair descending (%)	12.8	5.8	81.3

SVM, it corresponds to running the ANN predictor and then applying the hyperplane (in the current case of 2D representation, a line) estimated through the SVM on the training dataset.

In the future it would be useful to insert some update rules in the SVM classification scheme, as it has been done in the MAP approach, to let it take into account the temporal variations of the accelerometer patterns in a long-term scenario.

In conclusion, the availability of different classification schemes that can be profitably applied to single sensor data may help designing body sensor networks where the classification may be done on-board in each node, so that the data throughput can be substantially reduced, and the possibility to have accurate parameters for long-term monitoring can be pursued.

Acknowledgment

The authors would like to thank the participants who volunteered in the study and MSc. Flavio Tecca, who designed the inertial sensing units. This work has been partially funded by the Italian Ministry MIUR, under PRIN Grant no. 009X3L8SW 004, under the name "*Methods and interactive technologies building steps to an ecology of movement*."

References

[1] S. Patel, H. Park, P. Bonato, L. Chan, and M. Rodgers, "A review of wearable sensors and systems with application in rehabilitation," *Journal of NeuroEngineering and Rehabilitation*, p. 21, 2012.

[2] J. J. Kavanagh and H. B. Menz, "Accelerometry: a technique for quantifying movement patterns during walking," *Gait and Posture*, vol. 28, no. 1, pp. 1–15, 2008.

[3] K. Tong and M. H. Granat, "A practical gait analysis system using gyroscopes," *Medical Engineering and Physics*, vol. 21, no. 2, pp. 87–94, 1999.

[4] K. J. O'Donovan, R. Kamnik, D. T. O'Keeffe, and G. M. Lyons, "An inertial and magnetic sensor based technique for joint angle measurement," *Journal of Biomechanics*, vol. 40, no. 12, pp. 2604–2611, 2007.

[5] A. K. Bourke, J. V. O'Brien, and G. M. Lyons, "Evaluation of a threshold-based tri-axial accelerometer fall detection algorithm," *Gait and Posture*, vol. 26, no. 2, pp. 194–199, 2007.

[6] R. P. Troiano, D. Berrigan, K. W. Dodd, L. C. Mâsse, T. Tilert, and M. Mcdowell, "Physical activity in the United States measured by accelerometer," *Medicine and Science in Sports and Exercise*, vol. 40, no. 1, pp. 181–188, 2008.

[7] D. M. Karantonis, M. R. Narayanan, M. Mathie, N. H. Lovell, and B. G. Celler, "Implementation of a real-time human movement classifier using a triaxial accelerometer for ambulatory monitoring," *IEEE Transactions on Information Technology in Biomedicine*, vol. 10, no. 1, pp. 156–167, 2006.

[8] R. Muscillo, S. Conforto, M. Schmid, P. Caselli, and T. D'Alessio, "Classification of motor activities through derivative dynamic time warping applied on accelerometer data," in *Proceedings of the 29th Annual International Conference of IEEE-EMBS, Engineering in Medicine and Biology Society (EMBC '07)*, pp. 4930–4933, August 2007.

[9] C. V. C. Bouten, W. P. H. G. Verboeket-van de Venne, K. R. Westerterp, M. Verduin, and J. D. Janssen, "Daily physical activity assessment: comparison between movement registration and doubly labeled water," *Journal of Applied Physiology*, vol. 81, no. 2, pp. 1019–1026, 1996.

[10] E. P. Meijer, A. H. C. Goris, L. Wouters, and K. R. Westerterp, "Physical inactivity as a determinant of the physical activity level in the elderly," *International Journal of Obesity*, vol. 25, no. 7, pp. 935–939, 2001.

[11] M. Yoshioka, M. Ayabe, T. Yahiro et al., "Long-period accelerometer monitoring shows the role of physical activity in overweight and obesity," *International Journal of Obesity*, vol. 29, no. 5, pp. 502–508, 2005.

[12] C. V. C. Bouten, K. R. Westerterp, M. Verduin, and J. D. Janssen, "Assessment of energy expenditure for physical activity using a triaxial accelerometer," *Medicine and Science in Sports and Exercise*, vol. 26, no. 12, pp. 1516–1523, 1994.

[13] K. Y. Chen and M. Sun, "Improving energy expenditure estimation by using a triaxial accelerometer," *Journal of Applied Physiology*, vol. 83, no. 6, pp. 2112–2122, 1997.

[14] J. Staudenmayer, D. Pober, S. Crouter, D. Bassett, and P. Freedson, "An artificial neural network to estimate physical activity energy expenditure and identify physical activity type from an accelerometer," *Journal of Applied Physiology*, vol. 107, no. 4, pp. 1300–1307, 2009.

[15] Y. Hao and R. Foster, "Wireless body sensor networks for health-monitoring applications," *Physiological Measurement*, vol. 29, no. 11, pp. R27–R56, 2008.

[16] E. Jovanov, A. Milenkovic, C. Otto, and P. C. De Groen, "A wireless body area network of intelligent motion sensors for computer assisted physical rehabilitation," *Journal of NeuroEngineering and Rehabilitation*, vol. 2, article 6, 2005.

[17] D. Hendelman, K. Miller, C. Baggett, E. Debold, and P. Freedson, "Validity of accelerometry for the assessment of moderate intensity physical activity in the field," *Medicine and Science in Sports and Exercise*, vol. 32, no. 9, pp. S442–S449, 2000.

[18] S. J. Preece, J. Y. Goulermas, L. P. J. Kenney, and D. Howard, "A comparison of feature extraction methods for the classification of dynamic activities from accelerometer data," *IEEE Transactions on Biomedical Engineering*, vol. 56, no. 3, pp. 871–879, 2009.

[19] S. J. Preece, J. Y. Goulermas, L. P. J. Kenney, D. Howard, K. Meijer, and R. Crompton, "Activity identification using body-mounted sensors—a review of classification techniques," *Physiological Measurement*, vol. 30, no. 4, pp. R1–R33, 2009.

[20] S. Pirttikangas, K. Fujinami, and T. Nakajima, "Feature selection and activity recognition from wearable sensors," in *Proceedings of the 3rd International Symposium on Ubiquitous Computing Systems*, vol. 4239 of *Lecture Notes in Computer Science*, pp. 516–527, Seoul, Korea, 2006.

[21] P. H. Veltink, H. B. J. Bussmann, W. De Vries, W. L. J. Martens, and R. C. Van Lummel, "Detection of static and dynamic activities using uniaxial accelerometers," *IEEE Transactions on Rehabilitation Engineering*, vol. 4, no. 4, pp. 375–385, 1996.

[22] R. Muscillo, M. Schmid, S. Conforto, and T. D'Alessio, "Early recognition of upper limb motor tasks through accelerometers: real-time implementation of a DTW-based algorithm," *Computers in Biology and Medicine*, vol. 41, no. 3, pp. 164–172, 2011.

[23] B. Najafi, K. Aminian, A. Paraschiv-Ionescu, F. Loew, C. J. Büla, and P. Robert, "Ambulatory system for human motion analysis using a kinematic sensor: monitoring of daily physical activity in the elderly," *IEEE Transactions on Biomedical Engineering*, vol. 50, no. 6, pp. 711–723, 2003.

[24] J. Pärkkä, M. Ermes, P. Korpipää, J. Mäntyjärvi, J. Peltola, and I. Korhonen, "Activity classification using realistic data from wearable sensors," *IEEE Transactions on Information Technology in Biomedicine*, vol. 10, no. 1, pp. 119–128, 2006.

[25] D. Wu, K. Warwick, Z. Ma et al., "Prediction of parkinson's disease tremor onset using a radial basis function neural network based on particle swarm optimization," *International Journal of Neural Systems*, vol. 20, no. 2, pp. 109–116, 2010.

[26] F. Riganti Fulginei and A. Salvini, "Hysteresis model identification by the flock-of-starlings optimization," *International Journal of Applied Electromagnetics and Mechanics*, vol. 30, no. 3-4, pp. 321–331, 2009.

[27] S. Conforto and T. D'Alessio, "Real time monitoring of muscular fatigue from dynamic surface myoelectric signals using a complex covariance approach," *Medical Engineering and Physics*, vol. 21, no. 4, pp. 225–234, 1999.

[28] R. Muscillo, M. Schmid, S. Conforto, and T. D'Alessio, "An adaptive Kalman-based Bayes estimation technique to classify locomotor activities in young and elderly adults through accelerometers," *Medical Engineering and Physics*, vol. 32, no. 8, pp. 849–859, 2010.

[29] J. W. Sammon, "A non-linear mapping for data structure analysis," *IEEE Transactions on Computers*, no. 5, pp. 401–4099, 1969.

[30] F. R. Fulginei, A. Laudani, A. Salvini, and M. Parodi, "Automatic and parallel optimized learning for neural networks performing mimo applications," *Advances in Electrical and Computer Engineering*, vol. 13, no. 1, pp. 3–12, 2013.

[31] F. R. Fulginei, A. Salvini, and M. Parodi, "Learning optimization of neural networks used for MIMO applications based on multivariate functions decomposition," *Inverse Problems in Science and Engineering*, vol. 20, no. 1, pp. 29–39, 2012.

[32] F. R. Fulginei and A. Salvini, "Neural network approach for modelling hysteretic magnetic materials under distorted excitations," *IEEE Transactions on Magnetics*, vol. 48, no. 2, pp. 307–310, 2012.

[33] D. Marquardt, "An algorithm for least-squares estimation of nonlinear parameters," *SIAM Journal on Applied Mathematics*, vol. 11, pp. 431–441, 1963.

[34] M. Gneo, M. Schmid, S. Conforto, and T. D'Alessio, "A free geometry model-independent neural eye-gaze tracking system," *Journal of Neuroengineering and Rehabilitation*, vol. 9, p. 82, 2012.

[35] G. Capizzi, S. Coco, C. Giuffrida, and A. Laudani, "A neural network approach for the differentiation of numerical solutions of 3-D electromagnetic problems," *IEEE Transactions on Magnetics*, vol. 40, no. 2, pp. 953–956, 2004.

[36] P. Del Vecchio and A. Salvini, "Neural Network and Fourier Descriptor macromodeling dynamic hysteresis," *IEEE Transactions on Magnetics*, vol. 36, no. 4 I, pp. 1246–1249, 2000.

[37] A. Salvini and C. Coltelli, "Prediction of dynamic hysteresis under highly distorted exciting fields by neural networks and actual frequency transplantation," *IEEE Transactions on Magnetics*, vol. 37, no. 5 I, pp. 3315–3319, 2001.

[38] B. F. Mitchell, V. F. Dem'yanov, and V. N. Malozemov, "Finding the point of a polyhedron closest to the origin," *SIAM Journal on Control*, vol. 12, no. 1, pp. 19–26, 1974.

[39] D. Cai, X. He, and J. Han, "Document clustering using locality preserving indexing," *IEEE Transactions on Knowledge and Data Engineering*, vol. 17, no. 12, pp. 1624–1637, 2005.

[40] H. Chan, M. Yang, H. Wang et al., "Assessing gait patterns of healthy adults climbing stairs employing machine learning techniques," *International Journal of Intelligent Systems*, vol. 28, pp. 257–270, 2013.

Hindawi Publishing Corporation
Computational and Mathematical Methods in Medicine
Volume 2013, Article ID 512965, 6 pages
http://dx.doi.org/10.1155/2013/512965

Research Article

Evaluation of Motor Performances of Hemiplegic Patients Using a Virtual Cycling Wheelchair: An Exploratory Trial

Norihiro Sugita,[1] Makoto Yoshizawa,[2] Yoshihisa Kojima,[1] Makoto Abe,[1] Noriyasu Homma,[3] Kazunori Seki,[4] and Nobuyasu Handa[4]

[1] *Graduate School of Engineering, Tohoku University, Sendai, Miyagi 980-8579, Japan*
[2] *Cyberscience Center, Tohoku University, Sendai, Miyagi 980-8578, Japan*
[3] *Graduate School of Medicine, Tohoku University, Sendai, Miyagi 980-8575, Japan*
[4] *Sendai School of Health and Welfare, Sendai, Miyagi 981-3206, Japan*

Correspondence should be addressed to Norihiro Sugita; sugita@yoshizawa.ecei.tohoku.ac.jp

Received 27 September 2013; Accepted 2 November 2013

Academic Editor: Takashi Watanabe

Cycling is known to be an effective rehabilitation exercise for hemiplegic patients who face difficulty during walking because of stroke or other brain disorders. A cycling wheelchair (CWC) is a useful tool to provide exercise for these patients and improve their quality of life. In previous studies, our group developed a system that allows patients to safely practice driving a CWC in a virtual environment. However, it has been difficult to check their motor performances and determine the effects of the exercise on a daily basis. This study is an exploratory trial for developing a method to evaluate the motor performances of users based on their CWC pedaling patterns. An experiment with some hemiplegic patients and healthy subjects was conducted and their pedaling patterns were analyzed. Results showed a significant difference between the hemiplegic patients and healthy subjects in an index that reflects pedaling balance between the feet. This result indicates a possible method of evaluating the motor performances of users based on their pedaling patterns.

1. Introduction

Paralysis of the lower extremities can be caused by brain disorders (stroke, brain damage, and degenerative disease), neurologic diseases, or spinal cord injury. In general, patients with severe impairment of the leg use wheelchairs to move around in their daily lives. These patients generally never use their feet while moving with wheelchairs because most wheelchairs are made to be operated either by the user's hands or an electric motor. However, human legs act as a pump for carrying blood back to the heart [1]. Therefore, movement of the feet caused by the calves and the legs of patients does not occur for a long period of time, blood circulation in their lower limbs is reduced, and the risk of disuse syndromes such as muscle weakness and joint contractures is increased.

A cycling wheelchair (CWC) [2–5] is attracting attention as a tool to solve this problem because it provides physical exercise for hemiplegic patients. These individuals can move around more quickly and travel longer distances without fatigue using a CWC instead of a traditional wheelchair. In addition, they can also use their hands while driving a CWC. This encourages the patients to be independent and improves their quality of life. And some previous studies have reported the effectiveness of cycling for hemiplegic patients to improve their motor functions [6–10]. These findings support the possibility that a CWC is useful not only as a transportation device but also as a rehabilitation system for these patients.

Feedback regarding the training effects on patients is important to maintain their motivation for the rehabilitation. In previous studies, existing indices such as the Fugl-Meyer scale [11], the postural assessment scale for stroke patients (PASS) [12], and step length during treadmill use were used to show the effects of cycling. However, specialized instruments and medical staff are required to obtain these indices; therefore, it is difficult for patients to check their motor performances on a daily basis. Furthermore, it is

impossible to obtain information on the exercise on a real-time basis.

In preceding studies, we developed a virtual reality (VR) system, in which patients with motor dysfunction can safely drive a CWC without requiring a large open space to practice [13, 14]. This system allows us to measure user movements, such as pedaling, with a high degree of accuracy under several physical conditions. If motor performances and functions of the users are estimated using only their pedaling patterns that are characterized as changes in angular velocity or acceleration of the pedal, it is possible to develop not only a household testing system that checks the motor performances of the users on a daily basis but also new types of rehabilitation systems, for example, a system that automatically selects or plans a rehabilitation program suitable for each user based on their motor performances. In addition, it will be possible to automatically collect a large amount of pedaling data from several patients and to utilize the data for developing effective rehabilitation training methods. The indices obtained in real time will be useful for the development of a rehabilitation system with a biofeedback mechanism [15–18].

The purpose of this study is to develop a new method for assessing the motor performances of users by analyzing their CWC pedaling patterns. In particular, we have proposed new indices that are calculated based on the distribution of angular velocity of CWC pedals. We conducted an experiment to measure the angular velocity of CWC pedals from groups of patients and healthy subjects and discussed the differences in the indices between these groups.

2. Methods

2.1. Measurement of Pedal Angle. Figure 1 shows the experiment device used in this study. A CWC was fixed to a roller unit of the VR system developed in the preceding study [14]. The minimum torque required to rotate the pedal of the CWC was approximately 5.8 Nm in case of a user weighing 70 kg. Signals from a wireless acceleration sensor (WAA-006, Wireless Technologies, Inc.) attached to the wheel axis were recorded every 0.01 s and filtered through a low-pass filter with a cut-off frequency of 3 Hz. The pedal angle of the CWC θ (rad) was estimated on the basis of the inclination of the acceleration sensor as shown in Figure 2. The angle θ is defined as zero when the right pedal is at the highest point in a full revolution. The angular velocity of the pedal ω (rad/s) was calculated as the difference θ in the values.

2.2. Analysis. The distribution of the angular velocity ω in one revolution of a CWC pedal is graphically illustrated in a cobweb chart (Figure 3). In this figure, the θ-axis is set on the circumference of the cobweb chart, and the ω-axis is set as an axis perpendicular to the θ-axis. In general, healthy persons rotate the pedal primarily with their right leg, when θ is from 0 to π radian, hereinafter called right leg phase, and they rotate the pedal with their left leg when θ is from π to 2π radian, hereinafter called left leg phase.

Figure 4 shows examples of the ω distributions obtained from (a) a healthy subject and (b) a hemiplegic patient driving

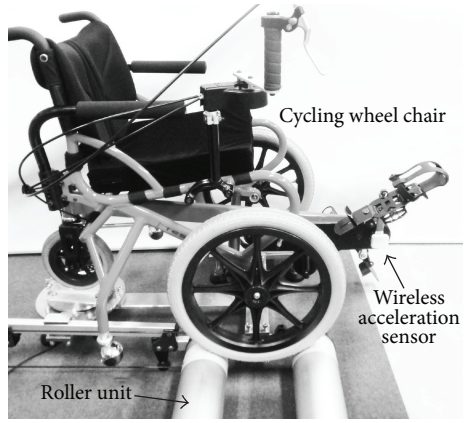

Figure 1: A cycling wheelchair (CWC) fixed to a roller unit of a virtual reality system and a wireless acceleration sensor to measure the angle of the pedal.

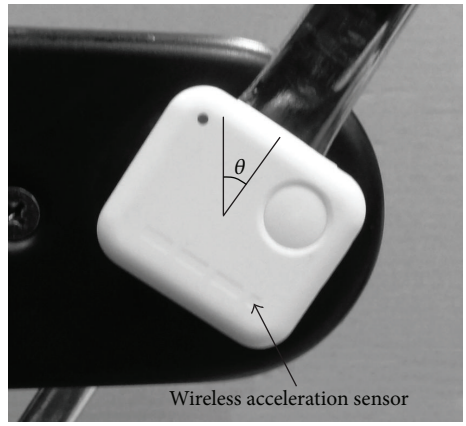

Figure 2: The pedal angle of CWC θ (rad) estimated on the basis of the inclination of a wireless acceleration sensor. The pedal angle θ is zero when the right pedal is the highest point in a full revolution.

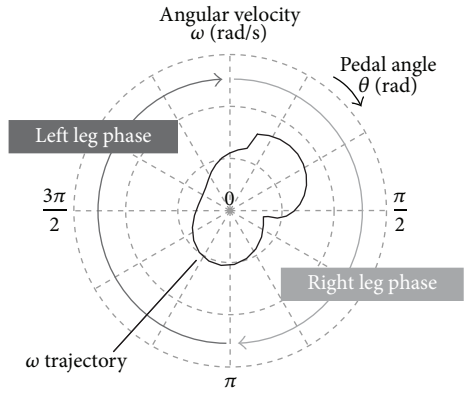

Figure 3: A cobweb chart to illustrate the distribution of the angular velocity in one revolution of the pedal. Right leg phase ($0 \le \theta < \pi$) and left leg phase ($\pi \le \theta < 2\pi$) are angular ranges in which the pedal is rotated primary with right or left leg, respectively.

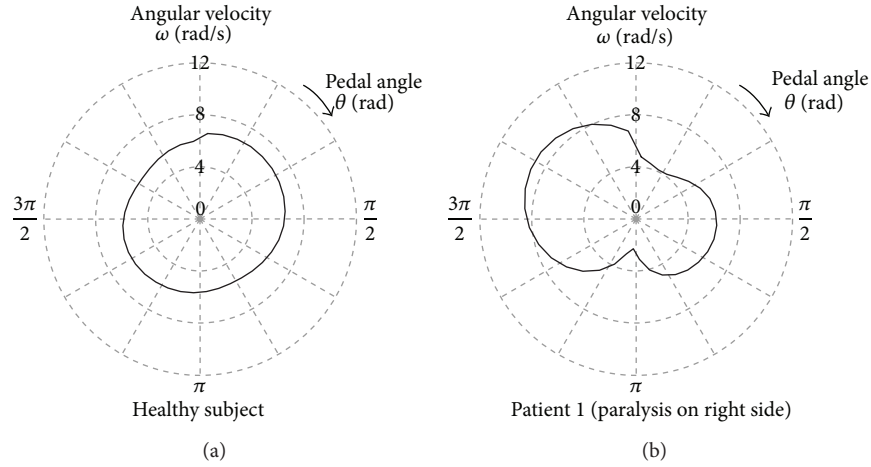

Figure 4: Examples of the angular velocity distribution of CWC pedals in one revolution obtained from (a) a healthy subject and (b) a hemiplegic patient.

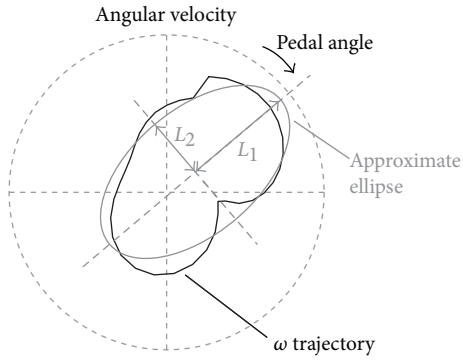

Figure 5: Elliptical approximation of the angular velocity distribution of CWC pedals in a full revolution. L_1 and L_2 are major and minor axes of the approximate ellipse, respectively.

the virtual CWC. The patient was paralyzed on his right side because of a stroke. As shown in Figure 4(a), ω of the healthy subject was kept relatively constant in one revolution. In contrast, for the patient, there was a difference in ω between the right and left leg phases as shown in Figure 4(b). Therefore, the shape of the ω distribution obtained from the patient tended to be an ellipse, while that from the healthy subject tended to be a true circle. Based on this observation, a new index, P_b, was proposed to evaluate pedaling balance between the feet. P_b is defined as follows:

$$P_b = \frac{L_2}{L_1}, \tag{1}$$

where L_1 and L_2 are the major and the minor axes of the approximate ellipse shown in Figure 5, respectively. P_b takes a value from 0 to 1, and the closer to 1 the P_b value, the better the pedaling balance. The ellipse that geometrically approximates the ω distribution is obtained by the method of least squares.

Users who are not hemiplegic patients but have some types of disability in their lower body cannot rotate the pedal smoothly during both the right and left leg phases. In this case, the variation in ω obtained will be large because the pressure exerted on the pedals is unstable. In this study, pedaling stability was evaluated by calculating an index P_s that is defined as follows:

$$P_s = \frac{C}{C_a}, \tag{2}$$

where C and C_a are the path length of the ω trajectory and the circumferential length of the approximate ellipse shown in Figure 5, respectively. P_s takes a value from 0 to 1, and the closer to 1 the P_s value, the more stable the rotation of pedaling.

3. Experiment

An experiment was conducted to evaluate the effectiveness of the proposed indices. Four hemiplegic patients (4 males; aged 65–75 years; mean age, 68.3 years) and 15 elderly healthy subjects (15 males; aged 61–77 years; mean age, 69.9 years) participated in the experiment. Two out of 4 patients were paralyzed on their right side, and the other 2 patients were paralyzed on their left side because of a stroke. None of the subjects had driven a CWC before this experiment.

A large-screen display was set in front of the experimental system shown in Figure 1 to display a VR image. The subjects sat on the CWC fixed to the system and rotated the pedals more than 10 revolutions while viewing the display. The image on display was updated according to the pedal rotation in real time. They could, therefore, experience a feeling of moving forward. They were instructed to rotate the pedals at a constant rate. But set values of the rate were not provided for them so that they can rotate the pedals in a natural state. The experiment was conducted twice, and data for the analysis was obtained from the second test.

The experimental protocol was approved by the Internal Review Board of the Tohoku University, and informed consent was obtained from all the subjects before the experiment.

Table 1: Comparison of mean ω, P_b, and P_s values between the patient and healthy subject groups.

	Patient ($n = 4$)	Healthy subject ($n = 15$)
Angular velocity (ω)	4.52 ± 1.59 rad/s	3.94 ± 1.07 rad/s
Pedaling balance (P_b)	0.66 ± 0.10*	0.80 ± 0.10*
Pedaling stability (P_s)	0.81 ± 0.16	0.91 ± 0.075

*$P < 0.05$; Mann-Whitney U-test.

4. Results

Table 1 shows mean values of ω, P_b, and P_s in the patient and the healthy subject groups. Each subject's ω, P_b, and P_s values were calculated on the basis of the data from the 2nd to 7th revolution of the pedals. No significant difference was observed in ω and P_s between the two groups in our study. In contrast, P_b of the patients was significantly smaller than that of the healthy subjects ($P < 0.05$; Mann-Whitney U-test).

Figure 6 shows the correlation between ω and P_b. This figure shows that P_b of the patients was lower than that of the healthy subjects, regardless of ω. The P_b value was higher than 0.7 for several subjects including the patients; however, P_b obtained from the subjects rotating the pedals at a rate less than 4.0 rad/s decreased even in the healthy group.

Figure 7 shows the correlation between ω and P_s. This result shows that the P_s value was higher than 0.7, except in 1 patient, and that P_s was proportional to ω. As is the case in P_b, P_s values of the patients were lower than those of the healthy subjects when they were compared without considering ω.

5. Discussion

There was no significant difference in the angular velocity ω between the patients and healthy subjects. This result may be related to the rotational load of the roller unit used in the experiment. That is, the rotational load was light enough, so that the patients could rotate the pedals at a high rate using only their unaffected leg.

In contrast, a significant difference was observed in the proposed index P_b that reflects the pedaling balance between the feet. This result indicates the possibility of P_b as an index that can identify hemiplegia symptoms. However, as shown in Figure 6, there were cases in which P_b of healthy subjects rotating the pedals at a low rate decreased considerably. This result implies that maintaining the pedaling balance between the feet at a low rotational rate is difficult even for healthy subjects, and P_b should be evaluated for users rotating the pedals at an adequate rate. From the results of this experiment, the minimum rotational rate desirable for the accurate evaluation of P_b is considered to be 4.0 rad/s.

Figure 8 shows examples of the ω distributions obtained from 3 patients. As shown in Figure 4(b) and Figure 8(a), the patients maintained pedal rotations by raising the rotational speed during the nonparalyze phase, which was the time period when they moved the pedals primarily with their unaffected leg. At the same time, there was a patient who increased the rotational speed during the paralyze phase as shown in Figure 8(b). This patient may have used the strength of his unaffected leg to lift the opposite pedal, on which he propped his affected leg, during the nonparalyze phase, and subsequently the pedal was gravitationally rotated during the paralyze phase. These results indicate that hemiplegic patients have different methods of rotating the pedals.

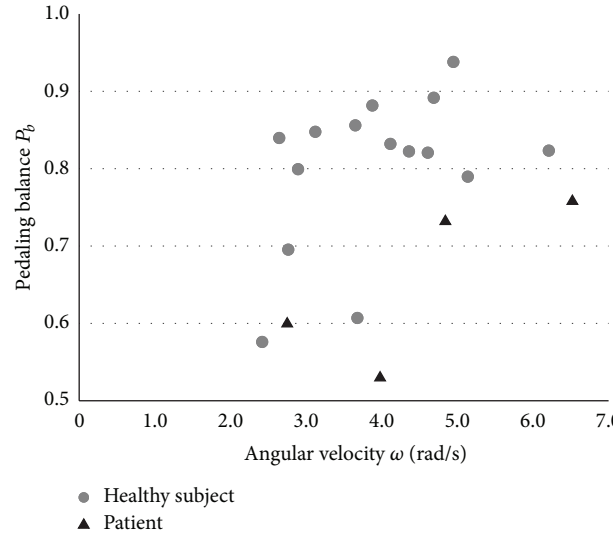

Figure 6: Correlation between angular velocity ω and pedaling balance P_b. Each subject's data were obtained as a value averaged from the 2nd to 7th revolution of the pedals.

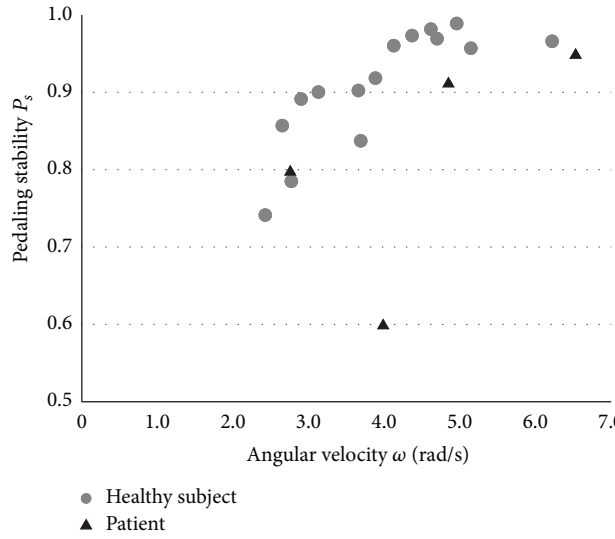

Figure 7: Correlation between angular velocity ω and pedaling stability P_s. Each subject's data were obtained as a value averaged from the 2nd to 7th revolution of the pedals.

As shown in Figure 7, the proposed index P_s that reflects pedaling stability was proportional to ω. This result is reasonable because the pedal rotation tends to be more stable by the action of the rotational inertia as the rotational rate increases. Figure 8(c) shows the ω distribution of the patient whose P_s was the lowest of all the subjects. This result shows that ω changed greatly, even during the nonparalyze phase.

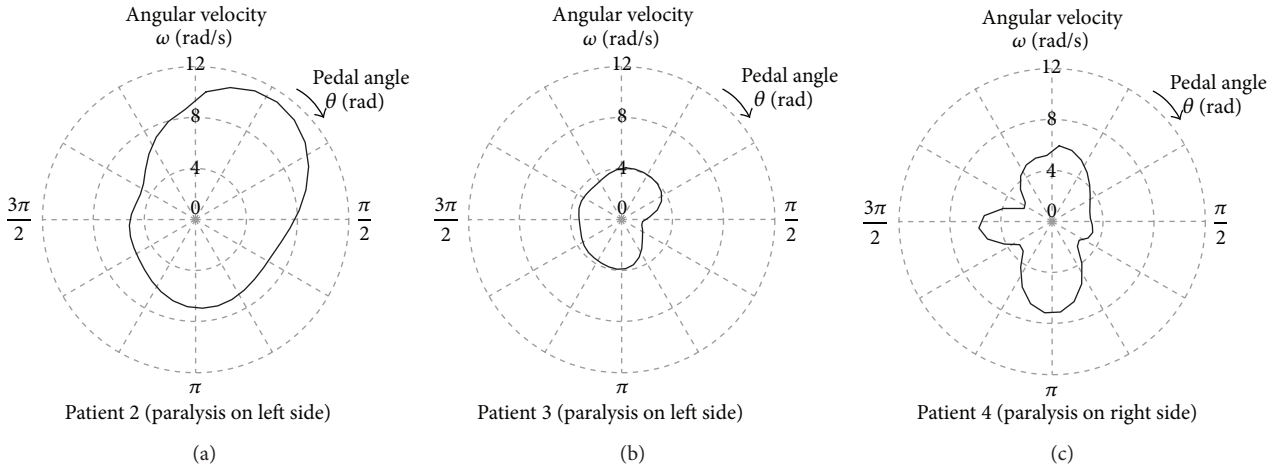

Figure 8: Examples of the angular velocity distribution of CWC pedals in one revolution obtained from (a) and (b) patients with left-sided paralysis and (c) a patient with right-sided paralysis.

In particular, ω suddenly increased at approximately the middle point of the nonparalyze phase, approximately $\theta = 3\pi/2$, which was the time when the joint angle of the affected leg was the smallest in a full revolution. Therefore, P_s is considered to have a relationship with the range of joint motion.

A center point or a rotational angle of the approximate ellipse of the ω distribution may also be useful indices to analyze pedaling patterns. For example, the center point of the approximate ellipse obtained from a patient with right-sided paralysis is considered to be in the left side of the cobweb chart. Furthermore, P_b and P_s can be obtained using a rotary torque or an angular acceleration of the pedal instead of the angular velocity. These indices may provide detailed information of pedaling characteristics in an easy-to-understand way because they are closely correlated with muscle activation patterns of users. However, a torque sensor requires major reorganization of the CWC, and the angular acceleration is easily influenced by noises such as wheel wobble; thus a higher-accuracy method for measuring the pedal angle is required.

The wireless acceleration sensor used in this study is easy to attach and is indestructible. It is, therefore, suitable for household systems to check the motor performances of users as noted in the Introduction. However, accuracy of the pedal angle obtained with the acceleration sensor is not considerably high compared with that with mechanical sensors such as a rotary encoder. Some noises, such as the centrifugal force and vibrations of the CWC, reduce the accuracy of the pedal angle. Estimation errors caused by these factors may be reduced by combining different types of sensors.

6. Conclusion

In this study, we analyzed pedaling patterns of the angular velocity obtained from hemiplegic patients and healthy subjects driving a CWC in a virtual environment. Two new indices based on the angular velocity of the CWC pedals were proposed to evaluate the motor performances of users.

The experimental results showed that a significant difference between the hemiplegic patients and healthy subjects was observed in the index related to the pedaling balance of the users between their feet. This result indicates a possibility of evaluating motor performances and functions of CWC users based on their pedaling patterns. In contrast, it was shown that accuracy of this index decreased for subjects rotating the pedals at a low rate.

In future works, changes to the proposed indices before and after rehabilitation trainings should be analyzed to test their efficiency. In addition, it is necessary to compare the proposed indices with general and traditional ones that are known to reflect the degree of motor dysfunctions [11, 12]. To investigate the relationship between the symptomatic states of users and pedaling patterns, more patient data are required. In addition, influences of rotational speed on the proposed indices should be removed as much as possible. A rotational rate appropriate for pedaling differs between the patient and healthy subject groups; therefore, a new index that is insusceptible to the rotational rate is required. Rotational loads of the CWC are considered to have significant influence on the pedaling patterns. A detailed analysis will be possible if data are obtained under conditions of some different rotational loads.

Conflict of Interests

The authors declare that there is no conflict of interests regarding the publication of this paper.

Acknowledgements

The authors would like to thank the participants of the experiment in this study. The authors would also like to thank the staff of TESS Co., Ltd. for their technical contributions.

References

[1] R. F. Rushmer, *Cardiovascular Dynamics*, W.B. Saunders, 2nd edition, 1976.

[2] K. Makino, N. Yoshimoto, H. Wada, and K. Hachisuka, "Usefulness of a Leg-pedaled Wheelchair for Hemiplegic Patients," *The Japanese Journal of Rehabilitation Medicine*, vol. 40, no. 9, pp. 617–620, 2003 (Japanese).

[3] K. Seki, M. Sato, T. Fujii, M. Ichie, and Y. Handa, "Activity of lower limb muscles during driving a cycling chair in hemiparetic stroke patients," in *Proceedings of the 15th Congress of the International Society of Electrophysiology and Kinesiology*, p. 221, Boston, Mass, USA, 2004.

[4] K. Seki, M. Sato, T. Fujii, and Y. Handa, "Driving a cycling chair without FES in the non-ambulatory hemiplegic patients," in *Proceedings of the 9th Annual Conference of the International FES Society*, pp. 245–246, Bournemouth, UK, 2004.

[5] K. Seki, M. Sato, and Y. Handa, "Increase of muscle activities in hemiplegic lower extremity during driving a cycling wheelchair," *Tohoku Journal of Experimental Medicine*, vol. 219, no. 2, pp. 129–138, 2009.

[6] T. Fujiwara, M. Liu, and N. Chino, "Effect of pedaling exercise on the hemiplegic lower limb," *American Journal of Physical Medicine and Rehabilitation*, vol. 82, no. 5, pp. 357–363, 2003.

[7] D. A. Brown, S. Nagpal, and S. Chi, "Limb-loaded cycling program for locomotor intervention following stroke," *Physical Therapy*, vol. 85, no. 2, pp. 159–168, 2005.

[8] M. Katz-Leurer, I. Sender, O. Keren, and Z. Dvir, "The influence of early cycling training on balance in stroke patients at the subacute stage. Results of a preliminary trial," *Clinical Rehabilitation*, vol. 20, no. 5, pp. 398–405, 2006.

[9] T. W. Janssen, J. M. Beltman, P. Elich et al., "Effects of electric stimulation-assisted cycling training in people with chronic stroke," *Archives of Physical Medicine and Rehabilitation*, vol. 89, no. 3, pp. 463–469, 2008.

[10] L. Johannsen, A. M. Wing, T. Pelton et al., "Seated bilateral leg exercise effects on hemiparetic lower extremity function in chronic stroke," *Neurorehabilitation and Neural Repair*, vol. 24, no. 3, pp. 243–253, 2010.

[11] A. R. Fugl-Meyer, L. Jääskö, I. Leyman, S. Olsson, and S. Steglind, "The post-stroke hemiplegic patient. 1. a method for evaluation of physical performance," *Scandinavian Journal of Rehabilitation Medicine*, vol. 7, no. 1, pp. 13–31, 1975.

[12] C. Benaim, D. A. Pérennou, J. Villy, M. Rousseaux, and J. Y. Pelissier, "Validation of a standardized assessment of postural control in stroke patients: the Postural Assessment Scale for Stroke patients (PASS)," *Stroke*, vol. 30, no. 9, pp. 1862–1868, 1999.

[13] S. Suzuki, A. Tanaka, T. Takahashi, K. Seki, Y. Handa, and M. Yoshizawa, "Developement of VR-based rehabilitation system for patients with leg paralysis using the cycling chair," in *Proceedings of the 9th Annual Conference Virtual Reality Society of Japan*, pp. 551–554, Kyoto, Japan, 2004 (Japanese).

[14] N. Sugita, Y. Kojima, M. Yoshizawa et al., "Development of a virtual reality system to evaluate skills needed to drive a cycling wheel-chair," in *Proceedings of the 34th Annual International Conference of the IEEE Engineering in Medicine and Biology Society*, pp. 6019–6022, San Diego, Calif, USA, 2012.

[15] H. Sveistrup, "Motor rehabilitation using virtual reality," *Journal of NeuroEngineering and Rehabilitation*, vol. 10, p. 10, 2004.

[16] R. Riener, L. Lünenburger, and G. Colombo, "Human-centered robotics applied to gait training and assessment," *Journal of Rehabilitation Research and Development*, vol. 43, no. 5, pp. 679–694, 2006.

[17] H. Huang, S. L. Wolf, and J. He, "Recent developments in biofeedback for neuromotor rehabilitation," *Journal of NeuroEngineering and Rehabilitation*, vol. 3, p. 11, 2006.

[18] S. Ferrante, E. Ambrosini, P. Ravelli et al., "A biofeedback cycling training to improve locomotion: a case series study based on gait pattern classification of 153 chronic stroke patients," *Journal of NeuroEngineering and Rehabilitation*, vol. 8, no. 1, article 47, 2011.

Hindawi Publishing Corporation
Computational and Mathematical Methods in Medicine
Volume 2013, Article ID 926858, 10 pages
http://dx.doi.org/10.1155/2013/926858

Research Article

Evaluation of Treatment in the Smart Home IRIS in terms of Functional Independence and Occupational Performance and Satisfaction

Julija Ocepek,[1] Anne E. K. Roberts,[2] and Gaj Vidmar[1]

[1] *University Rehabilitation Institute, Republic of Slovenia, Linhartova 51, SI-1000 Ljubljana, Slovenia*
[2] *Faculty of Health, Education and Society, University of Plymouth, SF18, Peninsula Allied Health Centre, College of St Mark & St John, Plymouth, Devon PL6 8BH, UK*

Correspondence should be addressed to Julija Ocepek; julija.ocepek@ir-rs.si

Received 5 August 2013; Revised 2 October 2013; Accepted 9 October 2013

Academic Editor: Imre Cikajlo

The development of assistive technologies, home modifications, and smart homes has rapidly advanced in the last two decades. Health professionals have recognised the benefits of these technologies in improving individual's quality of life. The Smart Home IRIS was established in 2008 within the University Rehabilitation Institute in Ljubljana with the aim to enable persons with disabilities and elderly people to test various assistive technologies and technical solutions for their independent living. We investigated the effect of treatments in the Smart Home IRIS. A convenience sample of 59 persons with disabilities and elderly people (aged 24–81 years) who were treated in the Smart Home IRIS from April to December 2011 participated. Standardised instruments—the Canadian Occupational Performance Measure (COPM) and the Functional Independence Measure (FIM)—were administered at the first assessment in the Smart Home IRIS and at a second assessment at the participant's home after 6–12 months. All the outcomes statistically significantly improved from the first to the second assessment. The treatments in the Smart Home IRIS appeared to contribute to higher occupational performance and satisfaction with performance and higher functional independence of persons with disabilities and elderly people.

1. Introduction

In the recent years, there has been an extended development and increased prescription of assistive technologies (ATs), including smart home technologies, that help persons with disabilities and elderly to live more independently. In Slovenia, there are several barriers that thwart the implementation of ATs, such as a lack of strong political initiatives towards AT development, the cost of ATs, and no possibility to test various ATs before buying them. Provision of ATs within the Slovenian health care system differs from many European countries in the sense that persons with disabilities and elderly must buy the majority of ATs.

One of the solutions for enabling persons with disabilities and elderly people to receive adequate information about ATs and to test appropriate ATs was the establishment of the Smart Home Independent Residing enabled by Intelligent Solutions (IRIS), in 2008. The main aim of the Smart Home IRIS is demonstration, testing, and application of contemporary technological solutions that compensate for diverse kinds of disabilities and thereby improve the quality of life of persons with disabilities [1]. The Smart Home IRIS is a demonstration apartment at the University Rehabilitation Institute in Ljubljana, founded on the basis of numerous European smart home projects. Its concept is presented in Figure 1.

The apartment is fitted with various assistive technologies, from simple to the most advanced, which assist persons with different disabilities as well as the elderly. The Smart Home IRIS enables persons with disabilities and the elderly to achieve the highest possible level of functional independence. Adapted equipment, technical aids, and numerous contemporary electronic systems which enable a user to control his or her living environment (open the doors and windows, pull the curtains, control the TV, radio, telephone, switch on/off

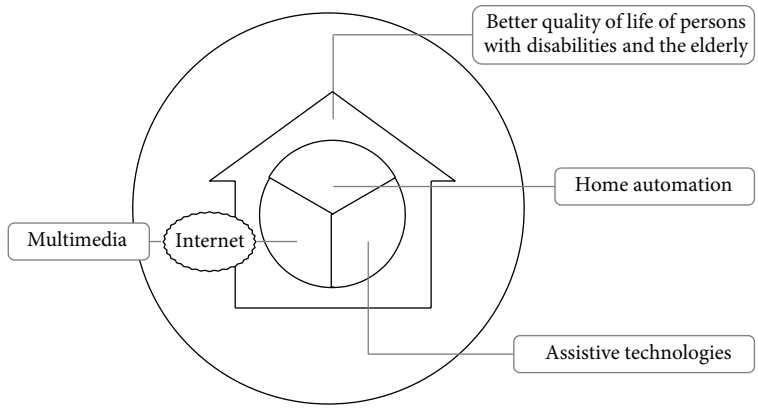

Figure 1: The concept of the Smart Home IRIS.

the heating system, etc.) in various manners (using switches, remote control, voice control, wheelchair joystick, eye control, ambient intelligence, etc.). The underlying rationale is our belief, based on our clinical experience, that controlling the living environment leads to a better quality of life.

The Smart Home IRIS is equipped with state-of-the-art information and communication technology, which is adapted to different levels and types of disability. This enables the users to communicate with the outside world, to receive remote care and remote monitoring of their health condition, and to partake in studying, work, leisure, and entertainment by means of electronic media. Individual treatments are client-centred—led by the problems identified by patients in the Canadian Occupational Performance Measure (COPM) [2] and performed by a multidisciplinary team (composed of a physiatrist, an occupational therapist, an engineer, and other professionals). The service is funded by the national health insurance company and incorporates several subservices.

Because five years have passed since the establishment of the Smart Home IRIS, evidence of its role and its contribution to the Slovenian health care system in general, and rehabilitation medicine in particular, is needed. Feedback from persons who have been treated in the Smart Home IRIS is also important for further planning of treatments, for initiating some changes of the daily practice, or for including additional services. A small initial study—a mail survey in which 117 persons with disabilities and elderly participated—was carried out during 2008 and 2009 [3]. The results provided important feedback about adequacy of treatments in the Smart Home IRIS and about satisfaction with the treatment from the users' point of view. However, due to the limitations of the research design, the acquired evidence was not strong. Therefore, the present study was conducted.

2. Materials and Methods

2.1. Study Design and Instruments. A quantitative quasi-experimental study was conducted, employing repeated measurement at two time-points without a control group. The dependent variables were the functional independence scores (total, motor, and cognitive scores on the Functional Independence Measure—FIM [4]) and the COPM performance and satisfaction ratings at the first treatment in the Smart Home IRIS and at the second assessment. The independent variables were the participants' characteristics: gender, diagnosis, age, and number of ATs used.

Three research hypotheses were tested. (1) The use of ATs and home modification has positive impact on functional independence of the persons treated in the Smart Home IRIS. (2) The use of ATs and home modification has positive impact on occupational performance and satisfaction with occupational performance of the persons treated in the Smart Home IRIS. (3) There are differences in progress with regard to the diagnosis of the persons who were treated in Smart Home IRIS and the number of assistive technologies that they used.

The COPM was used because the treatments in the Smart Home IRIS are client-centred in nature. It is a standardised individualized measure in the form of a semistructured interview designed to measure a client's self-perception of occupational performance. It also assists in setting the goals and can serve as an outcome measure to determine the degree of change in occupational performance over time as a result of intervention [5]. The focus of the COPM is on occupational performance areas, namely self-care, productivity, and leisure. The client's perspective is sought through the interview, and occupational performance problems are defined by the client. After the interview, the client uses a 0–10 scale to rate his or her perceived performance on each of the identified tasks and to rate his or her satisfaction with his or her own performance. The COPM has been reported to be a valid, reliable, clinically useful, and responsive outcome measure for occupational therapists [6]. Studies have reported the use of the COPM with a wide variety of clients in numerous different settings, including those with physical and mental health issues, all age groups, as well as clients in hospital, outpatient, and community settings [7–9]. Several studies have examined the test-retest reliability of the COPM [10–12] and the results indicate that the COPM is highly reliable (the reliability coefficients consistently exceed 0.80). The COPM has also demonstrated acceptable content, criterion, and construct validity [13–15]. Because the reproducibility of

the mean performance and satisfaction scores on the COPM has been found to be moderate but poor for the scores of the separate problems [16], the mean scores of performance and satisfaction were used.

The FIM is the most widely accepted functional assessment measure used with all diagnostic groups within the adult rehabilitation population, as evidenced in several studies all over the world [17–19]. It evaluates 18 activities in 6 categories (self-care, sphincter control, transfers, mobility, communication, and social cognition), which are grouped into two areas, motor and cognitive. Each item is scored on a 1–7 scale regarding the level of assistance required for the individual to perform the particular activity of daily living (1 indicates full assistance and 7 indicates full independence). The total score therefore ranges between 18 and 126 points. FIM scores differentiate between disabilities and levels of severity of impairment, correlate with the time taken for care, and correlate highly with the results of other relevant measures [17]. Reliability and validity of the FIM were proven through several studies [20, 21]. It has been found to have high rates of interrater and test-retest reliability (0.95).

2.2. Participants. In Slovenia, there are about 200,000 persons with disabilities and of those about 10,000 have the most severe types of disability [22]. The target population for our research were the persons with disabilities who were/are treated in the Smart Home IRIS. About 200 persons with different disabilities and of different ages are treated in the Smart Home IRIS each year. Among the persons treated in the study period from April to December 2011, 110 met the inclusion criteria listed below and were thus invited to take part in the study. Adults aged 18 years or more with adequate cognitive capacity who have been referred to the Smart Home IRIS for the first time were included. The age limit was imposed because of the financial and legislative autonomy/independence of the participants and because the FIM is normally only used for adults. Normal cognitive capacity was also required, so a score of at least 25 points on the Mini Mental State Examination (MMSE) [23] was another inclusion criterion. The final sample consisted of the 59 participants who agreed to participate, so a 54% response rate was obtained. The set minimum sample size requirement was met and exceeded, thus compensating for the slight loss of power when analysing data using nonparametric (i.e., rank-based; see Section 2.4) instead of the parametric method (i.e., normal distribution-based) that had been used for sample-size calculation.

2.3. Procedure. After receiving the ethical approval for the study, the recruitment of the participants began. Anyone who had already been seen in the Smart Home IRIS and met the inclusion criteria was invited to participate in the study. The recruitment letter with a brief introduction and describing the procedure of research was sent by surface mail to those patients. Those who agreed to take part in the research signed the consent form that was sent together with the recruitment letter and mailed it back in the prepared envelope. The FIM and COPM were completed at the outset of each individual's engagement with the Smart Home IRIS. They were administered in the Smart Home IRIS. This was followed by normal exposure to the smart home. Then the assessments were administered to the individuals again between 6 and 12 months from the initial assessment. Our clinical experience shows that this is an adequate period of time for the individual to realise the advised technical solutions or home modifications. The second set of assessments was conducted at the participants' homes. The recruitment letter, the consent form, and all data collection instruments were in Slovenian, so that they were fully understood by all the participants.

2.4. Data Analysis. The collected data were analysed using the PASW Statistics 18.0 software (SPSS Inc., IBM, Somers, NY, USA). Descriptive statistics were calculated for all variables and distributions were depicted graphically. Exact Wilcoxon signed-rank test (EWSRT) was used to test the null hypothesis of no change in the dependent variables between the first and the second assessments. In this way, the first two research hypotheses were addressed. In order to test the third research hypothesis, multiple linear regression was used. Three models were built, one for each dependent variable (FIM total score, COPM performance, and COPM satisfaction individual mean score). In each model, the independent variables were the two factors of interest (i.e., diagnosis type and number of ATs), the score at the first assessment (because it was reasonable to believe that the change in the outcome depended on baseline) and participant's age and gender (which also had to be statistically controlled for). Comprehensive regression diagnostics were performed to assure that the assumptions of the model were met. For illustrative purposes only (because the regression models provided proper inference), bivariate association of the number of assistive technologies with the three modelled outcomes were assessed using Spearman rank-correlation (Rho) and depicted using scatter-plots with linear fit.

3. Results

Fifty-nine adult persons with disability participated, 30 men and 29 women. The median age of the participants was 58 years (range 24–81 years). They had different diagnoses; the most frequent diagnosis was amputation of one leg (11 patients, 19%) followed by neuromuscular disease (10 patients, 17%), spinal cord injury (SCI) causing paraplegia (9 patients, 15%), and rheumatic disease or multiple skeletal injury (8 patients, 14%). Other diagnoses included SCI causing tetraplegia, cerebral vascular insult, amputation of one leg or an arm, and cerebral palsy (Figure 2).

For the purpose of further analysis, the diagnoses were divided into two groups: more severe (neuromuscular diseases, spinal cord injury—tetraplegia, and amputation of both legs) and less severe (amputation of one leg, spinal cord injury—paraplegia, multiple skeletal injury and rheumatoid arthritis, cerebral vascular insult, amputation of arm, cerebral palsy, and other). Eighteen participants (31%) belonged to the more severe group and 41 (69%) to the less severe group (Figure 2). In addition to clinical experience, the division was grounded in two established classifications used in the

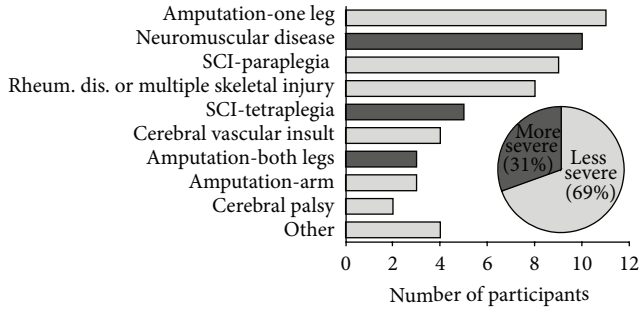

Figure 2: Diagnoses of the participants.

field of rehabilitation that combine medical diagnosis with functional status (FIM score), namely, the Functional Impairment Codes (FIC) and the Australian National Subacute and Nonacute Patient Casemix (AN-SNAP). The key benefit of using the division was that with fewer categories fewer degrees of freedom were spent in the multiple regression models (described further below) applied for testing the third hypothesis, thus making the cases-to-degrees-of-freedom ratio in those models sufficient for a valid analysis.

The number of assistive technologies that the participants used varied from zero (one patient) to five (one patient). The majority of the participants used one (21 patients, 36%) or two assistive technologies (24 patients, 41%). The most frequent assistive technologies were bath and shower seats (used by 31 participants, 53%), grab rails (used by 15 participants, 25%), and adaptations of computer (software and/or hardware; used by 12 participants, 20%).

Three FIM scores were analysed—motor sub-score, cognitive subscore and total score. For each of them, the null hypothesis to be statistically tested was that it would not change between the two assessments. All three scores statistically significantly improved (Table 1 and Figure 3). Median score increased by 15 and 13 points for total and motor FIM, respectively (median increase was 7 points for both). Because of the ceiling effect (the maximum possible score was attained by more than half of the patients already at the first assessment), the median cognitive FIM score could not increase (and median increase was zero), but the change in the score was nevertheless statistically significant and the lower quartile as well as the mean score did increase slightly. The distributions of differences in FIM scores between the two assessments (Figure 4) show that motor and total FIM score decreased in only one participant, and that cognitive FIM score did not decrease in any participant.

The problems identified by the participants through COPM were based on occupational performance areas, namely, self-care (personal care, functional mobility, and community management), productivity (work, household management, play, and school), and leisure (recreation, socializing). The number of identified problems varied from one to five; on average, the participants identified three problems. Barriers in home/work environment were identified as a problem by 41 participants (69%); dependence in performing activities of daily living was identified by 37 participants (63%); and limited mobility was identified as a problem by 30 participants (51%). They also identified problems with computer accessibility (17 participants, 29%), communication (8 participants, 14%), and controlling the home environment (6 participants, 8%).

Like for the three FIM scores, the null hypothesis to be statistically tested for the two COPM scores was that they would not change between the two assessments. At the second assessment the so-called reflective scoring was used, which means that the participants saw their score of each problem from the first assessment and then they scored the same problem taking into account the previous score. Both performance and satisfaction scores clearly and statistically significantly improved (Table 2 and Figure 5; the median and the mean both increased by about 4; the median increase was 3 for performance and 4 for satisfaction). The distributions of differences in COPM individual mean scores between the two assessments (Figure 6) show that neither performance nor satisfaction individual mean score decreased in any participant.

Multiple regression models for progress in the dependent variables were fitted next. Because of the ceiling effect for the cognitive FIM subscore and because a model for the motor FIM subscore would yield practically identical results, only the total FIM score was modelled as a comprehensive measure of independence in functioning. Complete regression diagnostics were performed, which showed that the data did not substantially violate the assumptions in any of the models. In all three models, VIF values were close to 1 and therefore far below the critical value of 5 (or even 10) that would indicate colinearity (last column in Tables 4, 5, and 6); Durbin-Watson statistic was close to 2, thus indicating no serial correlation (Table 3). Distributions of standardised residuals were not markedly skewed and no standardised residual was below −3 or above 3 (nearly all were between −2 and 2), and scatterplots of standardised residuals showed no clear indication of heteroscedasticity (all were approximately band-shaped).

All three models were statistically significant (i.e., the null model of predicting the mean of the dependent variable for all cases was rejected at $P < 0.001$; Table 3). The models explained an estimated 33%, 49%, and 36% of population variance for FIM total score, COPM performance individual mean score, and COPM satisfaction individual mean score, respectively (adjusted R^2 in Table 3). This percentages are quite high given the simplicity of the models (dictated by the limited sample size and available data), which speaks in favour of their validity. On the other hand, it is obvious that a substantial part of variance remains unexplained due to numerous individual and environmental factors that were not assessed and thus not included in the models.

In the model for FIM total score, diagnosis type was a statistically significant predictor ($P = 0.003$; Table 4), while the number of AT was marginally significant ($P = 0.061$; Table 4). The third research hypothesis could therefore be confirmed for FIM total score, whereby the estimated progress for patients in the more severe group was about 8 points less than for those in the less severe group, and for an additional AT the estimated progress was about 2 points larger, both given that all the other parameters in the model

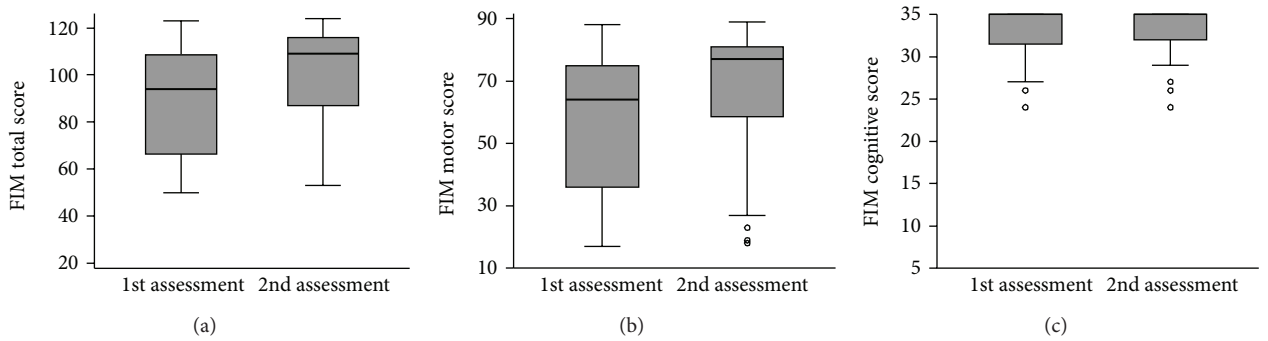

Figure 3: Boxplots of FIM scores at the first and the second assessment (thick line—median; box—interquartile range, IQR; whiskers—values within 1.5 IQR from the 1st and 3rd quartile; circles—outliers).

Table 1: Descriptive statistics and results of statistical tests for FIM scores.

Score	Assessment	Mean (SD)	Median (IQR)	*P* (EWSRT)
FIM total (possible range 18–126)	1st	89.6 (21.3)	94 (61–109)	<0.001
	2nd	100.2 (21.0)	109 (84–116)	
	Difference	10.6 (10.5)	7 (2–15)	
FIM motor (possible range 13–91)	1st	56.7 (21.3)	64 (34–75)	<0.001
	2nd	66.9 (21.0)	77 (57–81)	
	Difference	10.2 (10.3)	7 (2–15)	
FIM cognitive (possible range 5–35)	1st	32.9 (2.9)	35 (31–35)	0.004
	2nd	33.3 (2.6)	35 (32–35)	
	Difference	0.4 (1.1)	0 (0-0)	

IQR: interquartile range; EWSRT: exact Wilcoxon signed-rank test; difference = value at 2nd assessment − value at 1st assessment.

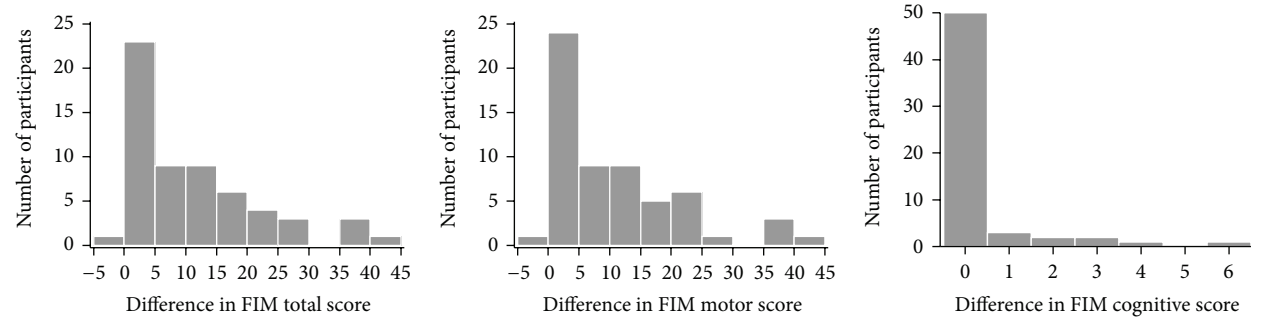

Figure 4: Distribution of differences in FIM scores between the first and the second assessment (histograms for total and motor score, bar chart for cognitive score).

Table 2: Descriptive statistics and results of statistical tests for COPM individual mean scores.

COPM	Assessment	Mean (SD)	Median (IQR)	*P* (EWSRT)
Performance (possible range 1–10)	1st	3.5 (1.9)	3.5 (1.7–4.8)	<0.001
	2nd	7.1 (2.0)	5.7 (7.3–9.0)	
	Difference	3.6 (2.7)	3.0 (1.5–5.3)	
Satisfaction (possible range 1–10)	1st	2.9 (1.8)	1.3 (2.7–3.7)	<0.001
	2nd	7.2 (2.2)	5.2 (7.5–9.0)	
	Difference	4.3 (2.6)	4.0 (2.0–5.7)	

IQR: interquartile range; EWSRT: exact Wilcoxon signed-rank test; difference = value at 2nd assessment − value at 1st assessment.

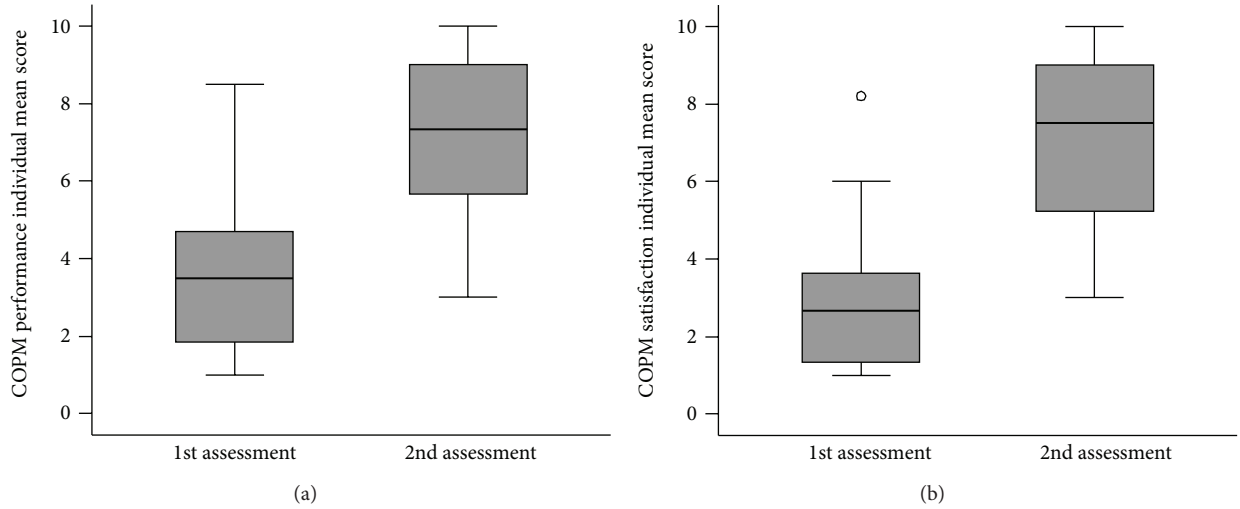

Figure 5: Box plots of COPM individual mean scores at the first and the second assessments (thick line—median; box—IQR: interquartile range, whiskers—values within 1.5 IQR from the 1st and 3rd quartile; circles—outliers).

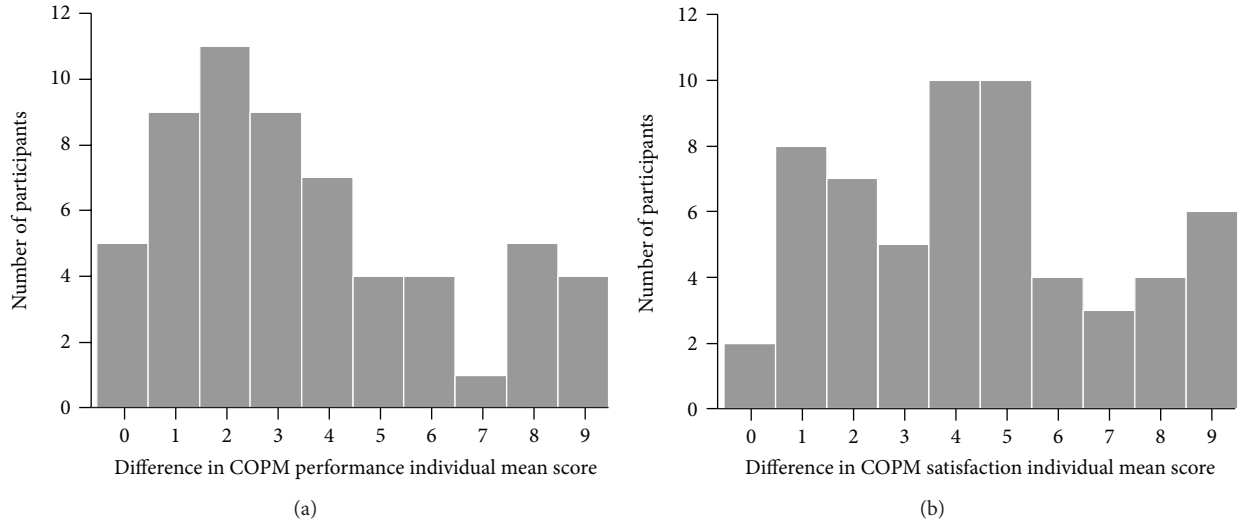

Figure 6: Distribution of differences in COPM individual mean scores between the first and the second assessment (bar charts of rounded values).

were held constant. The statistical significance of the baseline score ($P = 0.001$) is at least partly spurious, that is, artefact, because the difference score and either of its components are correlated by definition, so it should not be over-interpreted and only serves to adjust the patients' progress for the differences in initial functional independence.

The two models for COPM individual mean scores gave essentially equivalent results (Tables 5 and 6). In neither of the models for progress in COPM, diagnosis type was a statistically significant predictor ($P = 0.147$ and $P = 0.439$ for performance and satisfaction, resp.), whereby the estimated regression coefficient was negative (i.e., less progress predicted for the more severe group) as expected in both models. Because the number of ATs was statistically significant in both models ($P = 0.012$ and $P = 0.022$ for performance and satisfaction, resp., with expected progress about 0.7 points larger per additional AT for both outcomes), the third research hypothesis can therefore be at least partly confirmed for COPM scores as well. On a minor note, unlike in the model for FIM score, age was not a statistically significant predictor ($P = 0.936$ and $P = 0.754$), while there was a (nearly) statistically significant gender difference (with higher progress predicted for men) in both COPM models ($P = 0.034$ for performance; $P = 0.071$ for satisfaction). Like the finding regarding age for FIM progress, interpretation of gender difference in COPM progress is difficult and outside the scope of the present research. The same goes for the effect of the baseline score (for the reason outlined in the case of FIM), which was further inflated in case of COPM by the reflective scoring procedure (i.e., the patients seeing their scores at the first assessment during the second assessment), so the largest estimated standardised regression should not be

Table 3: Summary of multiple regression models.

Dependent variable	Adj. R^2	P (ANOVA)	Durbin-Watson
Change in FIM total score	0.325	<0.001	1.913
Change in COPM performance individual mean score	0.489	<0.001	2.432
Change in COPM satisfaction individual mean score	0.360	<0.001	2.688

Adj. R^2: adjusted coefficient of determination; P (ANOVA): statistical significance of the model as a whole; Durbin-Watson statistic: diagnostics of serial correlation.

Table 4: Parameter estimates and regression diagnostics of colinearity for multiple linear regression model of change in total FIM score.

Predictor	b	β	P	VIF
Constant	19.646		0.021	
Gender (male versus female)	0.559	0.027	0.816	1.141
Age (years)	0.244	0.352	0.002	1.030
FIM total score at 1st assessment	0.187	0.381	0.001	1.088
Diagnosis type (more versus less severe)	−8.267	−0.366	0.003	1.192
Number of assistive technologies	2.245	0.208	0.061	1.011

b: regression coefficient; β: standardised regression coefficient; VIF: variance inflation factor.

interpreted in terms of relative predictor importance or even causality.

Finally, only for clarification and illustration, bivariate (i.e., unadjusted) analysis of association of the number of ATs with the change scores was performed. The scatter plots with fitted regression lines (Figure 7) and the Spearman correlation coefficients (Rho = 0.328 for change in FIM total score, $P = 0.011$; Rho = 0.424 for change in COPM performance individual mean score, $P = 0.001$; and Rho = 0.387 for change in COPM satisfaction individual mean score; $P = 0.002$) agree with the finding from the regression models that the more ATs a patient uses, the more progress can be expected from him or her. The association is far from perfect, but it is clear especially for the two COPM scores.

4. Discussion

The aim of this study was to evaluate the treatments in the Smart Home IRIS in terms of their effect on occupational performance and functional independence of the treated persons. Three research hypotheses were addressed.

The first hypothesis stated that use of ATs and home modification has impact on increased functional independence for participants who have been treated in Smart Home IRIS. After the second assessment the participants showed a statistically significant improvement in all three

Table 5: Parameter estimates and regression diagnostics of colinearity for multiple linear regression model of change in COPM performance individual mean score.

Predictor	b	β	P	VIF
Constant	4.186		0.006	
Gender (male versus female)	1.174	0.221	0.034	1.168
Age (years)	−0.001	−0.008	0.936	1.031
COPM performance at 1st assessment	−0.757	−0.534	<0.001	1.118
Diagnosis type (more versus less severe)	−0.848	−0.147	0.147	1.126
Number of assistive technologies	0.697	0.252	0.012	1.064

b: regression coefficient; β: standardised regression coefficient; VIF: variance inflation factor.

Table 6: Parameter estimates and regression diagnostics of colinearity for multiple linear regression model of change in COPM satisfaction individual mean score.

Predictor	b	β	P	VIF
Constant	4.236		0.012	
Gender (male versus female)	1.089	0.208	0.071	1.154
Age (years)	−0.006	−0.034	0.754	1.035
COPM satisfaction at 1st assessment	−0.683	−0.454	<0.001	1.140
Diagnosis type (more versus less severe)	−0.498	−0.088	0.439	1.145
Number of assistive technologies	0.696	0.256	0.022	1.076

b: regression coefficient; β: standardised regression coefficient; VIF: variance inflation factor.

FIM scores—total ($P < 0.001$), motor ($P < 0.001$) and cognitive ($P = 0.004$). Though clearly beyond what would could be expected by chance (i.e., due to sampling error), the cognitive FIM could not increase much because of the ceiling effect (maximum possible score was attained by more than half of the patients already at the first assessment). Nevertheless, the increase in median score by 15 and 13 points for the total and the motor FIM, respectively, leaves no doubt that the observed improvement was substantial. In addition, the motor and the total FIM score decreased in only one participant, and the cognitive FIM score did not decrease in any participant. These findings indicate that the participants achieved a higher level of functional independence at the second assessment than at the first assessment. Hence, the first research hypothesis was supported, even though the causal link with the treatment in Smart Home IRIS cannot be firmly established because of the lack of a control group or other means to eliminate (or subtract) the possible effect of other factors.

The second hypothesis stated that the use of ATs and home modification has impact on occupational performance and satisfaction with occupational performance, which was

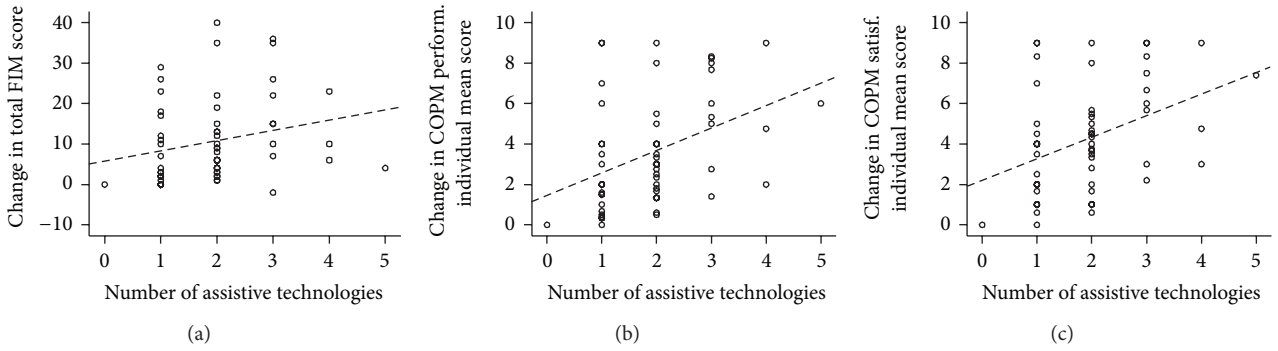

Figure 7: Scatter plots with linear regression lines (dashed; for illustrative purposes only) depicting association of the number of assistive technologies with progress in the outcome measures.

assessed using the COPM. At the second assessment, both the individual mean performance scores and the individual mean satisfaction scores were statistically significantly higher than at the first assessment ($P < 0.001$). The results also showed that neither performance nor satisfaction individual mean score decreased in any participant, which is very important for participants with progressive diseases (such as neuromuscular diseases). These findings are consistent with the findings of the previous studies [24–26]. The second hypothesis was therefore also supported, subject to the same cautionary note regarding causal interpretation as the first hypothesis.

The third hypothesis addressed the differences in progress with regard to the participant's characteristics, focusing on the diagnosis and the number of ATs while controlling for the possible confounding effect of gender, age, and score at the first assessment. Regarding functional independence, the difference with regard to diagnosis type (i.e., the difference between more severe diagnoses, namely, neuromuscular diseases, spinal cord injury causing tetraplegia, and amputation of both legs, and less severe diagnoses) appeared to be more certain ($P = 0.003$) than the positive effect of the number of ATs ($P = 0.061$). The opposite was observed with COPM individual mean scores: the difference with respect to diagnosis type was not statistically significant ($P = 0.147$ and $P = 0.439$ for performance and satisfaction, resp.) though it was in the same direction of more expected progress with less severe diagnoses, whereas the positive effect of the number of ATs was statistically significant in both models ($P = 0.012$ and $P = 0.022$). Nevertheless, the overall picture was the same and agreed with the third research hypothesis.

As already stressed, the association of the baseline score (i.e., at the first assessment) with the progress (i.e., the difference between the second and the first assessment) should not be overinterpreted because of purely mathematical reasons. In addition, the association may not be entirely related with the use of ATs but also with other factors, such as supplementary rehabilitation, concomitant health problems, and natural disease progress. Furthermore, as also already stressed regarding the two COPM scores, the effect of the baseline score status may be overestimated because of the reflective scoring procedure.

There are also other notable limitations to our study. We only considered the number of ATs in the statistical models, thus not taking into account the differences in the impact that a specific AT can have on functional independence. Having more devices does not necessarily lead to increased independence or satisfaction, because the change in independence is based on the match between the AT and the individual's needs, as well as on the degree to which the individual perceives that as leading to more independence. Hence, the distinction between useful ATs and those that are less may be blurred to some extent, which may also be reflected in the less evident positive statistical effect noted for the number of ATs.

It should also be noted that in addition to the number of ATs that a patients possesses and their appropriateness, better occupational performance and higher satisfaction with performance are impacted by the time of application of the ATs prescribed by the occupational therapist or other health care professionals. Appropriate ATs should be provided at the right time, considering the context, activity demands, and client factors (e.g., nature and prognosis of disease/disability) [27]. Late application of ATs leads to less effective usage or abandonment of the prescribed ATs [28]. Another important factor is the way of prescribing ATs, whereby each AT should be recommended and prescribed using a client-centred approach [29]. The present study does not directly assess timeliness of AT provision, though it does underline the need for individual and client-centred approach by occupational therapists and other health professionals who prescribe AT.

As already noted, the treatment in Smart Home IRIS cannot be firmly causally linked with the observed improvements, so a further limitation of our study is that it provides no evidence that factors which were not studied—such as capability of home care staff, specific AT factors (reliability/malfunctions and appropriateness with regard to the consumer's needs), and suitability of home environment—were not important in achieving the observed changes in functional independence, performance, and satisfaction with performance.

Finally, our choice of FIM as the measure of functional independence when using ATs and home modifications is also open to debate. It is not possible to obtain the highest score of 7 (i.e., attain the highest level of independence)

on several FIM items from the motor subscale (and hence attain the highest possible motor and total score) if assistive technology is used. Moreover, the FIM is primarily a medical assessment tool not aimed at AT evaluation. Measures such as the Psychosocial Impact of Assistive Devices Scale (PIADS) and Quebec User Evaluation of Satisfaction with Assistive Technology (QUEST) might have been used, which have demonstrated reliability and validity and have been used in evaluating the outcomes of AT interventions [30–32]. However, they have not been adapted for Slovenian language and environment yet, whereas the use of FIM has a relatively long tradition and the years of mandatory assessment of every rehabilitation inpatient at the University Rehabilitation Institute in Ljubljana, accompanied by extensive statistical analyses, vouch for the highest possible level of validity and reliability of the assessment procedure [33, 34].

5. Conclusions

The results showed that the use of assistive technologies and home modifications appears to have impact on increased functional independence and better performance and satisfaction. In addition, it was shown that progress differs with respect to the person's diagnosis and the number of assistive technologies he or she uses.

The findings obtained from the present study are important for Slovenian rehabilitation medicine and all health care professionals who work in the field of provision with assistive technologies in Slovenia. We attempted to fill the gap regarding the evidence on effectiveness of a smart home and our results suggest that the persons who use assistive technologies and home modifications may benefit from the treatment in Smart Home IRIS.

As the development of assistive technologies and smart home technologies is spreading, and rehabilitation professionals over the world are becoming aware of the benefits of assistive technologies, continued research in this area is essential. Further high-quality outcome studies, such as randomised controlled trials and longitudinal studies, would be beneficial. It would also be interesting to know whether using assistive technologies and home modifications for a longer period of time (at least for two years) results in long-term improvement.

Conflict of Interests

The authors declare that there is no conflict of interests regarding the publication of this paper.

References

[1] A. Zupan, R. Cugelj, and F. Hočevar, "Dom IRIS Smart Home," *Quark Magazine*, pp. 132–144, 2008.

[2] M. Law, S. Baptiste, A. Carswell, M. A. McColl, H. Polatajko, and N. Pollock, *The Canadian Occupational Performance Measure*, CAOT Publications ACE, Ottawa, Canada, 4th edition, 2005.

[3] J. Ocepek, M. Jenko, G. Vidmar, and A. Zupan, "Role of smart home IRIS in rehabilitation in Slovenia—findings from the user survey," *Informatica Medica Slovenica*, vol. 16, no. 2, pp. 1–5, 2011.

[4] C. V. Granger and G. E. Gresham, *Functional Assessment in Rehabilitation Medicine*, Williams & Wilkins, Baltimore, Md, USA, 1984.

[5] T. Sumsion, Ed., *Client-Centred Practice in Occupational Therapy. A Guide to Implementation*, Churchill Livingstone, Edinburgh, UK, 2nd edition, 2006.

[6] A. Carswell, M. A. McColl, S. Baptiste, M. Law, H. Polatajko, and N. Pollock, "The Canadian Occupational Performance Measure: a research and clinical literature review," *Canadian Journal of Occupational Therapy*, vol. 71, no. 4, pp. 210–222, 2004.

[7] A. Atwal, S. Owen, and R. Davies, "Struggling for occupational satisfaction: older people in care homes," *British Journal of Occupational Therapy*, vol. 66, no. 3, pp. 118–124, 2003.

[8] T. Lyons and P. Raghavendra, "Therapists' view on the usability of Canadian Occupational Performance Measure for an early intervention group by a multi-disciplinary team: a pilot study," *Australian Occupational Therapy Journal*, vol. 51, no. 2, 2003.

[9] C. Chesworth, R. Duffy, J. Hodnett, and A. Knight, "Measuring clinical effectiveness in mental health: is the Canadian occupational performance an appropriate measure?" *British Journal of Occupational Therapy*, vol. 65, no. 1, pp. 30–34, 2002.

[10] E. H. C. Cup, W. J. M. Scholte op Reimer, M. C. E. Thijssen, and M. A. H. van Kuyk-Minis, "Reliability and validity of the Canadian occupational performance measure in stroke patients," *Clinical Rehabilitation*, vol. 17, no. 4, pp. 402–409, 2003.

[11] A.-W. Pan, L. Chung, and G. Hsin-Hwei, "Reliability and validity of the Canadian Occupational Performance Measure for clients with psychiatric disorders in Taiwan," *Occupational Therapy International*, vol. 10, no. 4, pp. 269–277, 2003.

[12] L. Sewell and S. J. Singh, "The Canadian Occupational Performance Measure: is it a reliable measure in clients with chronic obstructive pulmonary disease?" *British Journal of Occupational Therapy*, vol. 64, no. 6, pp. 305–310, 2001.

[13] L. Carpenter, G. A. Baker, and B. Tyldesley, "The use of the Canadian occupational performance measure as an outcome of a pain management program," *Canadian Journal of Occupational Therapy*, vol. 68, no. 1, pp. 16–22, 2001.

[14] G. Boyer, R. Hachey, and C. Mercier, "Perceptions of occupational performance and subjective quality of life in persons with severe mental illness," *Occupational Therapy in Mental Health*, vol. 15, no. 2, pp. 1–15, 2000.

[15] M. A. McColl, M. Paterson, D. Davies, L. Doubt, and M. Law, "Validity and community utility of the Canadian Occupational Performance Measure," *Canadian Journal of Occupational Therapy*, vol. 67, no. 1, pp. 22–29, 2000.

[16] I. C. J. M. Eyssen, A. Beelen, C. Dedding, M. Cardol, and J. Dekker, "The reproducibility of the Canadian Occupational Performance Measure," *Clinical Rehabilitation*, vol. 19, no. 8, pp. 888–894, 2005.

[17] M. E. Cohen and R. J. Marino, "The tools of disability outcomes research functional status measures," *Archives of Physical Medicine and Rehabilitation*, vol. 81, no. 12, pp. S21–S29, 2000.

[18] M. Invernizzi, S. Carda, P. Milani et al., "Development and validation of the Italian version of the Spinal Cord Independence Measure III," *Disability and Rehabilitation*, vol. 32, no. 14, pp. 1194–1203, 2010.

[19] M. G. Stineman, R. N. Ross, S. V. Williams, J. E. Goin, and C. V. Granger, "A functional diagnostic complexity index for rehabilitation medicine: measuring the influence of many diagnoses on

functional independence and resource use," *Archives of Physical Medicine and Rehabilitation*, vol. 81, no. 5, pp. 549–557, 2000.

[20] Y. Young, M.-Y. Fan, J. R. Hebel, and C. Boult, "Concurrent validity of administering the functional independence measure (FIM) instrument by interview," *American Journal of Physical Medicine & Rehabilitation*, vol. 88, no. 9, pp. 766–770, 2009.

[21] J. M. Linacre, A. W. Heinemann, B. D. Wright, C. V. Granger, and B. B. Hamilton, "The structure and stability of the functional independence measure," *Archives of Physical Medicine and Rehabilitation*, vol. 75, no. 2, pp. 127–132, 1994.

[22] "Statistical Office of the Republic of Slovenia," Rapid Reports 15, 2010, http://www.stat.si/doc/statinf/05-si-007-1001.pdf.

[23] M. F. Folstein, S. E. Folstein, and P. R. McHugh, "Mini-Mental State: a practical method for grading the cognitive state of patients for the clinician," *Journal of Psychiatric Research*, vol. 12, pp. 189–198, 1975.

[24] I.-L. Boman, K. Tham, A. Granqvist, A. Bartfai, and H. Hemmingsson, "Using electronic aids to daily living after acquired brain injury: a study of the learning process and the usability," *Disability and Rehabilitation*, vol. 2, no. 1, pp. 23–33, 2007.

[25] J. Ripat, "Function and impact of electronic aids to daily living for experienced users," *Technology and Disability*, vol. 18, no. 2, pp. 79–87, 2006.

[26] L. S. Petty, L. McArthur, and J. Treviranus, "Clinical report: use of the Canadian Occupational Performance Measure in vision technology," *Canadian Journal of Occupational Therapy*, vol. 72, no. 5, pp. 309–312, 2005.

[27] D. J. Wilson, J. M. Mitchell, B. J. Kemp, R. H. Adkins, and W. Mann, "Effects of assistive technology on functional decline in people aging with a disability," *Assistive Technology*, vol. 21, no. 4, pp. 208–217, 2009.

[28] I. G. de Boer, A. Peeters, H. K. Ronday, B. J. A. Mertens, F. C. Breedveld, and T. P. M. Vliet Vlieland, "The usage of functional wrist orthoses in patients with rheumatoid arthritis," *Disability and Rehabilitation*, vol. 30, no. 4, pp. 286–295, 2008.

[29] T. Wielandt, K. McKenna, L. Tooth, and J. Strong, "Factors that predict the post-discharge use of recommended assistive technology (AT)," *Disability and Rehabilitation*, vol. 1, no. 1-2, pp. 29–40, 2006.

[30] L. Demers, M. Monette, M. Descent, J. Jutai, and C. Wolfson, "The psychosocial impact of assistive devices scale (PIADS): translation and preliminary psychometric evaluation of a Canadian-French version," *Quality of Life Research*, vol. 11, no. 6, pp. 583–592, 2002.

[31] L. Demers, R. Weiss-Lambrou, and B. Ska, "The Quebec User Evaluation of Satisfaction with Assistive Technology (QUEST 2.0): an overview and recent progress," *Technology and Disability*, vol. 14, no. 3, pp. 101–105, 2002.

[32] H.-F. Mao, W.-Y. Chen, G. Yao, S.-L. Huang, C.-C. Lin, and W.-N. W. Huang, "Cross-cultural adaptation and validation of the Quebec User Evaluation of Satisfaction with Assistive Technology (QUEST 2.0): the development of the Taiwanese version," *Clinical Rehabilitation*, vol. 24, no. 5, pp. 412–421, 2010.

[33] G. Vidmar, H. Burger, Č. Marinček, and R. Cugelj, "Analysis of data on assessment with the functional independent measure at the institute for rehabilitation, Republic of Slovenia," *Informatica Medica Slovenica*, vol. 13, no. 1, pp. 21–32, 2008.

[34] G. Vidmar, H. Burger, and Č. Marinček, "Time trends in ability level and functional outcome of stroke and multiple sclerosis patients undergoing comprehensive rehabilitation in slovenia," *Zdravstveno Varstvo*, vol. 50, no. 1, pp. 24–33, 2011.

Hindawi Publishing Corporation
Computational and Mathematical Methods in Medicine
Volume 2013, Article ID 895492, 12 pages
http://dx.doi.org/10.1155/2013/895492

Research Article

Haptic-Based Neurorehabilitation in Poststroke Patients: A Feasibility Prospective Multicentre Trial for Robotics Hand Rehabilitation

Andrea Turolla,[1,2] Omar A. Daud Albasini,[3] Roberto Oboe,[1,4] Michela Agostini,[1] Paolo Tonin,[1] Stefano Paolucci,[5] Giorgio Sandrini,[6] Annalena Venneri,[1,2] and Lamberto Piron[1]

[1] *Laboratory of Kinematics and Robotics, Fondazione IRCCS, Ospedale San Camillo, Via Alberoni, Venezia Lido, 30126 Venice, Italy*
[2] *Department of Neuroscience, University of Sheffield and Sheffield Teaching Hospital NHS Foundation Trust, Beech Hill Road, S10 2RX, Sheffield, UK*
[3] *AMTC, Universidad de Chile, Avenida Tupper 2007, Edificio AMTC, Santiago, Chile*
[4] *Dipartimento di Tecnica e Gestione dei Sistemi Industriali, Università di Padova Stradella S. Nicola, 36100 Vicenza, Italy*
[5] *Movement and Brain Laboratory, U.O.F. IRCCS Santa Lucia Foundation, Via Ardeatina, 00142 Rome, Italy*
[6] *IRCCS Casimiro Mondino Institute of Neurology Foundation, University of Pavia, Via Mondino, 27100 Pavia, Italy*

Correspondence should be addressed to Andrea Turolla; andrea.turolla@ospedalesancamillo.net

Received 17 July 2013; Accepted 11 September 2013

Academic Editor: Imre Cikajlo

Background. Haptic robots allow the exploitation of known motor learning mechanisms, representing a valuable option for motor treatment after stroke. The aim of this feasibility multicentre study was to test the clinical efficacy of a haptic prototype, for the recovery of hand function after stroke. *Methods*. A prospective pilot clinical trial was planned on 15 consecutive patients enrolled in 3 rehabilitation centre in Italy. All the framework features of the haptic robot (e.g., control loop, external communication, and graphic rendering for virtual reality) were implemented into a real-time MATLAB/Simulink environment, controlling a five-bar linkage able to provide forces up to 20 [N] at the end effector, used for finger and hand rehabilitation therapies. Clinical (i.e., Fugl-Meyer upper extremity scale; nine hold pegboard test) and kinematics (i.e., time; velocity; jerk metric; normalized jerk of standard movements) outcomes were assessed before and after treatment to detect changes in patients' motor performance. Reorganization of cortical activation was detected in one patient by fMRI. *Results and Conclusions*. All patients showed significant improvements in both clinical and kinematic outcomes. Additionally, fMRI results suggest that the proposed approach may promote a better cortical activation in the brain.

1. Background

Hand and finger dexterities are fundamental for many activities carried out by a person in order to be independent. Stroke can reduce motor function due to the resulting death of associated brain cells. Stroke leads to permanent neurological impairment in at least 12.6 million people worldwide [1, 2], and in up to 75% of the subjects, motor deficits involve the upper limb [3]. Nowadays, almost all the activities that deal with physical therapy and training tools for rehabilitation have focused on relearning movements of the abilities that the patients had stroke before. Currently, traditional rehabilitative interventions are mainly focused on the passive facilitation of isolated movements or on the promotion of alternative movements to those used before motor diseases [4, 5]. These need to emerge as a consequence of the increasing incidence of stroke patients and the related costs associated to rehabilitation care.

Recent findings from movement neuroscience demonstrated that the human neuromuscular system presents use-dependent plasticity, intended as changes in the pattern of neurons' connectivity [6], not only in healthy but also

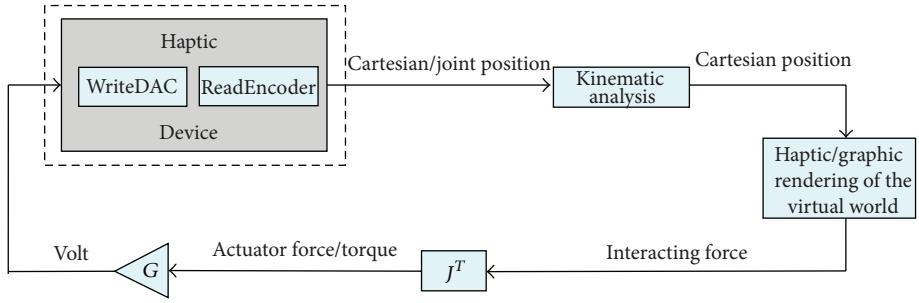

Figure 1: General framework architecture.

in neurologically diseased patients, so poststroke patients can experience significant benefits if treated with intensive rehabilitation sessions based on neurophysiologic learning principles [7]. Usually, robotic rehabilitation devices provide passive movement to the patient's arm; however, the use of haptics (i.e., manipulators able to provide force feedbacks), interfaced to VR environments, are becoming a common approach, as they allow intensive, frequent, and repetitive interactive exercise, more coherent with the principles of motor learning. Virtual-reality-based haptic rehabilitation is conceived as the interaction between a haptic device, which consists of a specific manipulator, and a virtual environment [8]. Indeed, a haptic interface enables the patient to move and interact with virtual objects inside a virtual space; hence, a correspondence between the end-effector of the haptic display and a virtual object (avatar) inside the virtual world is verified [9]. This avatar interacts with other virtual objects and the interaction force arising during contacts depends on the "penetration" the avatar performs on the other virtual objects, under a viscoelastic behaviour. As a VR-based application for rehabilitation, static objects are enough for representing the virtual environment [10]. In turn, the interaction force in the virtual environment is reproduced by the haptic device, so the patient receives a force response to his/her motion. This allows the patient to interact with different types of objects, which may have different kinds of properties [11, 12]. Several haptic robots for rehabilitation were developed and tested, such as the MIT-Manus [13, 14], the Mirror Image Movement Enabler (MIME) [15], the ARM-Guide [16], and the BiManu-Track [17].

The design of an effective haptic interface for rehabilitation is often a trial and error procedure and even a small change in the operating scenario or the addition of new features may require large modifications in hardware and software to better respond to the patient's needs. In our prototype the VR-based rehabilitation was conceived as the interaction through a haptic device (i.e., manipulator) with a virtual environment under a viscoelastic behaviour, with interaction forces depending on the "penetration" the avatar performs on the other virtual objects, allowing the patient to perform different motor tasks with different types of objects. Hence, the use of haptic-based therapy highly contributes to regain the mobility that was lost, while for therapists and doctors, this type of computer-based system is an efficient measurement tool, in which the kinematic outcomes for finger and hand rehabilitation (e.g., execution time, trajectory, velocity, and jerk) are accurately evaluated.

In order to merge known benefits of specific stimulation provided by VR and haptics devices, a general framework for virtual-reality- (VR-) based rehabilitation was developed, in which custom designed haptic devices could be easily plugged into the VR rehabilitation environment.

The aim of this study was to evaluate the efficacy of the proposed technological solution for the rehabilitation of hand and fingers motor function in poststroke patients. A feasibility prospective multicentre trial was conducted within a research project supported by the Italian Ministry of Health in three neurorehabilitation hospitals, respectively: Foundation San Camillo Hospital (Venice), Neurological National Institute Foundation "C. Mondino" (Pavia), and Foundation "Santa Lucia" (Rome).

2. Material and Methods

2.1. Patients. In each hospital, five consecutive stroke patients were enrolled according to the following inclusion criteria: affected by a single ischemic stroke in the region of the middle cerebral artery (MCA) at least six months before the entry; conventional physical therapy treatment received in the early period after stroke; and mild to intermediate motor impairment of the arm (defined as a Box and Blocks Test <45). Clinical history or evidence of memory impairment, neglect, apraxia, or aphasia interfering with verbal comprehension and treated depression were considered as exclusion criteria.

2.2. General Framework for VR-Based Haptic Rehabilitation. The haptic interface consists of a computer (e.g., a PC), a virtual reality engine, a data acquisition board, motor drivers, and a mechanism that constitutes the manipulated part of the haptic device. As shown in Figure 1, the positions (usually joint angles) of the haptic device are acquired via data acquisition board and converted into real world coordinates of the end effector, using a forward kinematic model. Such coordinates are then passed to the VR engine, which is in charge of displaying the exercises on the computer screen and computing the interaction force between the avatar and the virtual objects. The computed force is then converted into force/torque references to the actuators, using the Jacobian matrix of the mechanism, which is obtained by computing

the relation between the joint rates and the linear and angular velocity of the end-effector [18].

A general framework is developed in order to achieve the interaction described above. The proposed architecture is implemented inside MATLAB/Simulink. Every block of Figure 1, except the haptic/graphic rendering block, has an S-function associated with it. The VR engine can be selected among many available in the market. For this particular implementation, we chose the Handshake proSENSE Toolbox for haptic and graphic rendering [19]. In a nutshell, the Handshake proSENSE Toolbox adds haptic rendering to standard VRML-based environments. As a MATLAB/Simulink-based product, it works in a drag-and-drop fashion, thus, allowing even untrained users (e.g., doctors and therapists) to quickly develop and test models, and to do on-the-fly modifications on both, virtual environment and exercises, depending on the requirements and performances of the patient. Such general purpose framework achieves two important objectives.

(1) Hardware-independent solution: any modification on the hardware implies only minor parameter modifications on the software, mainly the ones related to the Jacobian matrix and the digital and analog channels that are used. This guarantees a fast and easy implementation of any new device, which better fits to some patient's condition and rehabilitation.

(2) Online modifications of the elements in the virtual environment: the exercises can be designed in order to fit the requirements and performances of the patient under analysis.

In turn, the proposed framework guarantees a fast and easy implementation for different types of devices, which must handle the corresponding settings and configurations, depending on the type of therapies to be implemented.

Additionally, it provides the haptic and graphic rendering, as well as the control algorithm of the five-bar linkage mechanism, and the external communication with the actuators; these features guarantee a real-time system.

The haptic interface implemented in the proposed framework is based on a PC running Microsoft Operating System (Windows XP), with a data acquisition card (Sensoray Model 626 PCI Multifunction I/O Board) that provides the interface to a five-bar linkage haptic device (detailed later), moved by two AC brushless servo motors (Mavilor Motors Model BLS-74) with the relative motor drivers (Infranor CD1-a). The setup and the prototype are shown in Figure 2. The software for controlling the haptic interface was completely developed within MATLAB/Simulink as a real-time application. The external communication to the acquisition board was implemented as an S-function, as well as the kinematic analysis for solving the mechanism, and the calculation of the transpose Jacobian matrix. The visual and haptic feedbacks were implemented using the Handshake proSENSE Toolbox.

The considerations for the design of the haptic device are focused on the implementation of a single finger haptic display, in which the force is exerted at the fingertip. Herein, all possible movements of each articulation that belongs to the finger are taken into account, along with the reachable

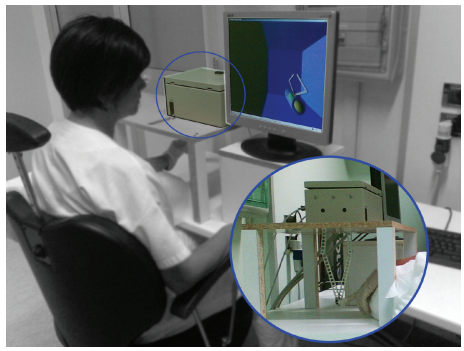

Figure 2: Haptic interface setup. The setup considers a PC with a control algorithm, a VR environment with graphic and haptic rendering, and a five-bar linkage mechanism with finger holder.

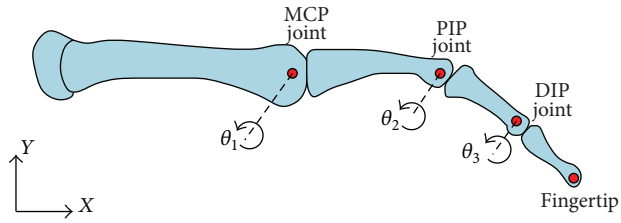

Figure 3: Planar skeletal model of the human finger.

Table 1: Finger joint motion ranges.

Finger joint	Angular motion range (degrees)	Link size (mm)
MCP	$-90 \le \theta_1 \le 45$	48.3
PIP	$-120 \le \theta_2 \le 0$	28.2
DIP	$-90 \le \theta_3 \le 50$	19.1

MCP: metacarpophalangeal; PIP: proximal interphalangeal; DIP: distal interphalangeal.

workspace of the finger itself. Therefore, this workspace must fit inside the workspace of the haptic device. The design is based on a male index finger (see Figure 3). The average dimensions of the finger were considered and a set of admissible movements (Table 1). This information was derived from the literature and based on statistical data [20].

The chosen mechanism was a five-bar linkage, where one bar is fixed to the frame, and the two cranks, fixed to the frame, are considered the moving members. The proposed mechanism has two active DOF and three passive DOF (rotations) at the fingertip. In this particular case, the driven joints are actuated by AC brushless motors, in which the maximum torque available is 3.4 [N-m], which corresponds to a force of 20 [N] at the fingertip. Each motor has an incremental encoder with a resolution of 32768 pulses per revolution, for which the manipulator position resolution is 0.022 [mm]. The design of the proposed mechanism was based on these three factors.

(i) The haptic device workspace must cover the whole reachable workspace of an average male's index finger.

(ii) Low inertia.

(iii) High performance.

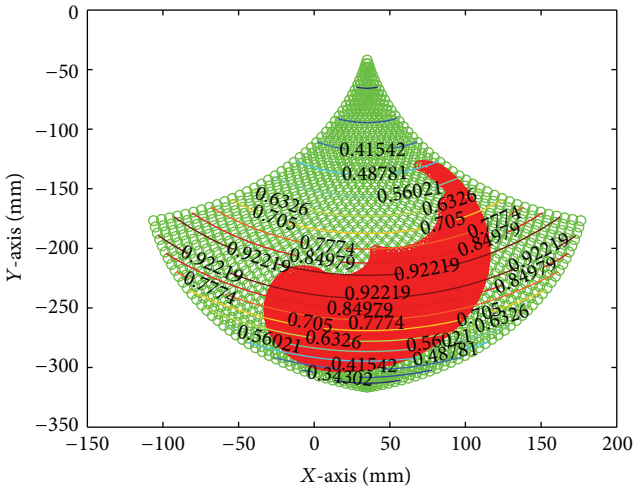

FIGURE 4: Reachable finger workspace, five-bar linkage workspace and ISO values.

The performance analysis is based on the evaluation of the mechanism isotropy (ISO), defined as follows:

$$\mu = \frac{\sigma_{\min}\left(J\left(\Theta\right)\right)}{\sigma_{\max}\left(J\left(\Theta\right)\right)}, \tag{1}$$

where $\sigma_{\min}$ and $\sigma_{\max}$ are the minimum and maximum singular value decomposition values of the Jacobian matrix $J(\Theta)$ that describes the five-bar linkage mechanism, respectively. Notice that $\Theta = [\theta_1, \theta_2, \theta_3, \theta_4]^T$. The mechanism isotropy is a function of the joint angles Θ and the value goes from 0 to 1. An ISO value of 0 means the mechanism is in a singular configuration. A typical singular configuration of the five-bar mechanism is obtained when the links are fully stretched. An ISO value of 1 means maximum performance, which also means that the mechanism can move equally well in all directions.

Link lengths were determined by maximizing the mechanism isotropy and by finding the best fitting between the average male's index finger workspace and the haptic device workspace. As a result, under normal conditions, which mean that the finger's motion is without obstacles and/or any load applied on it, the reachable workspace of a single finger is completely covered by the reachable workspace of the mechanism (link length [mm]: $L_1 = 140$; $L_2 = 180$; $L_3 = 180$; $L_4 = 140$; $L_5 = 70$) with ISO values always higher than 0.4 (i.e., good preservation of free movements in all directions) across the whole workspace, as shown in Figure 4.

In order to determine the end-effector position of the mechanism, forward kinematic analysis has to be done [18]. The angular positions θ_1 and θ_4 are known parameters because they can be read from the encoders that come with the AC brushless motors. The end-effector position of the haptic device is determined with respect to the origin of the x-y axis, which is placed in $P_1(x_1, y_1)$. Forward kinematics and force analysis are based on Figure 5. The Cartesian position $P(x_{ef}, y_{ef})$ of the end-effector of the device is as follows:

$$\begin{aligned} x_{ef} &= L_1 \cos\left(\theta_1\right) + L_2 \cos\left(\theta_2\right), \\ y_{ef} &= L_1 \sin\left(\theta_1\right) + L_2 \sin\left(\theta_2\right). \end{aligned} \tag{2}$$

The Jacobian matrix of the mechanism is defined as follows:

$$\begin{aligned} J\left(\Theta\right) &= \begin{bmatrix} a_{11} & a_{12} \\ a_{21} & a_{22} \end{bmatrix}, \\ a_{11} &= -\frac{1}{2}\frac{L_1\left(\cos\left(-\theta_2+\theta_1-\theta_3\right)-\cos\left(-\theta_2+\theta_1+\theta_3\right)\right)}{\sin\left(\theta_2-\theta_3\right)}, \\ a_{12} &= \frac{1}{2}\frac{L_4\left(\cos\left(\theta_2+\theta_3-\theta_4\right)-\cos\left(\theta_2-\theta_3+\theta_4\right)\right)}{\sin\left(\theta_2-\theta_3\right)}, \\ a_{21} &= \frac{1}{2}\frac{L_1\left(\sin\left(-\theta_2+\theta_1-\theta_3\right)+\sin\left(-\theta_2+\theta_1+\theta_3\right)\right)}{\sin\left(\theta_2-\theta_3\right)}, \\ a_{22} &= -\frac{1}{2}\frac{L_4\left(\sin\left(\theta_2-\theta_3+\theta_4\right)-\sin\left(\theta_2+\theta_3-\theta_4\right)\right)}{\sin\left(\theta_2-\theta_3\right)}. \end{aligned} \tag{3}$$

The relationship that links the applied force at the fingertip between the equivalent torques of the electric motors is expressed through the transpose Jacobian of the mechanism:

$$\tau_F = J^T\left(\Theta\right) F, \tag{4}$$

where F represents the generalized forces exerted on the end-effector and τ_F represents the torques exerted by the actuators in the joints. Considering the mechanism is used in a vertical plane, it is necessary to determine the equivalent torques in order to compensate the effects of gravity. Therefore, taking into account both, the generated forces at the fingertip and the forces due to the weight, the generated torques transmitted to the motors can be expressed as

$$\tau = J^T\left(\Theta\right) F + \eta\left(\Theta\right), \tag{5}$$

where $\eta(\Theta)$ represents the gravity compensation.

An open loop impedance control was used for the proposed five-bar linkage mechanism, in which the input in the physical model of the virtual world is the end-effector position of the device, expressed as a Cartesian position, and the output is the reaction force. The control scheme is described in Figure 6. As the position of the end-effector is known, the physical model algorithm detects a collision with a virtual object. Depending on the properties of the object, the algorithm determines the reaction force. The calculated force is then converted to motor torque through the transpose Jacobian matrix and then the contribution of the gravity compensation is added. As shown in Figure 6, the torque gain G is used to convert the signal into volt. A saturation block bounds it, preventing higher exertion forces, and avoiding any possible injury. However, this solution does not always guarantee safety. Hence, a hardware solution is needed in order to achieve safety. Such solution was implemented by

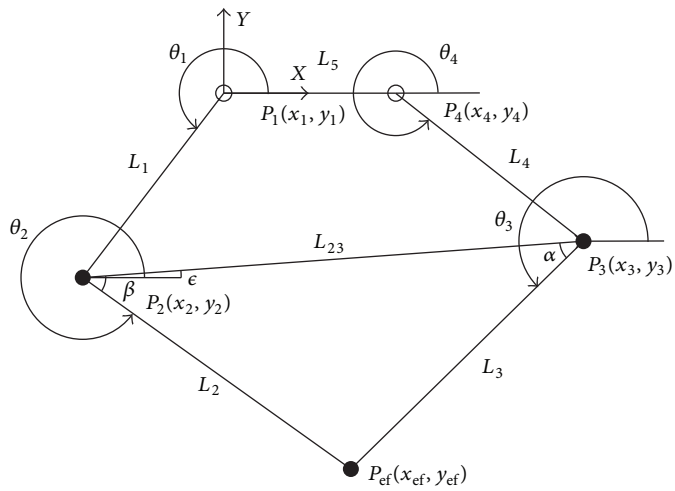

FIGURE 5: Five-bar linkage mechanism.

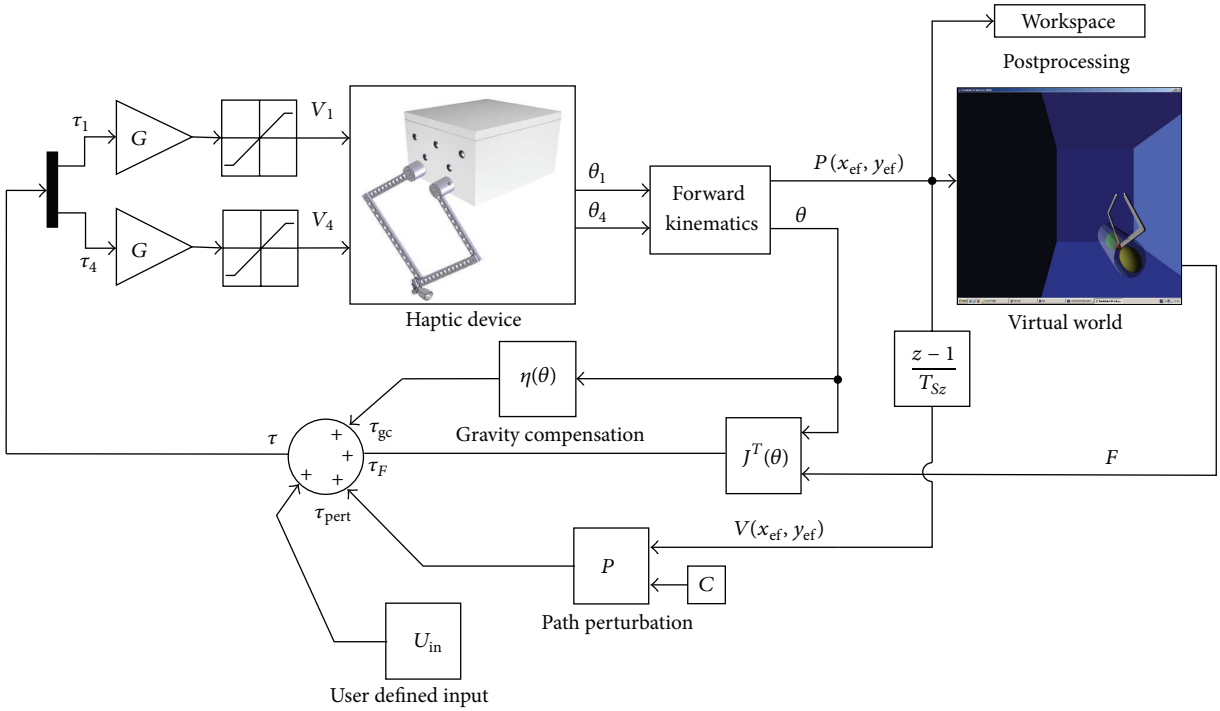

FIGURE 6: Control diagram of the haptic device and the virtual environment.

putting pressure sensitive safety edges along the moving bars of the mechanism. Using this hardware solution, the safety of the patient is guaranteed when unexpected higher forces occur and/or when the mechanism has unexpected behaviours.

The study was approved independently by the Institutional Review Boards of all participating hospitals and informed written consent was obtained by all participants at the time of enrolment.

2.3. Intervention. During the treatment the patients were comfortably seated in an ergonomic chair sustaining the trunk, in front of the haptic device, placed above an ergo nomic table. Both, the table and chair, were height adjustable in order to accomplish the best posture for the patients during the therapy (Figure 2). The robot was connected through a spherical passive joint (allowing three rotations around a pivotal point) to a finger or hand holder, depending on the patients' manipulation abilities (Figures 7 and 8). The rehabilitative exercises were developed by the therapist starting from the assessment scenes. The assessment scenes were never proposed as training exercises during the rehabilitation sessions. during the rehabilitation sessions. Following the initial assessment the therapist chose

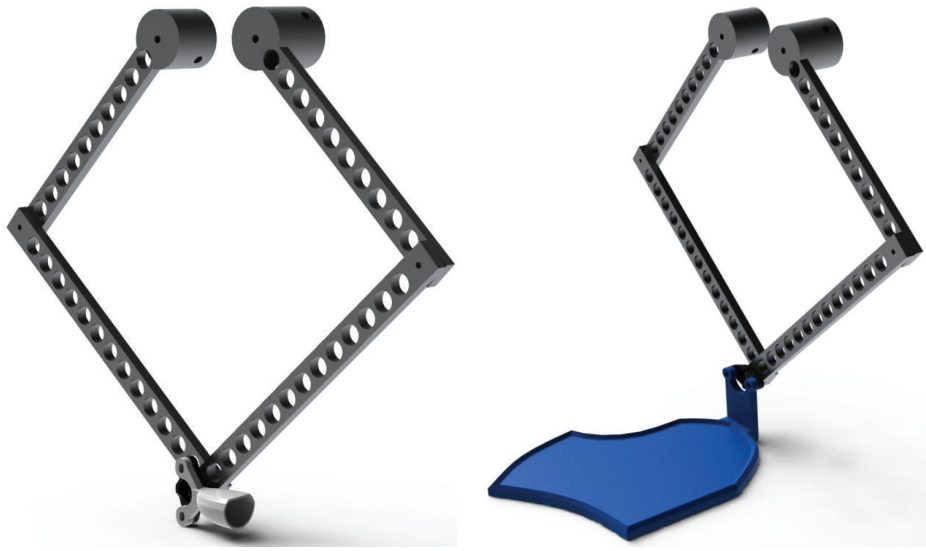

(a) (b)

Figure 7: Haptic device for finger/hand rehabilitation. (a) Finger rehabilitation. (b) Hand rehabilitation.

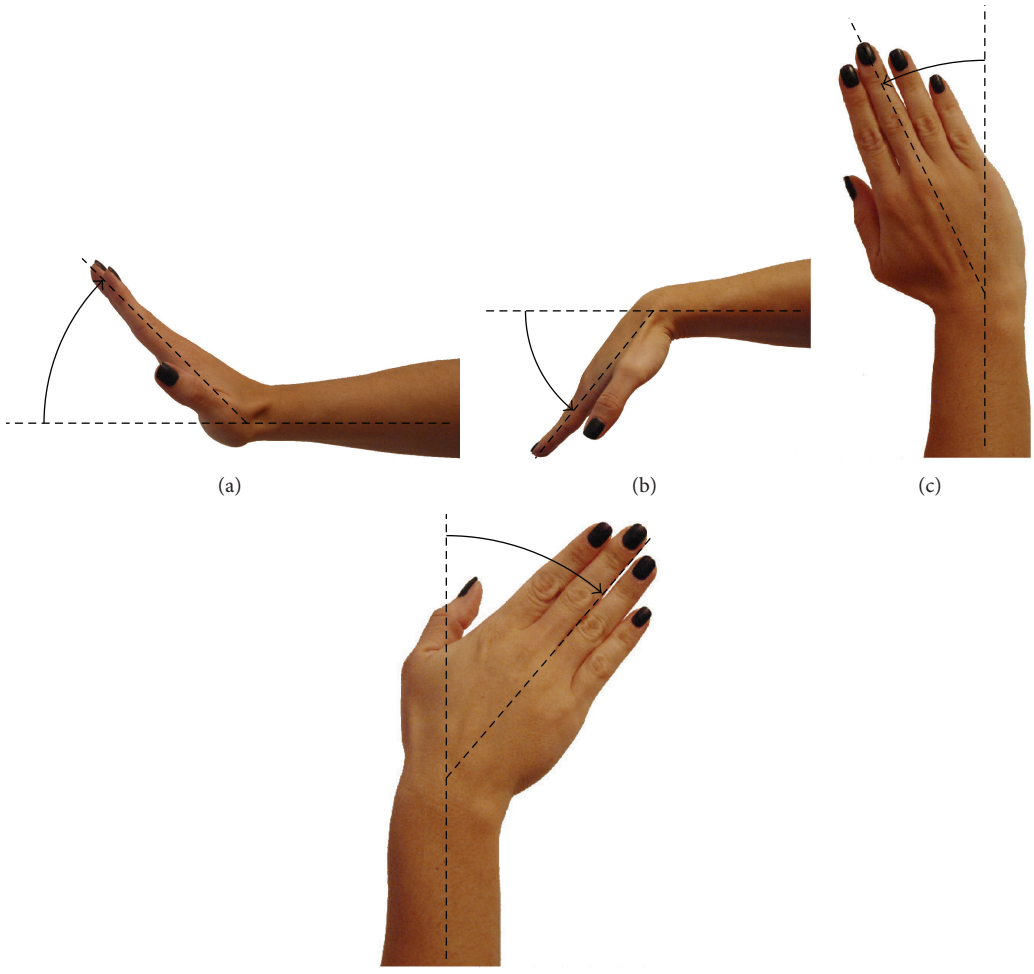

(a) (b) (c)

(d)

Figure 8: Possible movements for hand rehabilitation. (a) Extension. (b) Flexion. (c) Radial deviation. (d) Ulnar deviation.

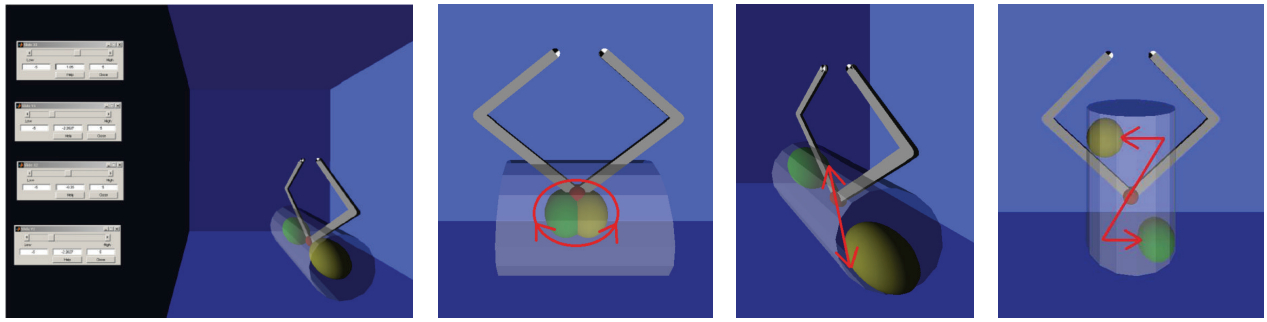

(a) (b) (c) (d)

Figure 9: The different scenarios for the exercises. The red arrows indicate the motor task to be accomplished. The environment managed by the therapist for the treatment (a) and examples of exercises proposed in horizontal (b), sagittal (c), and vertical (d) planes.

the best configuration of virtual objects to allow the patient to perform the most functional exercise autonomously, according to his/her motor function impairment. The new motor tasks were created by sliding the objects in the virtual environment by means of a graphical interface and adapting it online as the patient progressed during the therapy. During the treatment the subjects were asked to perform several different motor tasks (Figure 9); moreover, in order to interfere with the patient's path during the rehabilitation exercises, artificial perturbations in the system were implemented [21]. The perturbation was tested incrementally asking the patient to counteract the force received while moving on a linear path. Once the patient demonstrated to be unable to control the robot because the safety switches were touched with bars, this value was then set as the maximum threshold reachable. This perturbation was applied orthogonally to the patient's movement direction, affecting their actual path with a force proportional to the end effector velocity exerted by the patient, only in a subset of trials (at least 30% of the overall number of repetitions) and using random forces values within the range settle according to the described procedure. Every treatment session was supervised by the therapist that both instructed the patients on how to accomplish the exercises and also managed online the virtual environment and the user-defined perturbation. The aim of the online robot management by the therapist was to maintain the exercise strain adequate to the real time patients' capability, in order to prevent incoming muscles fatigue and avoiding frustration due to exceeding task challenges.

The treatment protocol lasted 3 weeks, every day 1 session of 45 minutes was provided for 5 days a week. The total amount of sessions performed was 15 for every patient.

2.4. Outcome Measures. As the haptics were developed to accomplish exercises targeted to hand and wrist motricity, outcomes describing both the clinical and kinematics domains were chosen. In order to quantify the upper limb motor impairment and hand dexterity of the paretic arm, two scales were administered, respectively: the Fugl-Meyer Upper Extremity (F-M UE) and the Nine Hole Pegboard Test (NHPT). The F-M UE is the most frequently used measure in stroke rehabilitation research. This is an ordinal scale whose scoring ranges from 0 to a maximum of 66 for the upper limb motor performance. The upper limb section has 33 items, which include reflex testing, movement observation, grasp testing, and assessment of coordination. The score for each item is 0 unable to perform; 1 able to perform in part; 2 able to perform [22]. Its clinimetric properties were known and the interrater reliability (r = 0.98 to 0.99) and intraclass correlation (ICC = 0.99) were estimated [23]. The NHPT is a test that assesses hand dexterity where the patients, sitting at a table, are asked to take 9 dowels (9 mm diameter, 32 mm long) from the table top and put them into 9 holes (10 mm diameter, 15 mm deep) spaced 50 mm apart on a board. The time to complete this task is recorded; the cut off is set at 50 seconds (when the number of peg placed is recorded). The number of pegs placed per second is then calculated [24]. Also the NHPT clinimetric properties were estimated, respectively, interrater reliability and test retest reliability (IRR and TRT: r = 0.68–0.99) [23].

The kinematic assessment of the patients motor behaviour was measured by means of two different motor tasks (Figure 10) each repeated 10 times, both executed in 3 different scenarios (Figure 11), for a total amount of 60 trials.

In the assessment exercises two spheres were displayed in the virtual environment arranged in a planar way, in the 3 different Cartesian planes, and put at the same distance. In the first motor task the patients were asked to touch alternatively the internal surface of the two spheres for 10 times, trying to perform the shorter executable path. In the second motor task the patients were asked to turn around the external surfaces of the two spheres, designing the narrower eight shape paths allowed by the haptics. In order to estimate the motor behaviour changes due to the therapy, we calculated four kinematic parameters describing the motor task performance.

(i) Average time needed to complete every trial [s]: the time the patient takes to execute the task he/she is asked to do.

(ii) Average velocity [m/s] is expressed as the mean of a proportion of the range of motion per unit time of the executed trials.

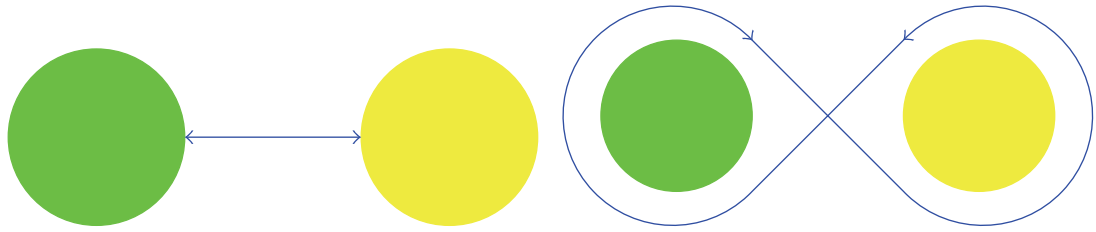

(a) (b)

Figure 10: The two motor tasks developed for the kinematic assessment. (a) The task of touching the spheres. (b) The eight shape path.

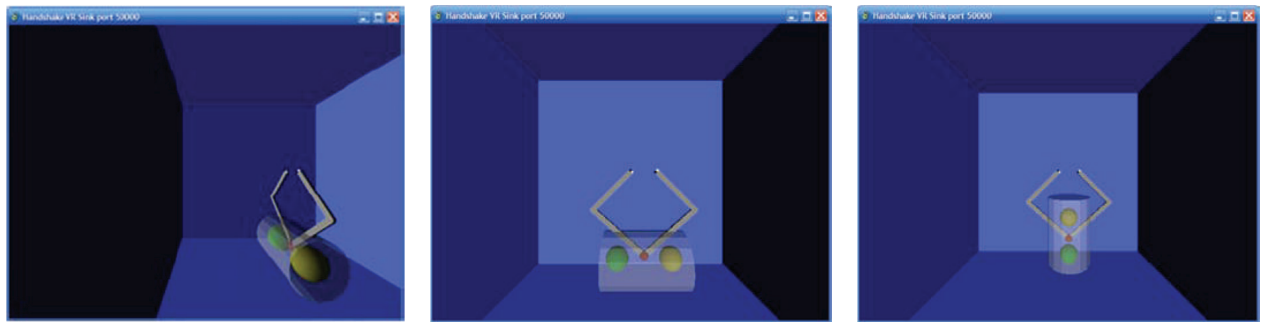

(a) (b) (c)

Figure 11: The three different assessment planes. (a) Sagittal. (b) Horizontal. (c) Vertical.

(iii) Jerk metric [1/s^2]: this parameter is used in order to characterize the average rate of change of acceleration in a movement [25]. It is defined as follows:

$$J_M = -\frac{1}{V_{\max}}\frac{1}{T}\int\sqrt{\left(\frac{d^3x}{dt}\right)^2+\left(\frac{d^3y}{dt}\right)^2}\,dt, \quad (6)$$

where J_M is the jerk metric, T is the duration, $V_{\max}$ is the maximum velocity, d^3x/dt is the jerk in x-axis, and d^3y/dt is the jerk in y-axis.

(iv) Normalized jerk [adim]: this parameter is a unit-free measure, which is used to compare coordination problems in patterns of different durations, shapes and sizes [26].

Consider

$$J_N = \sqrt{\frac{1}{2}\frac{T^5}{L^2}\int\left(\frac{d^3x}{dt}\right)^2+\left(\frac{d^3y}{dt}\right)^2}\,dt, \quad (7)$$

where J_N is the normalized jerk, T is the duration, L is the length, d^3x/dt is the jerk in x-axis, and d^3y/dt is the jerk in y-axis.

2.5. MRI Acquisition. In order to explore any neurophysiologic effect of the haptics on the cortical reorganization, a functional magnetic resonance imaging (fMRI) study was conducted on one sample patient. Scanning was on a 1.5 Tesla Philips (Achieva) scanner and included acquisition of high-resolution anatomical images, followed by fMRI of two side motor tasks. The patient's hand was fixed to a special cast by means of a binding leaving both the index fingers free to move in flexion-extension directions. The complete paradigm followed a block design in which 30 seconds of flexion-extension of the index finger were followed by 30 seconds of rest. In every run the patient was asked first to fix a black spot for 30 [s] without moving (rest) and then, when the command "move your index finger" appeared, to execute the task continuously in flexion-extension directions for another 30 [s] (movement). These blocks were repeated four times in every run, for a total acquisition of 120 volumes per run. There were 4 runs in which the patient was asked to perform the motor task, alternatively with the right and left index fingers. Scanning parameters included 25 axial 5 [mm] thick slices with no gap, 50 [volumes/series], TR = 2000 [ms], and TE = 40 [ms]. An investigator observed the subject's movements during scanning to verify task compliance.

2.6. Statistical and fMRI Analysis. The descriptive data were reported as mean and standard deviation. The analysis focused both on clinical and kinematics outcomes. For interval scales and ratio measures the variables distribution was explored by means of the Shapiro-Wilk test and parametric (Paired-Samples T test) or nonparametric (Wilcoxon signed-rank test) tests were used to determine scores' significant changes after treatment. For ordinal data a nonparametric (Wilcoxon signed-rank test) test was used to determine significant changes in scores after the treatment. SPSS Statistics

Table 2: Clinical changes due to the treatment.

Functional scales	Before treatment	After treatment	P value
Fugl-Meyer upper extremity	45.69 ± 12.88	53.77 ± 8.30	**0.002**[a]
Nine hole pegboard test	0.21 ± 0.14	0.26 ± 0.03	**0.002**[b]

The statistical significance value was considered for $P \leq 0.05$, emphasized in bold.
[a]Wilcoxon signed-rank test.
[b]Paired-Samples t test.

17.0 (IBM Inc. Chicago, Illinois) was used for the analysis and statistical significance was considered at $P = 0.05$. Using SPM8 [27], the fMRI images were realigned, normalized to MNI (Montreal Neurological Institute) space, and then spatially smoothed (FWHM = 8 mm). To estimate the cortical activations a general linear model (GLM) was applied (interscan interval: 2 s; microtime resolution: 16; microtime onset: 1) comparing the rest and movement period for the two fingers by means of t-contrast (P value = 0,01; extent threshold = 20). Finally the results were displayed overlapped on a 3D brain template.

3. Results

The sample was composed of 7 male and 8 female patients with a mean age of 54.00 ± 18.82 years and a mean distance from lesion of 16.59 ± 23.77 months. Six patients were affected by a lesion in the left hemisphere and nine in the right hemisphere. All the patients enrolled were assessed before and after the robotics treatment and completed the treatment protocol. No patients complained of any discomfort due to the interaction with the haptic interface. The baseline and posttreatment values, with their statistical significance, are reported in Tables 2 and 3, respectively, for the clinical and kinematics outcomes. From the explorative analysis both the F-M UE and NHPT were normally distributed (resp., $W = 0.931$, $P = 0.356$ and $W = 0.969$, $P = 0.887$), nevertheless the differences within group for the F-M UE was tested by means of nonparametric statistics, as this scale is considered an ordinal one. In the case of kinematics outcomes all the variables were estimated as normally distributed except the jerk normalized in both exercises (resp., Touch: $W = 0,814$, $P = 0,007$; 8 shape: $W = 0,652$, $P = 0,000$) and the time in the 8 shape exercise ($W = 0,871$, $P = 0,043$). The mean improvement on F-M UE was slightly bigger than 12% (i.e., 8.08 pts.), representing a change close to the minimal clinically important difference of 9 pts., reported for the F-M UE scale [28]. The NHPT increased 19% compared to baseline and despite the significant improvement observed, the lack of reference values in the literature made unreliable speculations on its clinical significance.

For kinematic assessment, both the mean time in trial execution and smoothness, intended as normalized jerk, significantly changed after the treatment, showing an optimization of the trajectories' morphology. We considered the normalized jerk as a smoothness parameter to avoid the differences in patients' functionalities that affect the jerk metric in the easiest task, as displayed in Table 3. On the contrary, the velocity did not change significantly in both the evaluated tasks. This evidence showed that the mean movement velocity should not be a parameter expected to change, in a workspace specifically designed for fingers/wrist movement.

The fMRI analysis (Figure 12) showed that before therapy the requested active finger movement induced, in the affected hemisphere, an activation of the frontal and parietal regions (presumably depending on semantic processes activated together with the motor area) and also an ipsilateral cortical activation of the nonaffected hemisphere. After treatment the ipsilateral activation almost disappeared, while, in the affected hemisphere, all the activations were brought back to a pattern close to the normal one, as for the right finger.

As a result, all patients showed evident improvements in kinematic performance and scored better results in clinical functional-scale assessment, even after a long time after stroke. Additionally, some results shown by fMRI suggest that the proposed approach stimulates the cortical reactivation of the brain.

4. Discussion

The motor therapy provided by means of the haptic interface showed statistical significant improvements in both clinical outcomes. As the F-M UE was known to improve significantly after intensive treatment focused on the upper limb, to our knowledge this is the first time that a significant improvement at NHPT induced by a hand robot therapy was observed in stabilized stroke patients. Similar results were already discussed but in multiple sclerosis patients [29, 30], while significant changing at NHPT in stroke patients were reported for other rehabilitative approaches (e.g., constraint induced movement therapy [31], botulinum toxin [32], passive joint mobilization [33], and task oriented intervention [34]). This result is encouraging and together with the possibility to reproduce reliably the NHPT by haptic interfaces [35], it unfolds new perspectives in assessing quantitatively hand motor recovery after stoke.

For the change in kinematics, we interpreted our result as related to the exercise specificity executed in a hand tailored space. Our setting constrained the patients to a high finalized interaction requiring an optimal end effector control, in this condition others parameters, better describing movement accuracy (such as smoothness), emerged as primary outcome of motor performance. In fact, the velocity in natural motor behaviour should be a movement characteristic mainly in charge of the entire upper limb and strictly dependent from the ability of a person to control trunk stability [36–38]. In our setting, on the contrary, the patients where well ergonomically supported in their posture, minimizing their voluntary control and were asked to enforce voluntary hands' movement to accomplish the exercises.

Finally, the fMRI data supplied a strong neurophysiological contribution to the possibility to induce a fine

Table 3: Kinematic changes due to the treatment.

Scenario	Before treatment	After treatment	P value
Touch			
Time [s]	4.42 ± 1.62	2.96 ± 0.65	**0.002**[a]
Velocity [m/s]	0.076 ± 0.021	0.082 ± 0.024	0.074[a]
Jerk metric [1/s^2]	−11.82 ± 2.56	−12.76 ± 2.44	0.273[a]
Normalized jerk [adim]	1332.55 ± 1336.04	341.00 ± 270.02	**0.006**[b]
8-shape			
Time [s]	16.64 ± 10.50	10.50 ± 3.96	**0.002**[b]
Velocity [m/s]	0.100 ± 0.022	0.089 ± 0.017	0.943[a]
Jerk metric [1/s^2]	−9.50 ± 2.49	−11.64 ± 2.15	**0.012**[a]
Normalized jerk [adim]	26304.06 ± 41387.15	7851.91 ± 21227.78	**0.013**[b]

The statistical significance value was considered for $P \leq 0.05$, emphasized in bold.
[a]Wilcoxon signed-rank test.
[b]Paired-Samples t test.

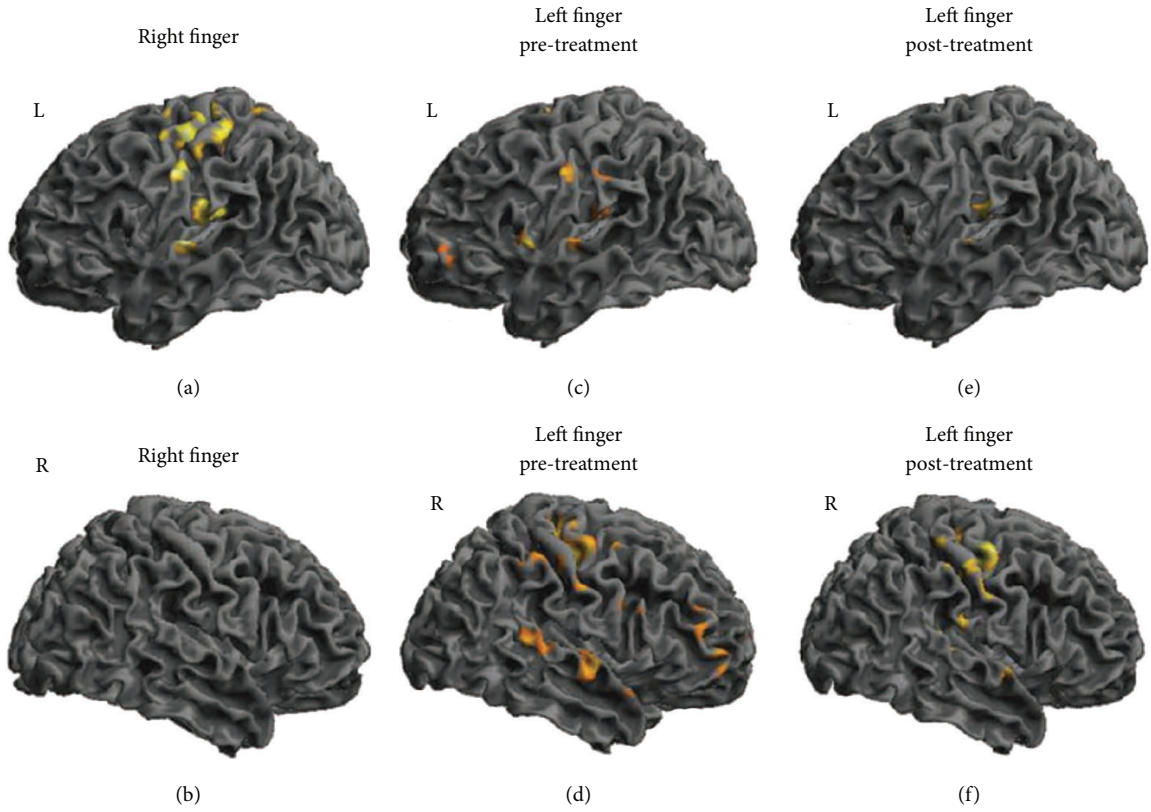

Figure 12: Cortical activation at fMRI. The cortical activation of the healthy (a, b) and impaired (c, d, e, f) finger movements are displayed. The activation of the right finger did not change one month later and was displayed for comparison. Before the treatment, the impaired finger movements induced bilateral activations. After the therapy the ipsilateral activations almost disappeared, while the contralateral activation tuned to M1 as for the healthy finger. L = left hemisphere; R = right hemisphere.

tuning of the motor cortex, by means of finalized robotics rehabilitation devices. Previous studies [39] already have shown how a finalized motor activity, also robot mediated [40], induced a cortical reorganization, nevertheless in our case it was mandatory to emphasize the continuity between the principles driving the hardware and software haptics' development, the motor rehabilitation protocol applied with the patients, and the experimental paradigm provided for the fMRI study. This data support the evidence that the specificity of the treatment, haptics mediated, could induced a fine tuning of the motor cortex activation, towards a normal pattern. These are the results from a multicenter proof of principle and feasibility study, so more data and controlled studies are needed to confirm robust inferences. The small sample size of the enrolled patients at this time and the absence of a control group should be considered as limitations

of the present study. Nevertheless clear and encouraging results emerge from the clinical and neurophysiologic points of view; moreover, the device safety was tested in a clinical setting sustaining its future development.

5. Conclusions

A general framework, completely developed in MATLAB/Simulink using the Handshake proSENSE Toolbox, was tested for a five-bar linkage mechanism used as a haptic device, for rehabilitative outcomes. The feasibility and clinical effectiveness of the developed system for a finger/hand rehabilitation program have been demonstrated. The proposed system includes a VR-based interface that allowed to evaluate robustly the finger/hand motion, supporting realtime update parameters and an online storage and retrieval database during the exercise, with the possibility to objectively measure the patients finger/hand functionality, as well as to fairly evaluate the rehabilitation program. The presented haptic interface trains finger and hand motion, while its application grants an excellent motor learning perspective. The presented application can further be improved by extending the haptic interface to more than one finger exercise. This type of application can provide new opportunities for creating more efficient treatments, extending the possibilities of success for the rehabilitation of poststroke patients. The realization of a general-purpose haptic interface, to be used in a multipurpose therapeutic application, is still a largely debated issue, since it is often preferred to use small devices, tailored around a specific pathology. This, however, leads to a large number of devices, each of them characterized by a different mechanical and electronic hardware. This paper addresses the problem of a modular design of the haptic devices for rehabilitation, in which any new device is integrated into the haptic rehabilitation environment as an easily designed S-function in MATLAB/Simulink. In terms of clinical perspectives some methodological issues should be faced in the future, extending the fMRI study both to a large sample of patients undergoing the robot therapy and to multiple followup in time, in order to better understand which plastic cortex mechanism could be really involved; designing bigger clinical trials, in order to avoid a low statistical power; controlling this approach with other recognized effective hands' motor treatments, in order to better estimate the magnitude of effectiveness.

Conflict of Interests

All the authors declared that they have no conflict of interests.

Authors' Contributions

Andrea Turolla, Omar A. Daud Albasini, Roberto Oboe, and Annalena Venneri were involved in analysis and interpretation of data, as well as in drafting and revising the paper. Andrea Turolla, Omar A. Daud Albasini, Roberto Oboe, Michela Agostini, Paolo Tonin, Stefano Paolucci, G iorgio Sandrini, and Lamberto Piron made substantial contributions to conception and design of the study. Andrea Turolla, Omar A. Daud Albasini, and Michela Agostini were involved in acquisition of data. All authors read and approved the final papers.

Acknowledgments

The authors acknowledge several colleagues who were involved in testing the device with patients in different hospitals: Alfonc Baba, Laura Cocco, Carla Zucconi, Giovanni Morone, Marco Iosa, Claudia Maggi, and Alice Rubbini. This project was firstly conceived, sustained, and animated by Lamberto Piron, who was granted as the Principal Investigator by the Italian Ministry of Health. On the January 3rd, 2011, Lamberto Piron died after a long illness. This paper is dedicated to his loving memory. This work was funded by the Italian Ministry of Health (Grant ART56-NMC-704763).

References

[1] WHO, *World Report on Disability. in Book World Report on Disability*, World Health Organization, 2011.

[2] R. W. V. Flynn, R. S. M. MacWalter, and A. S. F. Doney, "The cost of cerebral ischaemia," *Neuropharmacology*, vol. 55, no. 3, pp. 250–256, 2008.

[3] S. Prabhakaran, E. Zarahn, C. Riley et al., "Inter-individual variability in the capacity for motor recovery after ischemic stroke," *Neurorehabilitation and Neural Repair*, vol. 22, no. 1, pp. 64–71, 2008.

[4] R. P. S. Van Peppen, G. Kwakkel, S. Wood-Dauphinee, H. J. M. Hendriks, P. J. Van der Wees, and J. Dekker, "The impact of physical therapy on functional outcomes after stroke: What's the evidence?" *Clinical Rehabilitation*, vol. 18, no. 8, pp. 833–862, 2004.

[5] J. W. Krakauer, "Motor learning: its relevance to stroke recovery and neurorehabilitation," *Current Opinion in Neurology*, vol. 19, no. 1, pp. 84–90, 2006.

[6] L. Sawaki, "Use-dependent plasticity of the human motor cortex in health and disease," *IEEE Engineering in Medicine and Biology Magazine*, vol. 24, no. 1, pp. 36–39, 2005.

[7] S. J. Page, D. R. Gater, and P. Bach-Y-Rita, "Reconsidering the motor recovery plateau in stroke rehabilitation," *Archives of Physical Medicine and Rehabilitation*, vol. 85, no. 8, pp. 1377–1381, 2004.

[8] J. Broeren, M. Dixon, K. Stibrant Sunnerhagen, and M. Rydmark, "Rehabilitation after stroke using virtual reality, haptics (force feedback) and telemedicine," *Studies in health technology and informatics*, vol. 124, pp. 51–56, 2006.

[9] J. Broeren, K. S. Sunnerhagen, and M. Rydmark, "A kinematic analysis of a haptic handheld stylus in a virtual environment: a study in healthy subjects," *Journal of NeuroEngineering and Rehabilitation*, vol. 4, article 13, 2007.

[10] J. Broeren, A. Bjorkdahl, L. Claesson et al., "Virtual rehabilitation after stroke," *Stud Health Technol Inform*, vol. 136, pp. 77–82, 2008.

[11] J. Broeren, M. Rydmark, A. Björkdahl, and K. S. Sunnerhagen, "Assessment and training in a 3-dimensional virtual environment with haptics: a report on 5 cases of motor rehabilitation in the chronic stage after stroke," *Neurorehabilitation and Neural Repair*, vol. 21, no. 2, pp. 180–189, 2007.

[12] M. S. Cameirao, S. B. Badia, E. Duarte, A. Frisoli, and P. F. Verschure, "The combined impact of virtual reality neurorehabilitation and its interfaces on upper extremity functional recovery in patients with chronic stroke," *Stroke*, vol. 43, pp. 2720–2728, 2012.

[13] M. L. Aisen, H. I. Krebs, N. Hogan, F. McDowell, and B. T. Volpe, "The effect of robot-assisted therapy and rehabilitative training on motor recovery following stroke," *Archives of Neurology*, vol. 54, no. 4, pp. 443–446, 1997.

[14] S. E. Fasoli, H. I. Krebs, J. Stein, W. R. Frontera, and N. Hogan, "Effects of robotic therapy on motor impairment and recovery in chronic stroke," *Archives of Physical Medicine and Rehabilitation*, vol. 84, no. 4, pp. 477–482, 2003.

[15] P. S. Lum, C. G. Burgar, P. C. Shor, M. Majmundar, and M. Van der Loos, "Robot-assisted movement training compared with conventional therapy techniques for the rehabilitation of upper-limb motor function after stroke," *Archives of Physical Medicine and Rehabilitation*, vol. 83, no. 7, pp. 952–959, 2002.

[16] L. E. Kahn, M. L. Zygman, W. Z. Rymer, and D. J. Reinkensmeyer, "Robot-assisted reaching exercise promotes arm movement recovery in chronic hemiparetic stroke: a randomized controlled pilot study," *Journal of NeuroEngineering and Rehabilitation*, vol. 3, article 12, 2006.

[17] S. Hesse, C. Werner, M. Pohl, S. Rueckriem, J. Mehrholz, and M. L. Lingnau, "Computerized arm training improves the motor control of the severely affected arm after stroke: a single-blinded randomized trial in two centers," *Stroke*, vol. 36, no. 9, pp. 1960–1966, 2005.

[18] M. W. Spong, *Robot Dynamics and Control*, John Wiley & Sons, 1989.

[19] SouVR: Handshake proSENSETM Virtual Touch Toolbox v2.0 User's Guide.

[20] S. C. Venema and B. Hannaford, "A probabilistic representation of human workspace for use in the design of human interface mechanisms," *IEEE/ASME Transactions on Mechatronics*, vol. 6, no. 3, pp. 286–294, 2001.

[21] R. Shadmehr and F. A. Mussa-Ivaldi, "Adaptive representation of dynamics during learning of a motor task," *Journal of Neuroscience*, vol. 14, no. 5, pp. 3208–3224, 1994.

[22] A. Deakin, H. Hill, and V. M. Pomeroy, "Rough guide to the Fugl-Meyer assessment upper limb section," *Physiotherapy*, vol. 89, no. 12, pp. 751–758, 2003.

[23] E. Croarkin, J. Danoff, and C. Barnes, "Evidence-based rating of upper-extremity motor function tests used for people following a stroke," *Physical Therapy*, vol. 84, no. 1, pp. 62–74, 2004.

[24] A. Heller, D. T. Wade, and V. A. Wood, "Arm function after stroke: measurement and recovery over the first three months," *Journal of Neurology Neurosurgery and Psychiatry*, vol. 50, no. 6, pp. 714–719, 1987.

[25] B. Rohrer, S. Fasoli, H. I. Krebs et al., "Movement smoothness changes during stroke recovery," *Journal of Neuroscience*, vol. 22, no. 18, pp. 8297–8304, 2002.

[26] H.-L. Teulings, J. L. Contreras-Vidal, G. E. Stelmach, and C. H. Adler, "Parkinsonism reduces coordination of fingers, wrist, and arm in fine motor control," *Experimental Neurology*, vol. 146, no. 1, pp. 159–170, 1997.

[27] K. E. Stephan, N. Weiskopf, P. M. Drysdale, P. A. Robinson, and K. J. Friston, "Comparing hemodynamic models with DCM," *NeuroImage*, vol. 38, no. 3, pp. 387–401, 2007.

[28] K. N. Arya, R. Verma, and R. K. Garg, "Estimating the minimal clinically important difference of an upper extremity recovery measure in subacute stroke patients," *Topics in Stroke Rehabilitation*, vol. 18, no. 1, pp. 599–610, 2011.

[29] I. Carpinella, D. Cattaneo, S. Abuarqub, and M. Ferrarin, "Robot-based rehabilitation of the upper limbs in multiple sclerosis: feasibility and preliminary results," *Journal of Rehabilitation Medicine*, vol. 41, no. 12, pp. 966–970, 2009.

[30] E. Vergaro, V. Squeri, G. Brichetto et al., "Adaptive robot training for the treatment of incoordination in Multiple Sclerosis," *Journal of NeuroEngineering and Rehabilitation*, vol. 7, no. 1, article 37, 2010.

[31] I. C. Brunner, J. S. Skouen, and L. I. Strand, "Is modified constraint-induced movement therapy more effective than bimanual training in improving arm motor function in the subacute phase post stroke? A randomized controlled trial," *Clinical Rehabilitation*, vol. 26, no. 12, pp. 1078–1086, 2012.

[32] L. Shaw, H. Rodgers, C. Price et al., "BoTULS: a multicentre randomized controlled trial to evaluate the clinical effectiveness and cost-effectiveness of treating upper limb spasticity due to stroke with botulinum toxin type A," *Health Technology Assessment*, vol. 14, no. 26, 2010.

[33] P. Lindberg, C. Schmitz, H. Forssberg, M. Engardt, and J. Borg, "Effects of passive-active movement training on upper limb motor function and cortical activation in chronic patients with stroke: a pilot study," *Journal of Rehabilitation Medicine*, vol. 36, no. 3, pp. 117–123, 2004.

[34] J. Higgins, N. M. Salbach, S. Wood-Dauphinee, C. L. Richards, R. Côté, and N. E. Mayo, "The effect of a task-oriented intervention on arm function in people with stroke: a randomized controlled trial," *Clinical Rehabilitation*, vol. 20, no. 4, pp. 296–310, 2006.

[35] M. Bowler, F. Amirabdollahian, and K. Dautenhahn, "Using an embedded reality approach to improve test reliability for NHPT tasks," in *Proceedings of the IEEE International Conference on Rehabilitation Robotics (ICORR '11)*, July 2011.

[36] M. C. Cirstea and M. F. Levin, "Compensatory strategies for reaching in stroke," *Brain*, vol. 123, no. 5, pp. 940–953, 2000.

[37] A. D'Avella, A. Portone, L. Fernandez, and F. Lacquaniti, "Control of fast-reaching movements by muscle synergy combinations," *Journal of Neuroscience*, vol. 26, no. 30, pp. 7791–7810, 2006.

[38] A. Viau, A. G. Feldman, B. J. McFadyen, and M. F. Levin, "Reaching in reality and virtual reality: a comparison of movement kinematics in healthy subjects and in adults with hemiparesis," *Journal of NeuroEngineering and Rehabilitation*, vol. 1, p. 11, 2004.

[39] R. J. Nudo, B. M. Wise, F. SiFuentes, and G. W. Milliken, "Neural substrates for the effects of rehabilitative training on motor recovery after ischemic infarct," *Science*, vol. 272, no. 5269, pp. 1791–1794, 1996.

[40] C. D. Takahashi, L. Der-Yeghiaian, V. Le, R. R. Motiwala, and S. C. Cramer, "Robot-based hand motor therapy after stroke," *Brain*, vol. 131, no. 2, pp. 425–437, 2008.

Hindawi Publishing Corporation
Computational and Mathematical Methods in Medicine
Volume 2013, Article ID 398042, 12 pages
http://dx.doi.org/10.1155/2013/398042

Research Article

Effectiveness of Variable-Gain Kalman Filter Based on Angle Error Calculated from Acceleration Signals in Lower Limb Angle Measurement with Inertial Sensors

Yuta Teruyama and Takashi Watanabe

Graduate School of Biomedical Engineering, Tohoku University, Sendai 980-8579, Japan

Correspondence should be addressed to Yuta Teruyama; yuta.teruyama@bme.tohoku.ac.jp

Received 30 July 2013; Accepted 11 September 2013

Academic Editor: Imre Cikajlo

The wearable sensor system developed by our group, which measured lower limb angles using Kalman-filtering-based method, was suggested to be useful in evaluation of gait function for rehabilitation support. However, it was expected to reduce variations of measurement errors. In this paper, a variable-Kalman-gain method based on angle error that was calculated from acceleration signals was proposed to improve measurement accuracy. The proposed method was tested comparing to fixed-gain Kalman filter and a variable-Kalman-gain method that was based on acceleration magnitude used in previous studies. First, in angle measurement in treadmill walking, the proposed method measured lower limb angles with the highest measurement accuracy and improved significantly foot inclination angle measurement, while it improved slightly shank and thigh inclination angles. The variable-gain method based on acceleration magnitude was not effective for our Kalman filter system. Then, in angle measurement of a rigid body model, it was shown that the proposed method had measurement accuracy similar to or higher than results seen in other studies that used markers of camera-based motion measurement system fixing on a rigid plate together with a sensor or on the sensor directly. The proposed method was found to be effective in angle measurement with inertial sensors.

1. Introduction

Wearable inertial sensors have been used in many studies to estimate human kinetic data. Those sensors have advantages of low cost, small size, and practical usefulness compared to traditional lab tools such as optical motion measurement system or electric goniometers. As has been reported in previous studies, segment and joint angles [1–11], stride length [1, 3, 5], walking speed [1, 5], gait event timing [5, 12, 13], and so on can be estimated using inertial sensors. Therefore, a wearable inertial sensor system can be effective for objective and quantitative evaluation in rehabilitation of motor function. That is, inertial sensors are considered to be suitable for clinical applications.

In our previous studies, a method of measuring lower limb angles using wireless inertial sensors was developed to realize simplified wearable gait evaluation system for rehabilitation support. The method was tested in measurement of gait of healthy subjects [14, 15]. Although the method was shown to have practical accuracy, measurement errors varied depending on movement speeds or subjects. In the angle measurement method of our previous studies, Kalman filter was applied using angle calculated from acceleration signals. Many other studies also used accelerometers as inclinometers to measure inclination angles of body segments [2, 5, 7, 8]. However, the angle calculated from acceleration signals was influenced by impact and movement accelerations, since the angle was calculated from gravitational acceleration. Therefore, those impact and movement accelerations can be considered as one of the causes of variation of measurement error.

Low-pass filtering of acceleration signals is one of the methods to reduce influences of those impact and motion accelerations. In our previous studies, outputs of accelerometer were filtered with Butterworth low-pass filter with cutoff frequency of 0.5 Hz [14, 15]. However, low cutoff frequency is at risk for increasing measurement error because of its large time constant in the low-pass filtering. Therefore,

using higher cutoff frequency has a possibility to improve measurement error.

In this paper, in order to reduce influences of impact and movement accelerations in calculation of angles using Kalman filter, a variable-Kalman-gain method with higher cutoff frequency for the low-pass filtering was tested. In previous studies, a method to change Kalman gain based on the magnitude of acceleration signals was used [9, 16]. However, in this study, the method to change Kalman gain based on error of angle calculated from acceleration signals was proposed. This is because the Kalman filter of our system is applied using the angles calculated from acceleration signals.

The variable-gain method was evaluated in measurement of lower limb angles of healthy subjects in treadmill walking using a camera-based motion measurement system to measure reference angles for evaluation. The fixed-Kalman-gain method and the variable-gain method based on magnitude of acceleration signals were compared to the proposed method. Then, similar evaluation was performed in measurement of angles of a rigid body model, because some other studies evaluated angle measurement method with inertial sensors using a rigid plate that fixed a sensor together with markers of an optical motion measurement system or attaching the markers directly on the sensor [4, 8, 10, 11].

2. Angle Measurement Method Based on Kalman Filter

2.1. Fixed-Kalman-Gain Method. Figure 1(a) shows the block diagram of the angle measurement method used in our previous studies. An inclination angle of body segment is calculated by integrating an output of a gyroscope. Here, the integration error is corrected by Kalman filter using the angle calculated from outputs of an accelerometer. Then, joint angle is calculated from difference of inclination angles of the adjacent segments.

The state equation is represented by error of angle measured with a gyroscope $\Delta\theta$ and bias offset of outputs of the gyroscope Δb as follows:

$$\begin{bmatrix} \Delta\theta_{k+1} \\ \Delta b_{k+1} \end{bmatrix} = \begin{bmatrix} 1 & \Delta t \\ 0 & 1 \end{bmatrix} \begin{bmatrix} \Delta\theta_k \\ \Delta b_k \end{bmatrix} + \begin{bmatrix} \Delta t \\ 1 \end{bmatrix} w, \tag{1}$$

where w is error in measurement with the gyroscope and Δt is sampling period. Observation signal is deference of angles obtained from the gyroscope and an accelerometer Δy, which is given by

$$\Delta y_k = \begin{bmatrix} 1 & 0 \end{bmatrix} \begin{bmatrix} \Delta\theta_k \\ \Delta b_k \end{bmatrix} + v, \tag{2}$$

where v is error in measurement with the accelerometer. On this state-space model, Kalman filter repeats corrections (3) and predictions (4):

$$\begin{bmatrix} \Delta\widehat{\theta}_k \\ \Delta\widehat{b}_k \end{bmatrix} = \begin{bmatrix} \Delta\widehat{\theta}_k^- \\ \Delta\widehat{b}_k^- \end{bmatrix} + \begin{bmatrix} K_1 \\ K_2 \end{bmatrix} \left(\Delta y_k - \Delta\widehat{\theta}_k^- \right), \tag{3}$$

$$\begin{bmatrix} \Delta\widehat{\theta}_{k+1}^- \\ \Delta\widehat{b}_{k+1}^- \end{bmatrix} = \begin{bmatrix} 1 & \Delta t \\ 0 & 1 \end{bmatrix} \begin{bmatrix} \Delta\widehat{\theta}_k \\ \Delta\widehat{b}_k \end{bmatrix}, \tag{4}$$

where K_1 and K_2 represent Kalman gain for $\Delta\theta$ and Δb, respectively. Notations such as $\Delta\widehat{\theta}$ and $\Delta\widehat{\theta}^-$ represent estimated value and predicted value for $\Delta\theta$, respectively. For the initial condition, $\Delta\widehat{\theta}_0^-$ was set as 0, and $\Delta\widehat{b}_0^-$ was set as $\Delta\widehat{b}$ at the last measurement. The Kalman filter was applied repeatedly until its output converged.

Values of Kalman gain were fixed in angle calculation in our previous studies. Those gain values are determined by the noise ratio, that is, the ratio of the covariance of observation noise and covariance of process noise. In our system, value of Kalman gain increases as the noise ratio decreases and decreases as the noise ratio increases.

As shown in (3) and (4), the Kalman filter estimates $\Delta\theta$ and Δb by using the angle difference Δy. Therefore, large value of Kalman gain (small noise ratio) means that calculation results become highly dependent on accelerometer, while small Kalman gain (large noise ratio) means that calculation results become highly dependent on gyroscope. Considering power of the correction by Kalman filter, values of the noise ratio were determined by trial and error method.

2.2. Variable-Kalman-Gain Method. The fixed-Kalman-gain method shown in the previous section was found to be useful in measurement of angles during gait of healthy subjects [14, 15]. However, impact and movement accelerations were considered to increase measurement error and its variation. That is, those accelerations are considered to cause inappropriate correction by the Kalman filter. As described in the previous section, Kalman gain means correction power of the Kalman filter. Therefore, in this paper, following two methods of changing the noise ratio to determine Kalman gain were tested.

(a) *Acceleration Magnitude-Based Method*. Figure 1(b) shows the variable-gain method based on acceleration magnitude, which was introduced in reference to previous studies [9, 16]. Value of the noise ratio is adjusted based on the magnitude of impact and motion acceleration signals. Here, the magnitude of impact and motion acceleration signals was calculated by subtracting gravitational acceleration (1 G) from magnitude of measured acceleration vector. That is, the value of noise ratio is varied as follows:

$$\begin{aligned} n &= n_1, \quad \text{for } |\alpha| \le \alpha_1, \\ n &= n_2, \quad \text{for } \alpha_1 < |\alpha| \le \alpha_2, \\ n &= n_3, \quad \text{for } \alpha_2 < |\alpha| \le \alpha_3, \\ n &= n_4, \quad \text{for } \alpha_3 < |\alpha|, \end{aligned} \tag{5}$$

where n and $|\alpha|$ represent the noise ratio and the magnitude of impact and motion acceleration signals, respectively. α_1, α_2, and α_3 show thresholds to change the value of noise ratio, respectively.

(b) *Angle Error-Based Method.* Figure 1(c) shows the method proposed in this paper, in which the noise ratio is adjusted based on the difference between the angle estimated by the Kalman filter and the angle calculated from acceleration signals. Here, the angle difference was used approximately as the

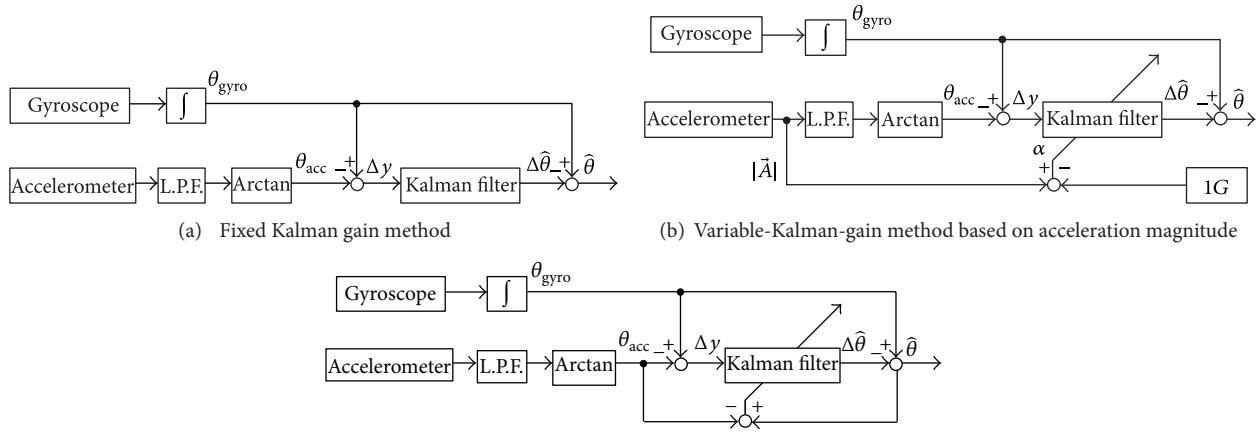

(a) Fixed Kalman gain method

(b) Variable-Kalman-gain method based on acceleration magnitude

(c) Variable-Kalman-gain method based on angle error

Figure 1: Block diagrams of the angle calculation methods using Kalman filter tested in this paper.

magnitude of influence of impact and motion accelerations. That is, it was assumed that the angle difference involves substantial error of angle calculated from acceleration signals, which is caused by impact and movement accelerations. The value of noise ratio is varied as follows:

$$\begin{aligned} n &= n_1, \quad \text{for } \left|\widehat{\theta} - \theta_{\text{acc}}\right| \le \theta_1, \\ n &= n_2, \quad \text{for } \theta_1 < \left|\widehat{\theta} - \theta_{\text{acc}}\right| \le \theta_2, \\ n &= n_3, \quad \text{for } \theta_2 < \left|\widehat{\theta} - \theta_{\text{acc}}\right| \le \theta_3, \\ n &= n_4, \quad \text{for } \theta_3 < \left|\widehat{\theta} - \theta_{\text{acc}}\right|, \end{aligned} \tag{6}$$

where, n and $|\widehat{\theta} - \theta_{\text{acc}}|$ represent the noise ratio and the angle difference between the angle estimated by the Kalman filter $\widehat{\theta}$ and the angle calculated from acceleration signals θ_{acc}, respectively. The angle difference $|\widehat{\theta} - \theta_{\text{acc}}|$ shows approximately the magnitude of influence of impact and motion accelerations. θ_1, θ_2, and θ_3 show thresholds to change values of the noise ratio, respectively.

3. Methods of Validation Tests

The angle calculation methods were applied to data measured with inertial sensors and evaluated in comparison to those angles measured with an optical motion measurement system. First, the evaluation was performed in measurement of lower limb angles in treadmill walking with healthy subjects. Then, angles of a rigid body model were measured for evaluation of the methods, because some other studies evaluated their angle measurement method with inertial sensors using the rigid plate that fixed a sensor together with markers of an optical motion measurement system [4, 8, 10, 11].

3.1. Measurement of Lower Limb Angles in Treadmill Walking. Inclination angles of lower limb segments in treadmill walking were measured with 3 healthy subjects (male, 22-23 y.o.). The subjects walked on a treadmill for about 90 sec at speeds of 1 km/h (slow), 3 km/h (normal), and 5 km/h (fast). Five trials were performed for each walking speed.

Seven wireless inertial sensors (WAA-006, Wireless Technologies) were attached on the feet, the shanks and the thighs of both legs, and lumbar region with stretchable bands (Figure 2(a)). The sensors were put inside of pocket of the band. Acceleration and angular velocity signals of each sensor were measured with a sampling frequency of 100 Hz and were transmitted to a PC via Bluetooth network.

The optical motion measurement system (Optotrak, Northern Digital, Inc.) was used to measure reference data for evaluating angles calculated by the methods from data measured with the inertial sensors. Markers for reference data were attached on the left side of the body (Figure 2(a)). The maker positions were measured with a sampling frequency of 100 Hz.

3.2. Measurement of Angles with a Rigid Body Model. Figure 2(b) shows the schematic diagram of the rigid body model used in the measurement. The rigid body model simulated motion of the thigh, the shank, and the knee joint. The optical motion measurement system (Optotrak, Northern Digital, Inc.) was also used to measure reference data for evaluating the angle calculation method. Sensors and markers were attached on the rigid body model as shown in Figure 2(b). Acceleration and angular velocity signals of each sensor and the marker positions were measured with sampling frequency of 100 Hz.

Inclination angles of the thigh and the shank parts were measured for 35 sec with angle ranges of ±15, ±30, ±45, ±60, and ±75 deg for the thigh part. Zero degree means the direction of gravitational force. The shank part was moved freely associated with movement of the thigh part. The cycle period of the movements was 2 sec, and five trials were conducted for each target angle range.

4. Results of Validation Tests

Two variable-Kalman-gain methods were evaluated in comparison to the previous fixed-Kalman-gain method. Here, for

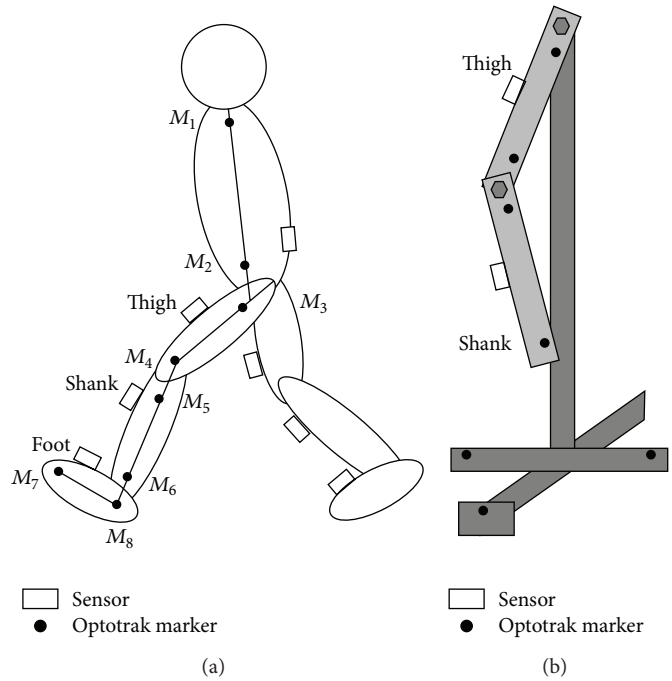

Figure 2: Experimental setup for the angle measurement during treadmill walking (a) and the angle measurement using rigid body model (b). M1: the acromion, M2: along the long axis of the trunk at the same height as the iliospinale anterius, M3: the great trochanter, M4: the lateral femoral condyle, M5: the caput fibulae, M6: the lateral malleolus, M7: the metatarsale fibulare, and M8: on the foot at the same height as the metatarsale fibulare along the line of shank markers.

the fixed-gain method, values of the noise ratio n to determine Kalman gain and the cutoff frequency of Butterworth low-pass filter for acceleration signals f_c are shown below.

Method 1 (previous fixed Kalman gain method)

$$n = 10^6, \qquad f_c = 0.5\,\text{Hz}. \tag{7}$$

Method 2 (fixed Kalman gain method)

$$n = 10^6, \qquad f_c = 10\,\text{Hz}. \tag{8}$$

Method 1 is the previous method used in our research group, in which the noise ratio of Kalman filter was fixed and cutoff frequency of the low-pass filter for acceleration signals was determined to remove impact and motion accelerations. Method 2 is the fixed-Kalman-gain method with higher cutoff frequency of the low-pass filter, which was tested to make clear the influence of low cutoff frequency on measurement error.

There was offset difference between the sensor system and camera-based motion analysis system, because the markers for the reference signals were not attached on the sensors. Therefore, the difference was calculated as the mean value of the first 100 samples of the 1st measurement and removed the value for evaluation. Then, root mean squared error (RMSE) and correlation coefficient (ρ) between measured angles with sensors and reference values were calculated for evaluating measurement accuracy. In this paper, inclination angles of lower limb segments in the sagittal plane were evaluated.

4.1. Measurement of Lower Limb Angles in Treadmill Walking. For the variable-Kalman-gain methods, values of the noise ratio n and threshold values were determined by trial and error as shown below.

Method 3 (variable-gain method based on acceleration magnitude)

$$\begin{aligned} n &= 10^4, \quad \text{for } |\alpha| \le 20\,\text{mG}, \\ n &= 10^6, \quad \text{for } 20\,\text{mG} < |\alpha| \le 300\,\text{mG}, \\ n &= 10^8, \quad \text{for } 300\,\text{mG} < |\alpha| \le 1\,\text{G}, \\ n &= 10^{13}, \quad \text{for } 1\,\text{G} < |\alpha|. \end{aligned} \tag{9}$$

Method 4 (variable-gain method based on angle error)

$$\begin{aligned} n &= 10^4, \quad \text{for } \left|\widehat{\theta} - \theta_{\text{acc}}\right| \le 1\ \text{deg}, \\ n &= 10^6, \quad \text{for } 1\ \text{deg} < \left|\widehat{\theta} - \theta_{\text{acc}}\right| \le 15\ \text{deg}, \\ n &= 10^8, \quad \text{for } 15\ \text{deg} < \left|\widehat{\theta} - \theta_{\text{acc}}\right| \le 60\ \text{deg}, \\ n &= 10^{13}, \quad \text{for } 60\ \text{deg} < \left|\widehat{\theta} - \theta_{\text{acc}}\right|. \end{aligned} \tag{10}$$

Here, the cutoff frequency of the low-pass filter for acceleration signals f_c was 10 Hz for both methods.

Figures 3 and 4 show RMSE values and ρ values of measured inclination angles, respectively. The proposed variable-gain method (Method 4) showed the smallest average RMSE

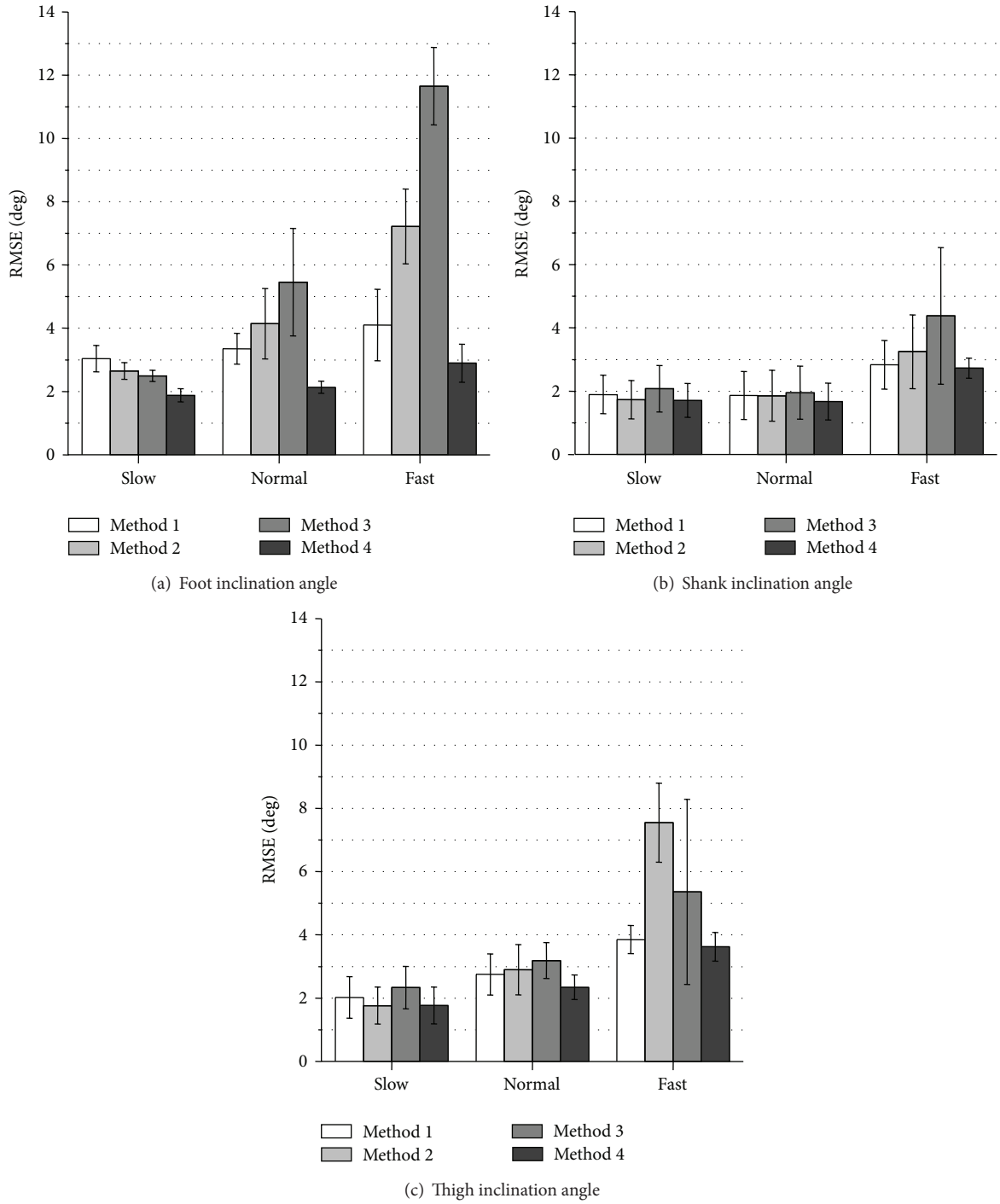

(a) Foot inclination angle

(b) Shank inclination angle

(c) Thigh inclination angle

Figure 3: Evaluation results of RMSE of measured inclination angles during treadmill walking. Average values obtained from the results of 5 trials of all subjects are shown for each walking speed.

values and the largest ρ values for all of measurement conditions. Method 4 achieved average RMSE values of less than 3.0 deg except for thigh angle at fast walking speed and average values of correlation coefficient larger than 0.994 for all the measurement conditions.

The measurement accuracy of foot inclination angle was improved significantly with Method 4 for all walking speeds comparing to the results of Method 1 used in our previous studies (Figures 3(a) and 4(a)). For the shank and the thigh inclination angles, slight improvement of RMSE values and ρ values was shown for all walking speeds with Method 4 compared to the results of Method 1 (Figures 3(b), 3(c) and 4(b), 4(c)).

The values of RMSE with Method 2 (fixed-gain method with higher cut-off frequency) decreased compared to the results of Method 1 in all the segments at slow walking

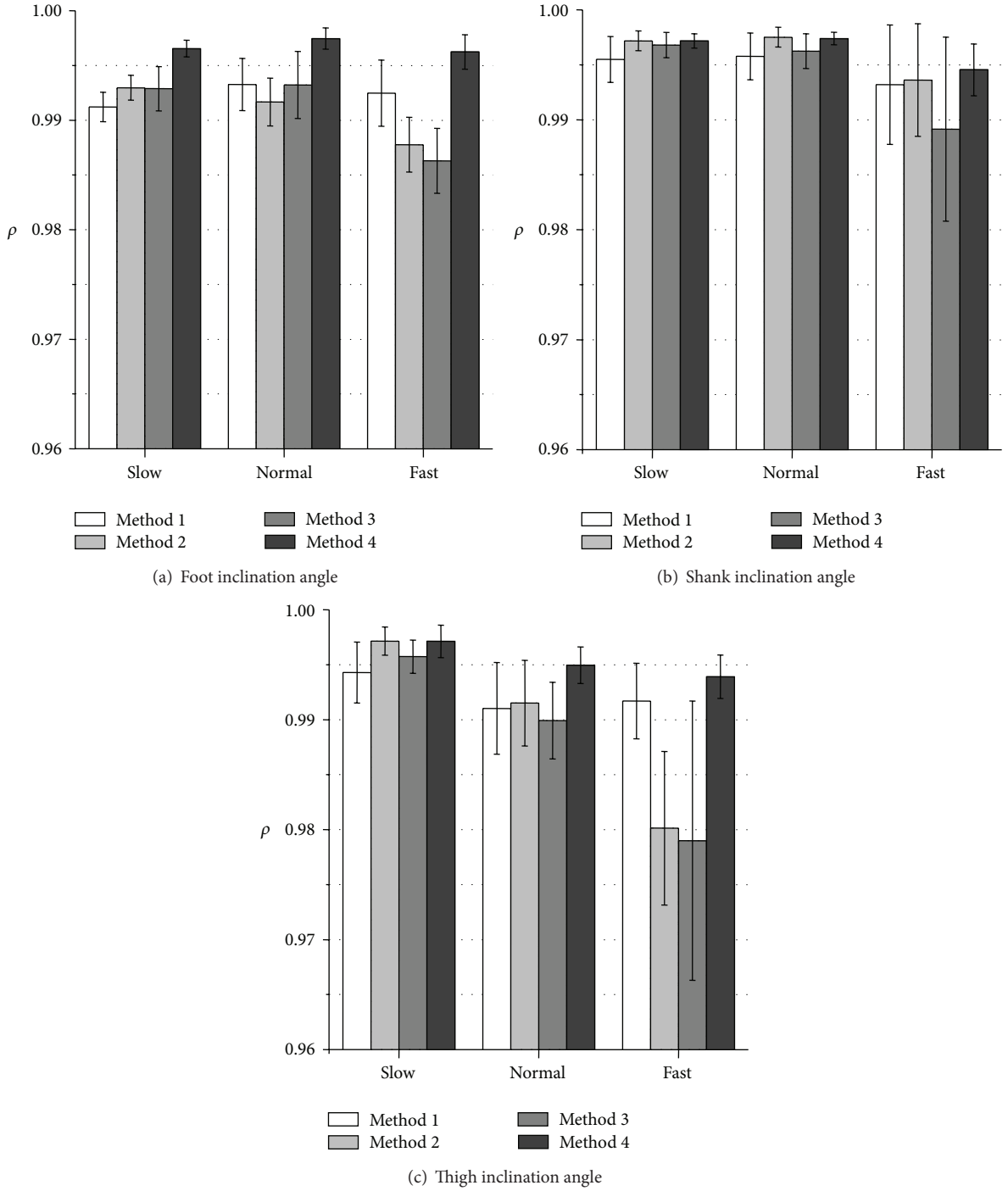

(a) Foot inclination angle

(b) Shank inclination angle

(c) Thigh inclination angle

Figure 4: Evaluation results of correlation coefficient (ρ) of measured inclination angles during treadmill walking. Average values obtained from the results of 5 trials of all subjects are shown for each walking speed.

speed. However, at normal and fast walking speeds, the values of RMSE with Method 2 increased compared to the results of Method 1. Method 3 (variable-gain method based on acceleration magnitude) reduced measurement accuracy especially for fast waking speed and for foot inclination angle.

4.2. Measurement of Angles Using Rigid Body Model. The parameter values used for Methods 3 and 4 are shown below.

Method 3 (variable-gain method based on acceleration magnitude)

$$\begin{aligned} n &= 10^4, \quad \text{for } |\alpha| \le 10\,\text{mG}, \\ n &= 3 \times 10^6, \quad \text{for } 10\,\text{mG} < |\alpha| \le 200\,\text{mG}, \\ n &= 10^7, \quad \text{for } 200\,\text{mG} < |\alpha| \le 400\,\text{mG}, \\ n &= 2 \times 10^7, \quad \text{for } 400\,\text{mG} < |\alpha|. \end{aligned} \tag{11}$$

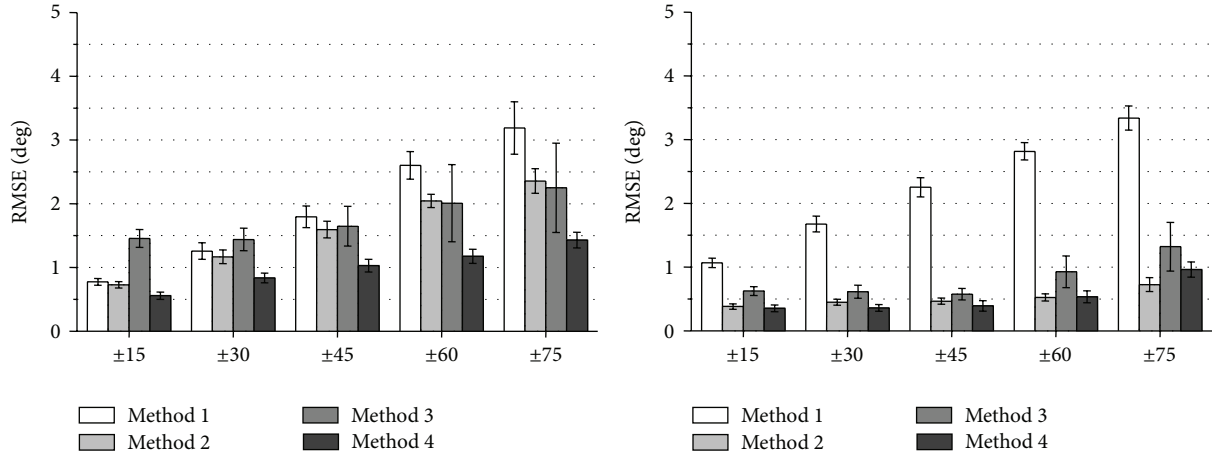

(a) Shank inclination angle (b) Thigh inclination angle

Figure 5: Evaluation results of RMSE of measured inclination angles using rigid body model. Average values obtained from the results of 5 trials are shown for each target angle range.

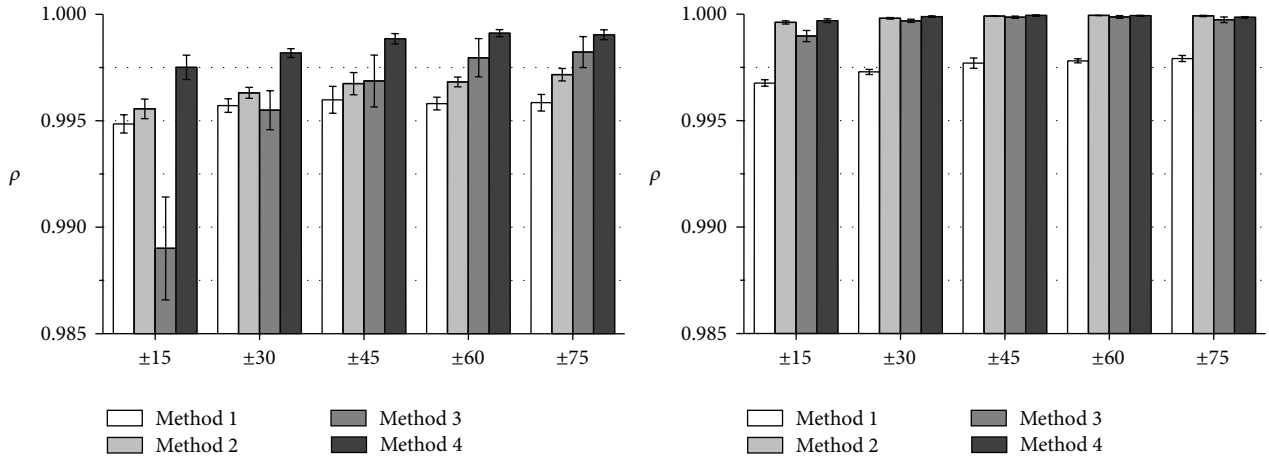

(a) Shank inclination angle (b) Thigh inclination angle

Figure 6: Evaluation results of correlation coefficient (ρ) of measured inclination angles using rigid body model. Average values obtained from the results of 5 trials are shown for each target angle range.

Method 4 (variable-gain method based on angle error)

$$\begin{aligned} n &= 10^4, \quad \text{for } \left|\widehat{\theta} - \theta_{\text{acc}}\right| \le 1 \text{ deg}, \\ n &= 3 \times 10^6, \quad \text{for } 1 \text{ deg} < \left|\widehat{\theta} - \theta_{\text{acc}}\right| \le 20 \text{ deg}, \\ n &= 10^7, \quad \text{for } 20 \text{ deg} < \left|\widehat{\theta} - \theta_{\text{acc}}\right| \le 30 \text{ deg}, \\ n &= 2 \times 10^7, \quad \text{for } 30 \text{ deg} < \left|\widehat{\theta} - \theta_{\text{acc}}\right|. \end{aligned} \tag{12}$$

Here, the cutoff frequency of the low-pass filter for acceleration signals f_c was 10 Hz for both methods. The parameter values of Methods 3 and 4 were changed from those values in angle measurement with human subjects, since magnitude of impact and motion acceleration signals and angle difference $|\widehat{\theta} - \theta_{\text{acc}}|$ were smaller than that in the measurement with human subjects.

Figures 5 and 6 show RMSE values and ρ values of measured inclination angles, respectively. The proposed variable-gain method (Method 4) showed highest measurement accuracy almost for all the target angle ranges. Average values of RMSE and correlation coefficient with Method 4 were less than 1.5 deg and larger than 0.9975, respectively. Although Methods 2 and 3 were also effective to improve measurement accuracy, Method 3 could not improve shank angle in movements of target angle range of ±15 deg and ±30 deg.

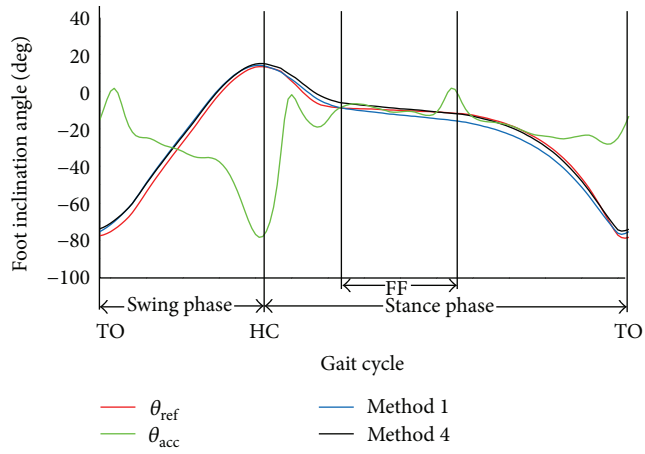

Figure 7: An example of waveforms of reference and measured foot inclination angles at normal walking speed. θ_{ref} and θ_{acc} represent reference angle and angle calculated from acceleration signals, respectively. The x-axis shows the gait cycle. The toe off, the heel contact, and the foot flat are represented by TO, HC, and FF, respectively.

5. Discussion

The proposed variable-Kalman-gain method (Method 4) measured lower limb angles in treadmill walking with the smallest average values of RMSE and the largest average values of correlation coefficient. In particular, Method 4 showed significant improvement in calculation of foot inclination angle in treadmill walking compared to our previous method (Method 1). It is a useful result that measurement accuracy of foot inclination angle was improved, because evaluation of foot movements in walking is important for gait of motor disabled subjects and elderly persons. In measurement of shank and thigh angles, values of the noise ratio were not so greatly varied, since magnitude of the angle difference $|\widehat{\theta} - \theta_{acc}|$ did not fluctuate significantly during movements. This is one of the reasons why improvement of measurement accuracy was not so large in shank and thigh angles with Method 4.

The proposed variable-Kalman-gain method (Method 4) was highly effective in calculation of foot inclination angle. Figure 7 shows the reference and calculated foot inclination angles of one gait cycle at normal walking speed. As seen in Figure 7, the calculated angle with Method 4 was almost equal to that with Method 1 between around the TO and the HC in the swing phase. Method 4 improved angle calculation between around the FF and the TO in the stance phase. It is considered that the sensor attached on the foot was close to the stationary state at around the FF. At that time, the variable-Kalman-gain method corrected the angle significantly increasing values of Kalman gain (decreasing noise ratio), since the angle difference $|\widehat{\theta} - \theta_{acc}|$ was small as the influence of impact and movement accelerations was small. It is possible to decrease angle measurement error between the FF and the TO by reducing noise ratio with Method 1. However, in that case, angle error between around the TO and the HC is increased by the influence of impact and movement accelerations. Method 4 reduced Kalman gain effectively at around the TO and the HC, since the angle difference $|\widehat{\theta} - \theta_{acc}|$ increased. Therefore, the Method 4 could be effective especially in foot angle measurement, decreasing the influence of impact and motion accelerations.

As shown in Figure 3, RMSE values of measured inclination angles in treadmill walking with Method 2 decreased at slow walking speed compared to the results of Method 1 in all segments. In addition, as shown in Figure 5, RMSE values of measured inclination angles of the rigid body model with Method 2 decreased at all target angle ranges compared to the results of Method 1 for both segments. These suggest that very low cutoff frequency for the low-pass filtering of the acceleration signal increases measurement error if impact and movement accelerations are not so large. The cause of error increases in treadmill walking at the normal and fast walking speeds with Method 2 is considered to be influences of impact and motion accelerations. It is considered that although 0.5 Hz of cutoff frequency is reasonable value for removing impact and motion accelerations in angle calculation of human gait, error increase is caused by the large delay in the low pass filtering.

The variable-gain method based on acceleration magnitude (Method 3) did not show improvement of measurement accuracy of lower limb angles of human gait. For most of measurement conditions, average values of RMSE increased, and those of correlation coefficient decreased. The parameter values that are good for changing Kalman gain used in (9)–(12) were determined by trial and error method for both variable-gain methods. Although there is a possibility of improving measurement accuracy with Methods 3 and 4, the results of this paper suggest that the proposed method of changing the Kalman gain based on angle error was more suitable to the Kalman filter used in our system than that based on acceleration magnitude.

In angle measurement of the rigid body model, the values of RMSE with Method 4 were less than 1.5 deg for all segments and all target angle ranges. Those RMSE values

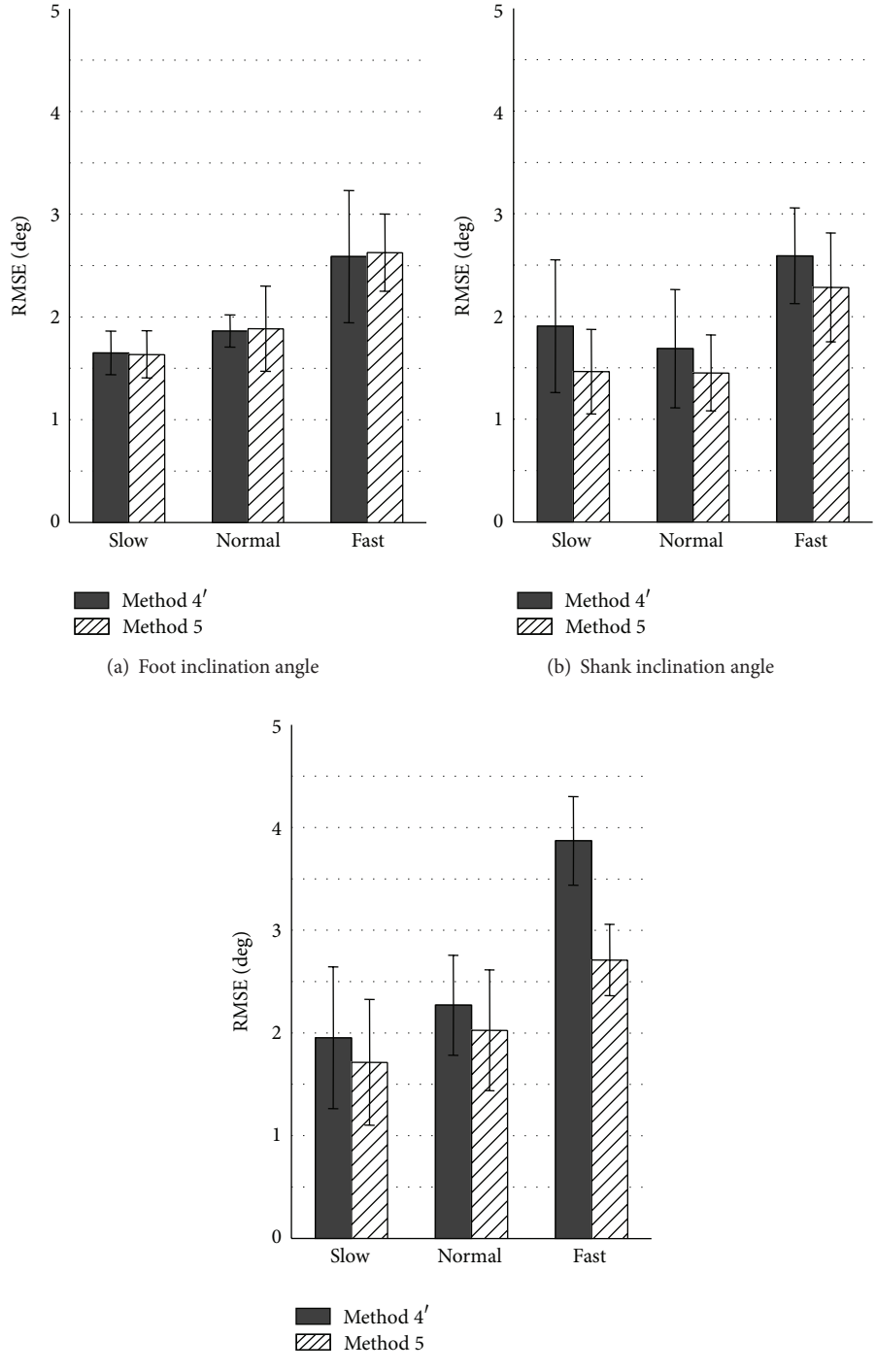

Figure 8: Average values of RMSE of measured inclination angles during treadmill walking calculated by using Methods 4 and 5.

show measurement accuracy similar to or higher than results seen in other studies that used markers of camera-based motion measurement system fixing on a rigid plate together with the sensor or on the sensor directly [4, 8, 10, 11]. It is considered that the proposed variable-gain method became effective in measurement of human gait.

In the proposed variable-gain method, influence of impact and motion accelerations was approximately represented by $|\widehat{\theta} - \theta_{acc}|$. Here, the approximation was validated by comparing to results of using $|\theta_{ref} - \theta_{acc}|$ as shown in Figure 8, in which θ_{ref} shows reference value measured with the camera-based motion measurement system. In the

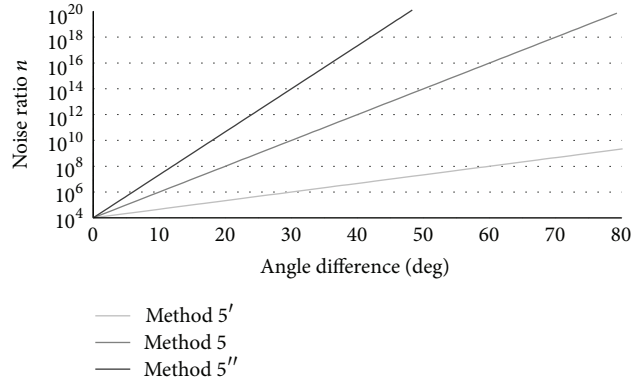

Figure 9: Relationships between the noise ratio and the angle difference used in the test of influence of the noise ratio.

comparison, the noise ratio (Kalman gain) was determined as continuous value by the followings from the angle difference.

Method 4′:

$$n = 10^4 e^{0.46 \cdot |\hat{\theta} - \theta_{\text{acc}}|}. \tag{13}$$

Method 5:

$$n = 10^4 e^{0.46 \cdot |\theta_{\text{ref}} - \theta_{\text{acc}}|}. \tag{14}$$

Here, (13) and (14) were derived by linear approximation of discrete values of the noise ratio n in (10). That is,

$$\log n = ax + \log b, \tag{15}$$

where a and b represent constant values and x represents the angle difference. The constant value a was determined to decrease RMSE values by trial and error method, and b was set 10^4 from (10). As shown in Figure 8, for foot inclination angles, measurement results with Method 5 were similar to the results with Method 4′ for all walking speeds. Measurement results for the shank and the thigh inclination angles were improved for all walking speeds with Method 5 using reference values. Average values of RMSE with Method 5 were less than 3.0 deg for all walking speeds and all segments. This result suggests that the proposed variable-Kalman-gain method based on angle error is effective to improve measurement accuracy of angle during human gait. It is also suggested that measurement accuracy with Method 4′ can be improved if error in $|\hat{\theta} - \theta_{\text{acc}}|$ is reduced.

Angle measurement accuracy depends on the noise ratio. In this paper, parameter values to calculate values of noise ratio used in (9)–(14) were determined to decrease RMSE values by trial and error method. Here, different relationships between the noise ratio and the angle difference described by (14) were examined. Figures 9 and 10 show the tested relationships and results of their measurement accuracy, respectively. Method 5′ used smaller noise ratio and Method 5″ used larger noise ratio than Method 5. In Figure 10, the results obtained by Method 1 (fixed-gain method) are also shown. The RMSE values were decreased with variable-gain method in any parameter setting compared to the fixed-gain method. However, Method 5′ (smaller noise ratio) showed larger RMSE values than Method 5 for all the measurement conditions. It is considered that the influence of impact and movement accelerations was not decreased sufficiently with Method 5′ because of large value of Kalman gain (small noise ratio). On the other hand, RMSE values with Method 5″ (larger noise ratio) were similar to that of Method 5 for almost all the measurement conditions. However, Method 5″ has a tendency to increase RMSE values of the thigh and the shank inclination angles for the fast walking speed. Therefore, further studies on the method to determine appropriate Kalman gain are expected. In addition, this paper focused only on the error of angle calculated from acceleration signals in determination of Kalman gain. It is considered that the noise ratio also depends on magnitude of the offset drift of gyroscope. This is also required to be studied more for measurement of angles with the variable-gain Kalman filter. Finally, the proposed variable-Kalman-gain method was validated in measurement of inclination angles of lower limb segments in the sagittal plane in this paper. It is expected to show the effectiveness of the proposed method in measurement of 3 dimensional angles.

6. Conclusion

In this paper, variable-gain Kalman filter was tested to improve measurement accuracy of lower limb angles during gait, in which two calculation methods of Kalman gain were compared to fixed-gain Kalman filter. In measurements of lower limb angles of healthy subjects in treadmill walking and that of angles of a rigid body model, the variable-gain method based on the angle difference proposed in this study showed the highest measurement accuracy for most of measurement conditions. In particular, the proposed variable-gain method improved significantly measurement accuracy of foot inclination angle in human gait. On the other hand, measurement results of the shank and the thigh inclination angles show slight improvement of measurement accuracy. The proposed variable-gain method was found to be effective in angle measurement with inertial sensors. The

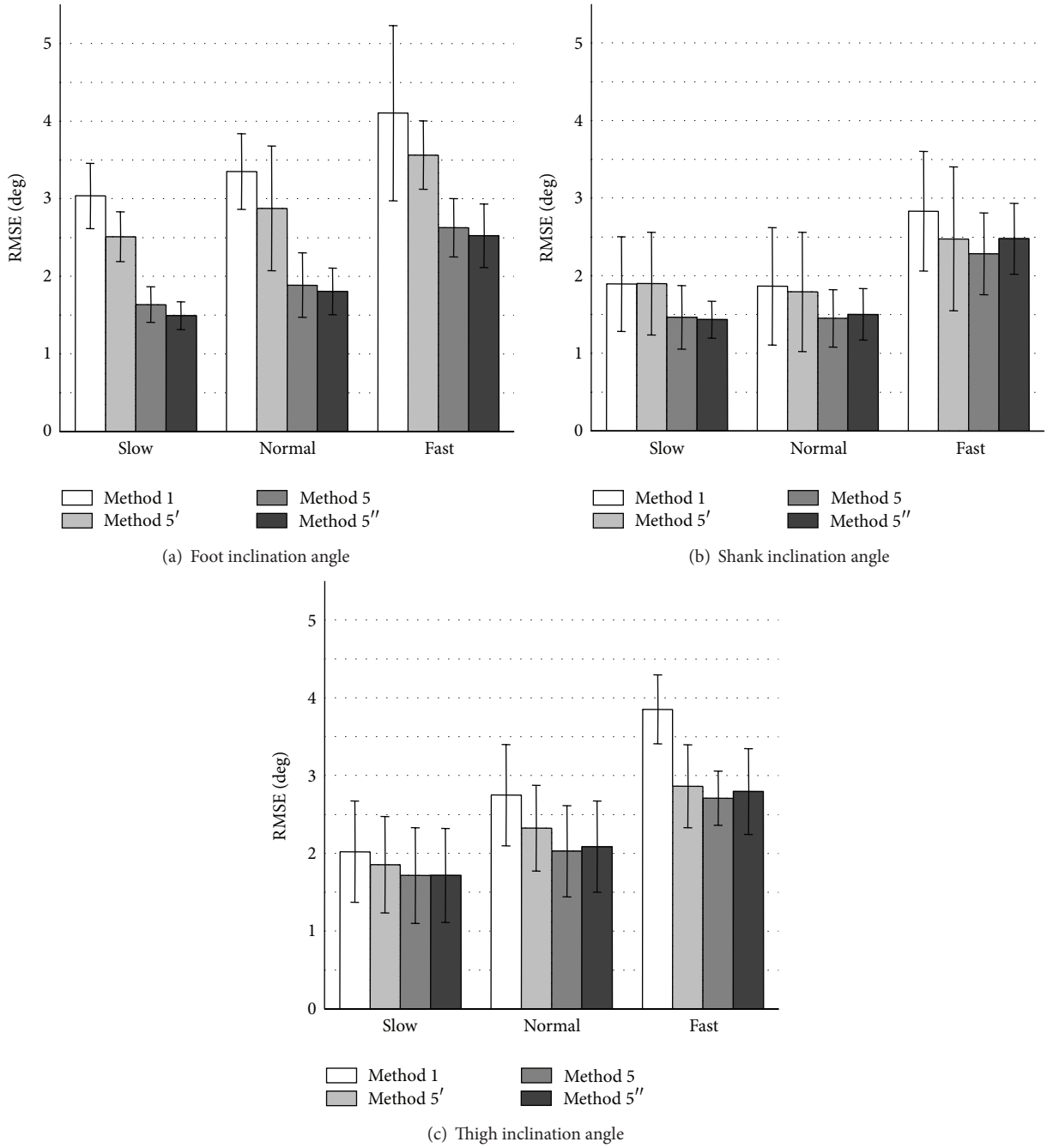

(a) Foot inclination angle

(b) Shank inclination angle

(c) Thigh inclination angle

Figure 10: Average RMSE values of measured inclination angles during treadmill walking calculated by fixed-gain method (Method 1) and variable-gain method with 3 different parameter settings for the noise ratio.

results also suggested that more accurate measurement can be realized by improving estimation accuracy of the angle difference $|\theta_{\text{ref}} - \theta_{\text{acc}}|$. Further studies on this point and to find appropriate method to determine Kalman gain using the angle difference and other parameters are expected.

Acknowledgment

This work was supported in part by the Ministry of Education, Culture, Sports, Science and Technology of Japan under a Grant-in-Aid for Challenging Exploratory Research.

References

[1] K. Tong and M. H. Granat, "A practical gait analysis system using gyroscopes," *Medical Engineering and Physics*, vol. 21, no. 2, pp. 87–94, 1999.

[2] H. Dejnabadi, B. M. Jolles, and K. Aminian, "A new approach to accurate measurement of uniaxial joint angles based on a combination of accelerometers and gyroscopes," *IEEE Transactions on Biomedical Engineering*, vol. 52, no. 8, pp. 1478–1484, 2005.

[3] J. C. Alvarez, R. C. González, D. Alvarez, A. M. López, and J. Rodríguez-Uría, "Multisensor approach to walking distance estimation with foot inertial sensing," in *Proceedings of the 29th*

Annual International Conference of IEEE-EMBS, Engineering in Medicine and Biology Society (EMBC '07), pp. 5719–5722, August 2007.

[4] D. Roetenberg, P. J. Slycke, and P. H. Veltink, "Ambulatory position and orientation tracking fusing magnetic and inertial sensing," *Transactions on Biomedical Engineering*, vol. 54, no. 5, pp. 883–890, 2007.

[5] S. J. M. Bamberg, A. Y. Benbasat, D. M. Scarborough, D. E. Krebs, and J. A. Paradiso, "Gait analysis using a shoe-integrated wireless sensor system," *IEEE Transactions on Information Technology in Biomedicine*, vol. 12, no. 4, pp. 413–423, 2008.

[6] A. Findlow, J. Y. Goulermas, C. Nester, D. Howard, and L. P. J. Kenney, "Predicting lower limb joint kinematics using wearable motion sensors," *Gait and Posture*, vol. 28, no. 1, pp. 120–126, 2008.

[7] R. Takeda, S. Tadano, A. Natorigawa, M. Todoh, and S. Yoshinari, "Gait posture estimation using wearable acceleration and gyro sensors," *Journal of Biomechanics*, vol. 42, no. 15, pp. 2486–2494, 2009.

[8] M. D. Djurić-Jovičić, N. S. Jovicic, D. B. Popović, and A. R. Djordjević, "Nonlinear optimization for drift removal in estimation of gait kinematics based on accelerometers," *Journal of Biomechanics*, vol. 45, no. 16, pp. 2849–2854, 2012.

[9] C. Mazzà, M. Donati, J. McCamley, P. Picerno, and A. Cappozzo, "An optimized Kalman filter for the estimate of trunk orientation from inertial sensors data during treadmill walking," *Gait and Posture*, vol. 35, no. 1, pp. 138–142, 2012.

[10] B. J. E. Misgeld, D. Ruschen, S. Kim, and S. Leonhardt, "Body sensor network-based strapdown orientation estimation: application to human locomotion," in *International Conference on Rehabilitation Robotics (ICORR '13)*, 2013.

[11] A. Caroselli, F. Bagala, and A. Cappello, "Quasi-real time estimation of angular kinematics using single-axis accelerometers," *Sensors*, vol. 13, no. 1, pp. 918–937, 2013.

[12] J. M. Jasiewicz, J. H. J. Allum, J. W. Middleton et al., "Gait event detection using linear accelerometers or angular velocity transducers in able-bodied and spinal-cord injured individuals," *Gait and Posture*, vol. 24, no. 4, pp. 502–509, 2006.

[13] H. Lau and K. Tong, "The reliability of using accelerometer and gyroscope for gait event identification on persons with dropped foot," *Gait and Posture*, vol. 27, no. 2, pp. 248–257, 2008.

[14] H. Saito and T. Watanabe, "Kalman-filtering-based joint angle measurement with wireless wearable sensor system for simplified gait analysis," *IEICE Transactions on Information and Systems*, vol. 94, no. 8, pp. 1716–1720, 2011.

[15] T. Watanabe and H. Saito, "Tests of wireless wearable sensor system in joint angle measurement of lower limbs," in *Proceedings of the 33rd Annual International Conference of the IEEE Engineering in Medicine and Biology Society (EMBS '11)*, pp. 5469–5472, September 2011.

[16] A. M. Sabatini, "Quaternion-based extended Kalman filter for determining orientation by inertial and magnetic sensing," *IEEE Transactions on Biomedical Engineering*, vol. 53, no. 7, pp. 1346–1356, 2006.

Hindawi Publishing Corporation
Computational and Mathematical Methods in Medicine
Volume 2013, Article ID 592328, 9 pages
http://dx.doi.org/10.1155/2013/592328

Research Article

Experimental Evaluation of Balance Prediction Models for Sit-to-Stand Movement in the Sagittal Plane

Oscar David Pena Cabra[1] and Takashi Watanabe[2]

[1] *Graduate School of Engineering, Tohoku University, Aramaki-aza-Aoba 6-6-11-901-7, Aoba-ku, Sendai 980-8579, Japan*
[2] *Graduate School of Biomedical Engineering, Tohoku University, Aramaki-aza-Aoba 6-6-11-901-7, Aoba-ku, Sendai 980-8579, Japan*

Correspondence should be addressed to Oscar David Pena Cabra; oscar.dpc@bme.tohoku.ac.jp

Received 27 July 2013; Revised 4 September 2013; Accepted 5 September 2013

Academic Editor: Imre Cikajlo

Evaluation of balance control ability would become important in the rehabilitation training. In this paper, in order to make clear usefulness and limitation of a traditional simple inverted pendulum model in balance prediction in sit-to-stand movements, the traditional simple model was compared to an inertia (rotational radius) variable inverted pendulum model including multiple-joint influence in the balance predictions. The predictions were tested upon experimentation with six healthy subjects. The evaluation showed that the multiple-joint influence model is more accurate in predicting balance under demanding sit-to-stand conditions. On the other hand, the evaluation also showed that the traditionally used simple inverted pendulum model is still reliable in predicting balance during sit-to-stand movement under non-demanding (normal) condition. Especially, the simple model was shown to be effective for sit-to-stand movements with low center of mass velocity at the seat-off. Moreover, almost all trajectories under the normal condition seemed to follow the same control strategy, in which the subjects used extra energy than the minimum one necessary for standing up. This suggests that the safety considerations come first than the energy efficiency considerations during a sit to stand, since the most energy efficient trajectory is close to the backward fall boundary.

1. Introduction

Lower limb motor functions are important for the activities of daily living (ADL), participating in social activities, and preventing bedridden state. Therefore, rehabilitation training of sit-to-stand movement is considered to be the first step to prevent motor-disabled patients and elderly people from being bedridden. In the rehabilitation, joint angle trajectories and/or joint torques are commonly measured for evaluation of motor function. During lower limb movement, however, balance control is also required for developing the movement safely. Since sit-to-stand movement requires control of stability in addition to muscular strength [1, 2], balance control ability in sit-to-stand movement should also be evaluated in rehabilitation training.

Bipedal balance has been studied since it is expected to have important applications in preventing health problems associated with falls [3–6] and in designing better and safer rehabilitation techniques for lower limb function impairment [7]. Bipedal dynamic stability has also been studied as the ability to restore static balance [8, 9]. In those studies, it has been theoretically shown that the ability to restore balance is described by conditions of the center of mass (CM) velocity-position with respect to the base of support (BOS).

In order to calculate these BOS-CM conditions for predicting the ability to control gait balance, those previous studies modeled human bipedal gait as a single joint, simple inverted pendulum [3, 6, 8, 9]. Based on the method using the simple inverted pendulum model, dynamic balance during sit-to-stand movement has also been studied [10–12]. However, sit-to-stand movements have multiple joint interactions that present significant variation of the CM rotational radius of the inverted pendulum model. In spite of the aspect of sit-to-stand movements, it has not been studied sufficiently if a simple inverted pendulum would suffice to describe the balance in the sit-to-stand movements or not.

In this paper, in order to make clear usefulness and limitation of the traditional simple inverted pendulum model

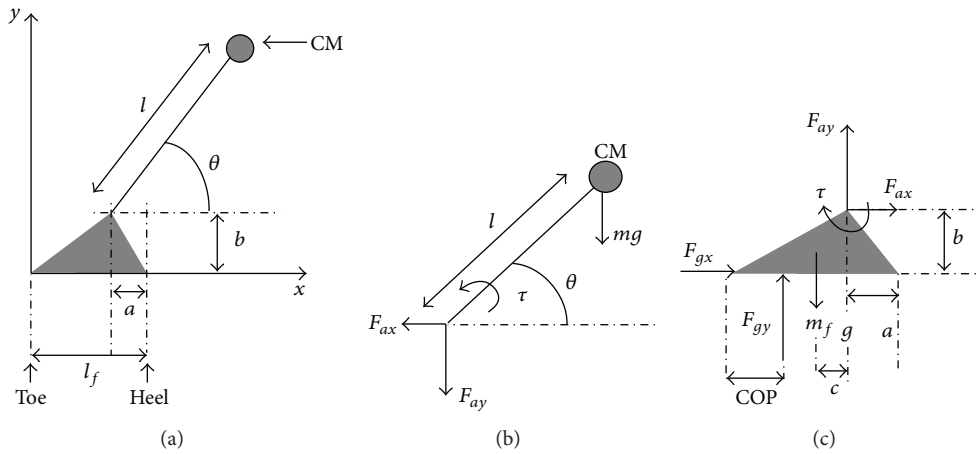

Figure 1: The inverted pendulum used for modeling sit-to-stand movement in the sagittal plane. Note that the length l is constant for the traditional simple inverted pendulum model and is represented by a function of the angle θ in order to include multiple-joint influence for the complex model used in this paper.

in balance prediction in sit-to-stand movements, the balance prediction obtained by the method of using the traditional simple model was compared to the prediction of a complex model that included multiple-joint influence. Here, since a telescopic pendulum model has been shown to be no less informative than more demanding multisegment models [13], an inertia variable inverted pendulum model, in which rotational radius was varied during sit-to-stand movement, was used as the complex model. The model predictions were tested upon experimentation by measuring sit-to-stands performed by healthy subjects. In addition, normal sit-to-stand CM trajectories were discussed from the measured data for evaluating balance control ability.

2. Methods

2.1. Outline of Balance Prediction. In the sit-to-stand movement, the center of mass (CM) velocity-position is in a given initial state when the subject leaves the chair. Then, the task of sit-to-stand consists of stopping the CM somewhere over the base of support (BOS) while satisfying the restrictions imposed by the friction coefficient, the foot geometry, maximum and minimum physiological ankle torque, and the condition that the foot segment should not move.

The sit-to-stand balance control feasibility can be calculated by finding all the CM velocity-position conditions when leaving the chair that allow the CM to arrive and stop over the base of support using the inverted pendulum model shown in Figure 1 with the maximum ankle plantar flexion and the maximum ankle dorsiflexion. The results were plotted in the form of a map as shown in Figure 2, in which the solid lines are the theoretical balance control boundaries. The upper boundary is the trajectory where the subject manages to stop the CM just over the toe using maximum plantar flexion, and therefore velocity-position conditions over the top boundary would result in a forward fall. The lower boundary is the trajectory where the subject manages to take the CM just over the heel using maximum dorsiflexion, and velocity-position conditions below the bottom boundary would result in a backward fall. The broken line shows the conditions that would allow recovering static balance without using ankle torque after the seat-off.

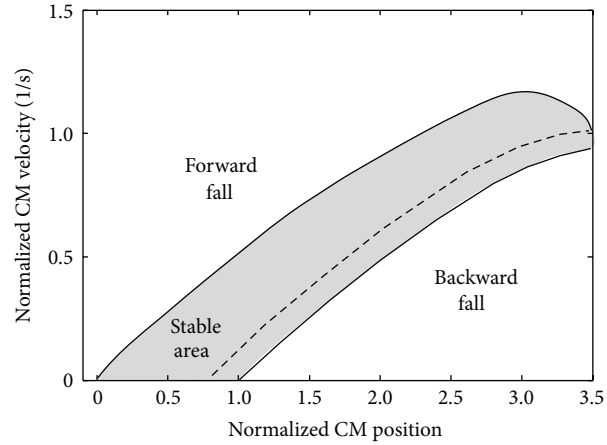

Figure 2: An example of the dynamic balance condition obtained through a simple inverted pendulum. The horizontal axis represents the posterior position of the CM, measured with respect to the toe and normalized to the subject's foot length (thus the 0 and 1 represent the toe and heel position, resp.). The vertical axis represents the anterior velocity of the CM normalized to the subject's height. The solid lines enclose the CM velocity-position conditions that allow recovering static balance (gray-shaded area), that is, the dynamic balance conditions. The broken line represents the most energy-efficient trajectory (zero external torque).

2.2. Models. The inverted pendulum model with a static support segment (Figure 1) has a physical state that can be described with two variables, the angle and the angular velocity. If the joint torque is known, the behavior of the pendulum is completely described. However, in order to maintain the conditions of no support segment movement,

this torque is subjected to several physical constraints. Rewriting every torque constraint as a function of the state variables, it is possible to find the torque ranges for every possible state of the system (see appendix for details). These torque ranges will be the allowed control ranges and therefore can be used to simulate the pendulum movement and to measure the controllability of the system. The models used in this paper for balance prediction in sit-to-stand movement are described below (see appendix for details).

2.2.1. Simple Inverted Pendulum Model. In previous studies, a simple inverted pendulum model with constant pendulum length l was used in Figure 1 for predicting the ability to control gait balance, since it had no redundancy and only one degree of freedom. A biped can be modeled by a support segment (foot) that does not move and the rest of the body that rotates around the ankle. Previous studies on dynamic balance during sit-to-stand movement also used the simple inverted pendulum model [10–12]. The total external torque measured with respect to the ankle τ is equal to the time variation of the angular momentum of the body. This was described by the following [8]:

$$\sum \tau = \frac{d}{dt}\left(I\dot{\theta}\right). \tag{1}$$

That is,

$$\tau - mgl\cos\theta = ml^2\ddot{\theta}, \tag{2}$$

where I, θ, m, g, and l stand for the CM rotational inertia, the angle of rotation of the CM, the body mass, the gravitational acceleration, and the pendulum length, respectively.

2.2.2. Inertia (Rotational Radius) Variable Inverted Pendulum Model. In this paper, the methodology presented by Pai and Patton [8] was expanded for predicting balance in sit-to-stand movement. Since the CM rotational radius of the inverted pendulum model (l in Figure 1) varies significantly in the sit-to-stand movement due to multiple joint interactions, a telescopic inverted pendulum model [13] that was shown to be useful to represent movements including multiple joint interactions was used. Here, variation of rotation radius of the pendulum was represented by variation of the CM rotational inertia $I(t)$. Therefore, the total external torque measured with respect to the ankle τ can be written as the following equation:

$$\sum \tau = \frac{d}{dt}\left(I\dot{\theta}\right) = \frac{dI}{dt}\dot{\theta} + I\frac{d\dot{\theta}}{dt}. \tag{3}$$

Assuming that the different joints of the body move synchronized for a given movement, it is possible to define the rotational inertia of the body as a function of the rotational angle of the CM $I(\theta)$. This assumption leads to the following equation:

$$\tau - mgl\cos\theta = \frac{dI(\theta)}{d\theta}\dot{\theta}^2 + I(\theta)\ddot{\theta}. \tag{4}$$

By defining the total body inertia as only a function of the rotational angle, the pendulum model reduces to a one degree of freedom system. Thus, it becomes possible to use the same methodology developed by Pai and Patton [8] to predict balance in the sit-to-stand movement.

It is important to mention that the inclusion of the inertia (rotational radius) variation affects not only the rotational movement equation (3), but also all the constraints equations (refer to the appendix).

2.3. Experimental Methods. Six healthy male subjects (25.3 ± 7.7 years old) participated in measurements of sit-to-stand movements for determination of their inertia function and for evaluation of the balance predictions. The CM velocity-position was estimated by measuring the position of the head, trunk, thigh, shank, and foot segments and estimating their mass distribution from the subject's weight [14]. The arm position was not used because a preliminary experiment performed in our study showed that it did not have much influence on the CM position calculation. It was assumed that the mass of each segment was uniformly distributed in each of the segments, and therefore the CM of a given body segment would be at the center of each of the segments. The body CM can be finally calculated from the position of the CM of all the segments.

Experimental data were recorded using 15 reflective markers with an 8-camera, 3D motion analysis system at a data sampling rate of 120 Hz (Vicon, Oxford Metrics, UK). Force plates were used for finding the timing of seat-off. All the theoretical balance predictions were calculated using MATLAB (Math Works, Inc., USA).

First, every subject was asked to perform two self-selected most natural sit-to-stands, to measure their sit-to-stand inertia function. The rotational inertia function was estimated by assigning the measured CM rotational radius ($l(\theta)$) to the rotational angle (θ):

$$I(\theta) = ml(\theta)^2, \tag{5}$$

$$l(\theta) = a_0\theta^3 + a_1\theta^2 + a_3\theta + a_4. \tag{6}$$

Here, $a_0 \sim a_4$ are parameters to approximate measured CM rotational radius. These functions were used to calculate the balance predictions during the sit-to-stand by the complex model that included multiple-joint influence.

Next, the subjects were asked to stand up at different initial conditions of the CM position which in turn will lead to different initial conditions of the CM velocity-position when the subject leaves the chair. In order to create different velocity-position CM conditions at the seat-off, the horizontal position of the feet was varied while sitting. The feet were shifted −0.2~1.2 foot lengths forward from the foot position where the ankle was at 90 degree, since those distances were showed to include successful and not successful stand ups. Every subject was asked to perform a total of 23 to 25 sit-to-stands. It is important to note that the actual position of the feet is rather unimportant since the real important information will be the horizontal BOS-CM distance that is precisely known from the markers position measurements.

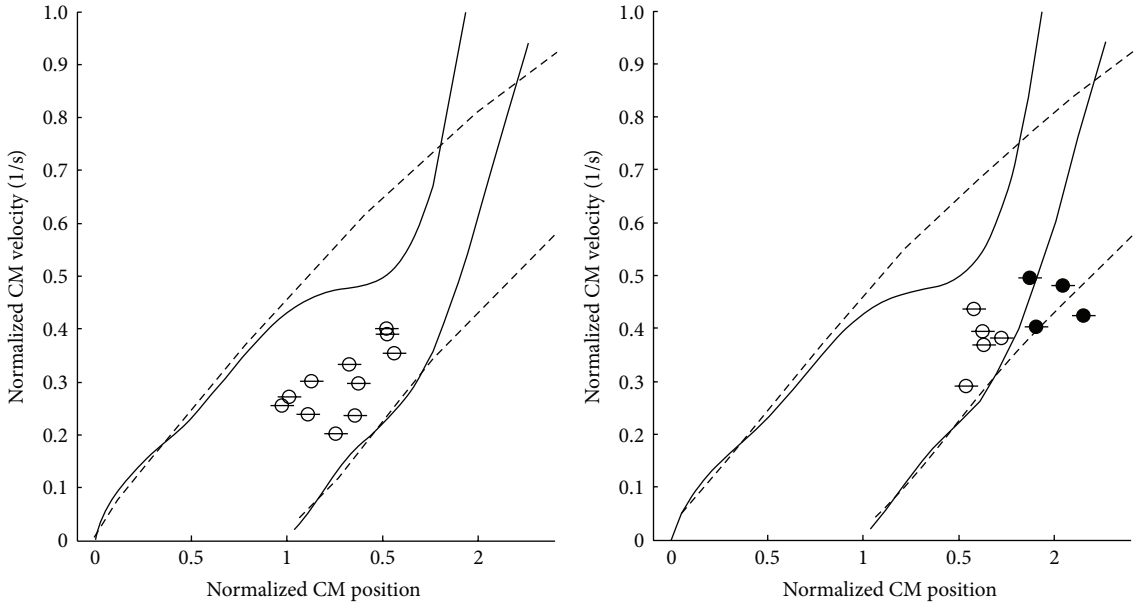

(a) Normal sit-to-stand data

(b) Demanding sit-to-stand data

Figure 3: An example of balance control prediction for normal sit-to-stand conditions (a) and demanding sit-to-stand conditions (b) (subject C). The solid lines show the boundaries for sit-to-stand balance control calculated with the inertia variable model, while the broken lines show the boundaries calculated with a simple inverted pendulum model. The open circles represent the successful sit-to-stand data while the closed circles represent the unsuccessful sit-to-stand data. In order to consider a data to be stable, the whole error bar on the point should be inside the boundaries.

3. Results

The BOS-CM horizontal position was gradually increased to demanding standing up conditions for every subject. A threshold of the BOS-CM horizontal distance of the first unsuccessful sit-to-stand was set to divide the data into two groups. The first group would be the conditions where every subject was able to make a successful sit-to-stand (normal condition). The second group would be all the data after the threshold (demanding condition), which was used for evaluating the theoretical balance predictions since it would include unstable sit-to-stand movements. From the results, the sitting BOS-CM horizontal distance threshold was 2.48 foot length. A total of 146 sit-to-stand measurements were performed, but due to markers disappearances or subjects' mistakes (BOS movement), 127 valid sit-to-stands were analyzed, in which 80 sit-to-stands were classified as the normal condition and 47 sit-to-stands as the demanding one.

Figure 3 shows an example of the balance control predictions calculated for one of the subjects. The plots on the maps show the CM velocity-position conditions of the measured sit-to-stands at the seat-off. The horizontal line in every data plot shows the error of the CM position estimation (±1.5 cm), which was calculated from the standard deviation of the mass distribution of the biomechanical model used to estimate the mass of each segment of subjects [14]. Data were considered to be stable only if the whole error bar was inside the boundaries. The results for all the subjects were that both the simple inverted pendulum model method and the inertia variable model method correctly classified all the 80 normal sit-to-stands as seen in Figure 3(a). As for the 47 demanding sit-to-stands, the complex model including multiple-joint influence showed a stability sensitivity of 100% and a specificity of 82.4% in the balance prediction. For the same data, the simple inverted pendulum prediction showed a sensitivity of 100%, but a specificity of 41.2%.

From the 80 normal sit-to-stands measured, it was found that 72 (90%) of them had extra kinetic energy compared to the (calculated) zero torque trajectory, while the other 8 data were almost on their zero torque trajectories crossing the zero torque condition after leaving chair. Figure 4 shows all of the 72 trajectories divided by the subject and plotted over their corresponding stability map. The broken line shows the zero torque trajectory which would be the most energy-efficient trajectory to make a successful sit-to-stand [8]. The gray lines show the measured CM sit-to-stand trajectories. On the other hand, only a few data (8 measured trajectories) did cross the zero torque condition. Figure 5 shows an example of this CM behavior during a sit-to-stand performed by subject A.

4. Discussion

The results from the demanding sit-to-stand conditions showed that the inertia variable pendulum model is better than a simple inverted pendulum model for evaluating the stability of a sit-to-stand movement. The specificity for the demanding sit-to-stand was improved from 41% to 82% by using the model including multiple-joint influences. On

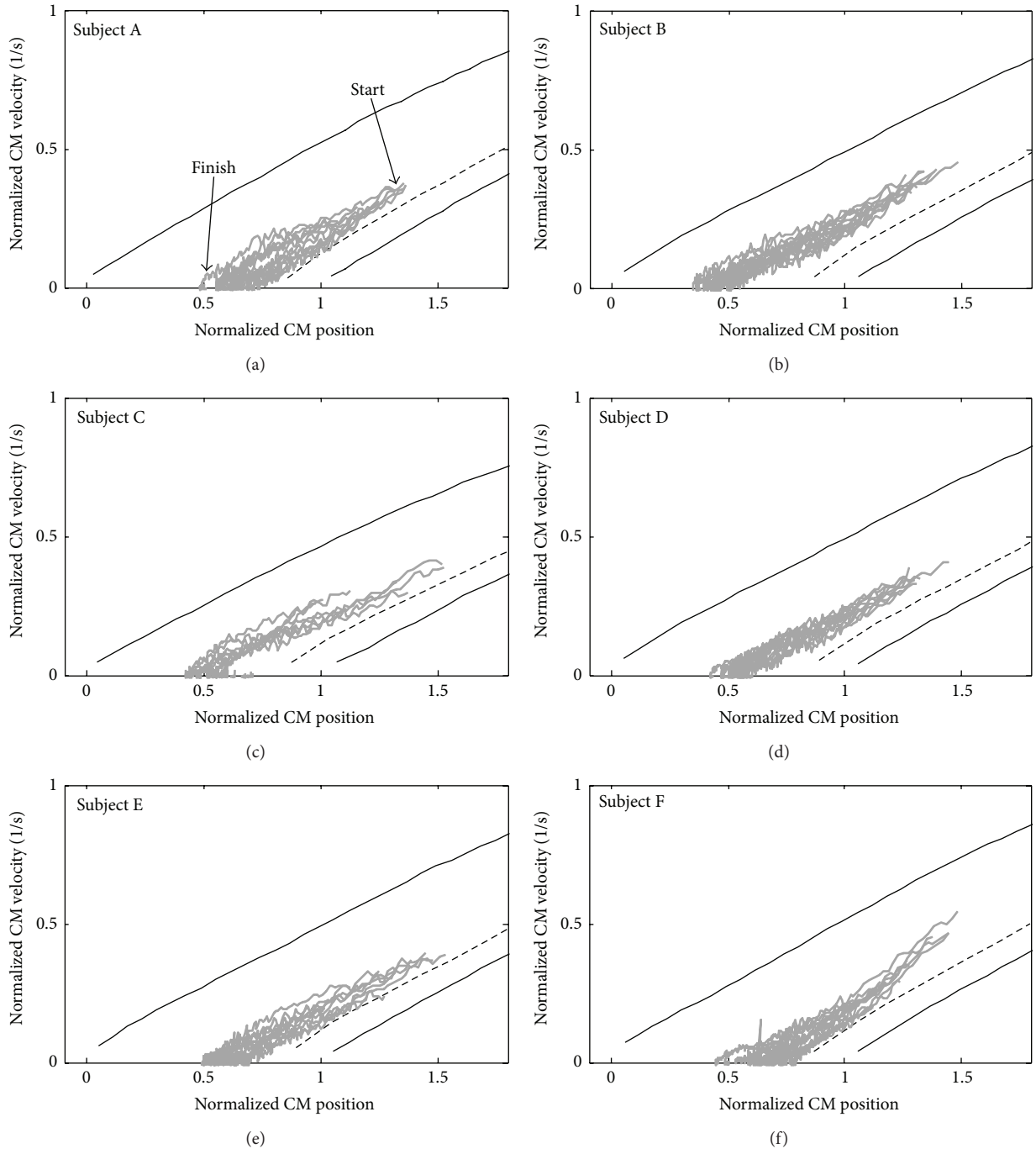

Figure 4: Measured CM sit-to-stand trajectories after leaving chair. Here, the 72 trajectories that showed a more energetic (faster) CM trajectory than the most efficient zero torque trajectory (in broken lines) are shown.

the other hand, both of the maps correctly classified all the normal (natural) sit-to-stand data as seen in Figure 3(a). Here, a similarity threshold between the maps was defined as the value that was calculated as the difference of the position control tolerance (the horizontal distance of the boundaries of the maps) becomes less than a certain value. For example, by setting the similarity threshold of 85%, it was found that the simple inverted pendulum prediction for sit-to-stands showed similar results as the inertia variable pendulum model up to CM velocities of 0.4 heights per second (see Figure 6). The CM velocity of 0.4 heights per second is much higher than the average velocity of the normal sit-to-stand data (0.24 ± 0.03 heights per second) measured with healthy subjects in this paper. Therefore, the simple inverted pendulum model can be valid for normal sit-to-stand movements.

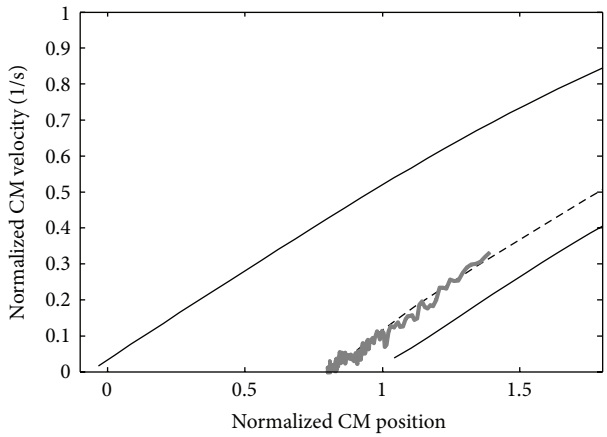

Figure 5: An example of a nonstandard control strategy performed by subject A. The CM position at the seat-off was 1.39 foot length. It is possible to see that at the moment of the seat-off, the CM is in a backward position near the most efficient zero torque compared to the trajectories of the same subject in Figure 4.

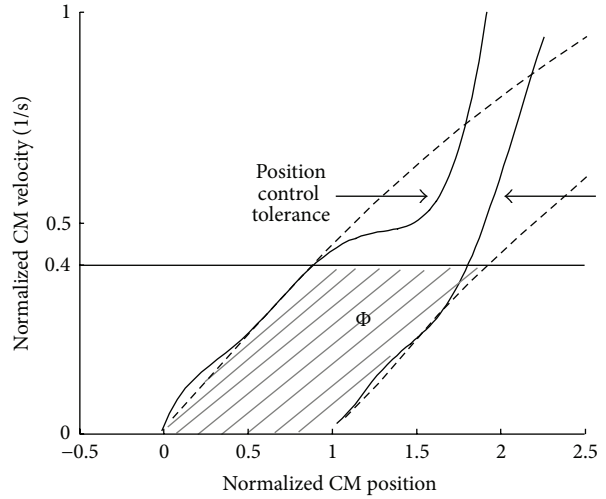

Figure 6: An example of validity threshold for the simple inverted pendulum model. The plot on the map shows average velocity at the seat-off for a natural sit-to-stand.

The simple inverted pendulum model is also considered to be reliable for rehabilitation assessment and balance analysis in sit-to-stand movements of motor-disabled subjects and elderly persons. For sit-to stand movements that have low CM velocity at the seat-off, there was no large difference in the map between the simple inverted pendulum model and the inertia variable pendulum model as shown in Figure 6. In the studies on dynamic balance during sit-to-stand movement, CM velocities at the seat-off of elderly persons were similar to or lower than young subjects [11] and those of persons with Parkinson disease were lower than those of healthy elderly subjects [12]. These suggest that normal sit-to-stand movements of motor-disabled subjects and elderly persons show lower CM velocities than those of natural (normal) sit-to-stand of healthy young subjects, which could be evaluated by the simple inverted pendulum model.

As seen in Figure 4, the CM control strategy in a normal sit-to-stand condition is different from the most energy-efficient strategy shown by the broken lines. For a given CM position, it is possible to see that the CM velocity is higher than the velocity required for achieving a successful sit-to-stand. This extra velocity would come from an extra effort before the subject leaves the chair and then would require an extra effort to absorb it after the subject leaves the chair. These suggest that the natural sit-to-stand control strategy has a velocity-position target that satisfies very stable physical conditions even if that means an extra energy cost. These can also be understood when comparing the CM trajectories and the balance control boundaries in Figure 4. It is clear that this energy inefficiency allows a greater balance control tolerance, improving the stability against a dangerous backward fall (lower boundary).

It seems that the natural gait control strategy first tries to satisfy the stability requirements rather than optimizing the energy usage. However, energy considerations are often used when analyzing gait and designing assistive and rehabilitation technology [15, 16]. It is suggested that not only energy but also stability may play a major role in control strategy and therefore should be also taken into consideration.

As for the data that crossed the zero torque line as shown in Figure 5, it was found that most of them had a backward CM position at the seat-off. During the measurements, the subjects were asked to stand up in different CM conditions including very backward positioned CM conditions. It is considered that the subjects did not use the standard control strategy or they tried but failed to achieve their intended forward velocity when they were standing up in different foot positions than usual.

5. Conclusions

The balance prediction in sit-to-stand movements obtained using a traditional simple inverted pendulum was compared to the prediction of an inertia variable inverted pendulum model including multiple-joint influence. The results showed that the multiple-joint influence model is more accurate in predicting balance during sit-to-stand movements under demanding conditions and also that the traditionally used simple inverted pendulum is still reliable in predicting balance during normal or nondemanding sit-to-stand movements. Especially, the simple inverted pendulum model could be effective for sit-to-stand movements with low CM velocity at the seat-off. In addition, almost all CM trajectories during normal sit-to-stands seemed to follow the same control strategy, in which the subjects used extra energy than the minimum one necessary for standing up. This suggests that the safety considerations come first before the energy-efficiency considerations during a sit-to-stand since the most energy efficient trajectory is close to the backward fall boundary.

Appendix

Equations (A.1)–(A.6) describe the motion of the pendulum and the BOS (see Figure 1). Notice that the inertia variation is introduced making the pendulum length a function of the angle (see (3)–(5))

$$\sum \tau = \frac{d}{dt}\left(I\dot{\theta}\right) = \frac{dI}{dt}\dot{\theta} + I\frac{d\dot{\theta}}{dt}\,(\mathrm{CM}),$$
$$\tau - mgl\cos\theta = \frac{dI}{d\theta}\dot{\theta}^2 + I\ddot{\theta} = 2ml\frac{dl}{d\theta}\dot{\theta}^2 + ml^2\ddot{\theta}, \quad (A.1)$$
$$\ddot{\theta} = \frac{\tau - mgl\cos\theta - 2ml\,(dl/d\theta)\,\dot{\theta}^2}{ml^2} = \frac{\tau - mlJ}{ml^2}.$$

Here, $J = g\cos\theta + 2(dl/d\theta)\dot{\theta}^2$.

For the CM,

$$-F_{ax} = m\ddot{x}_{\mathrm{CM}}, \quad (A.2)$$
$$-F_{ay} - mg = m\ddot{y}_{\mathrm{CM}}. \quad (A.3)$$

For the foot,

$$\tau + \left(l_f - a - \mathrm{COP}\right)F_{gy} - bF_{gx} - cm_f g = 0,$$
$$\mathrm{COP} = l_f - \left(\frac{bF_{gx} - \tau + cm_f g}{F_{gy}} + a\right), \quad (A.4)$$
$$F_{gx} = -F_{ax}, \quad (A.5)$$
$$F_{gy} = m_f g - F_{\mathrm{ay}}. \quad (A.6)$$

Transforming the constraints shown by (A.7)–(A.10) into restrictions of the ankle torque would make it possible to find the feasible torque for the simulation

$$F_{gy} \geq 0, \quad (A.7)$$
$$\left|F_{gx}\right| \leq \mu F_{gy}, \quad (A.8)$$
$$0 < \mathrm{COP} < l_f, \quad (A.9)$$
$$\tau_{\text{maximum Plantarflexion}} < \tau < \tau_{\text{maximum Dorsiflexion}}. \quad (A.10)$$

From the constraint of the ground reaction force (A.7) and (A.3) and (A.6),

$$m\ddot{y}_{\mathrm{CM}} + \left(m_f + m\right)g \geq 0,$$
$$\ddot{y}_{\mathrm{CM}} + \left(\frac{m_f}{m} + 1\right)g \geq 0,$$
$$\left(\ddot{\theta}A_1 + \dot{\theta}^2 B_1\right) + \left(\frac{m_f}{m} + 1\right)g \geq 0, \quad (A.11)$$
$$\left(\ddot{\theta}A_1 + \dot{\theta}^2 B_1\right) + K_1 \geq 0,$$

where,

$$A_1 = \frac{dl}{d\theta}\sin\theta + l\cos\theta,$$
$$B_1 = \frac{d^2 l}{d\theta^2}\sin\theta + 2\frac{dl}{d\theta}\cos\theta - l\sin\theta, \quad (A.12)$$
$$K_1 = \left(\frac{m_f}{m} + 1\right)g.$$

From (A.1), it becomes

$$(\tau - mlJ)\,A_1 \geq -ml^2\left(\dot{\theta}^2 B_1 + K_1\right). \quad (A.13)$$

Then, solving for τ

$$\tau \geq -\frac{ml^2}{|A_1|}\left(\dot{\theta}^2 B_1 + K_1\right) + mlJ, \quad \text{for } A_1 > 0,$$
$$\tau \leq -\frac{ml^2}{|A_1|}\left(\dot{\theta}^2 B_1 + K_1\right) + mlJ, \quad \text{for } A_1 < 0. \quad (A.14)$$

Equation (A.8) gives the friction anterior and friction posterior constraints. For the maximum anterior friction condition, (A.8) becomes

$$F_{gx} \geq -\mu F_{gy}. \quad (A.15)$$

From (A.2), (A.5) and (A.3), (A.6),

$$m\ddot{x}_{\mathrm{CM}} \geq -\mu\left\{m\ddot{y}_{\mathrm{CM}} + \left(m_f + m\right)g\right\},$$
$$\ddot{x}_{\mathrm{CM}} \geq -\mu\ddot{y}_{\mathrm{CM}} - \left(\frac{m_f}{m} + 1\right)g\mu, \quad (A.16)$$
$$\ddot{\theta}A_x + \dot{\theta}^2 B_x \geq -\mu\left(\ddot{\theta}A_1 + \dot{\theta}^2 B_1\right) + K_2,$$

where,

$$A_x = \frac{dl}{d\theta}\cos\theta - l\sin\theta,$$
$$B_x = \frac{d^2 l}{d\theta^2}\cos\theta - 2\frac{dl}{d\theta}\sin\theta - l\cos\theta, \quad (A.17)$$
$$K_2 = -\mu K_1.$$

Then,

$$\ddot{\theta}A_2 \geq \dot{\theta}^2 B_2 + K_2, \quad (A.18)$$

where,

$$A_2 = \mu A_1 + A_x,$$
$$B_2 = -\mu B_1 - B_x. \quad (A.19)$$

From (A.1),

$$(\tau - mlJ)\,A_2 \geq ml^2\left(\dot{\theta}^2 B_2 + K_2\right). \quad (A.20)$$

Solving for τ,

$$\tau \geq \frac{ml^2}{|A_2|}\left(\dot{\theta}^2 B_2 + K_2\right) + mlJ, \quad \text{for } A_2 > 0,$$
$$\tau \leq \frac{ml^2}{|A_2|}\left(\dot{\theta}^2 B_2 + K_2\right) + mlJ, \quad \text{for } A_2 < 0. \tag{A.21}$$

For the maximum posterior friction condition, (A.8) becomes

$$F_{gx} \leq \mu F_{gy}. \tag{A.22}$$

From (A.2), (A.5) and (A.3), (A.6),

$$m\ddot{x}_{\mathrm{CM}} \leq \mu\left\{m\ddot{y}_{\mathrm{CM}} + \left(m_f + m\right)g\right\},$$
$$\ddot{x}_{\mathrm{CM}} \leq \mu\ddot{y}_{\mathrm{CM}} + \left(\frac{m_f}{m} + 1\right)g\mu, \tag{A.23}$$
$$\ddot{\theta}A_3 \leq \dot{\theta}^2 B_3 + K_3,$$

where,

$$A_3 = A_x - \mu A_1 = A_2 - 2\mu A_1,$$
$$B_3 = \mu B_1 - B_x = B_2 + 2\mu B_1, \tag{A.24}$$
$$K_3 = \mu K_1 = -K_2;$$

from (A.1)

$$(\tau - mlJ)\,A_3 \leq ml^2\left(\dot{\theta}^2 B_3 + K_3\right); \tag{A.25}$$

solving for τ

$$\tau \leq \frac{ml^2}{|A_3|}\left(\dot{\theta}^2 B_3 + K_3\right) + mlJ, \quad \text{for } A_3 > 0,$$
$$\tau \geq \frac{ml^2}{|A_3|}\left(\dot{\theta}^2 B_3 + K_3\right) + mlJ, \quad \text{for } A_3 < 0. \tag{A.26}$$

Equation (A.9) gives the COP heel and COP toe constraints. For the COP behind the heel condition, (A.9) becomes

$$\mathrm{COP} < l_f. \tag{A.27}$$

Equation (A.4) becomes

$$l_f \geq l_f - \left(\frac{bF_{gx} - \tau + cm_f g}{F_{gy}} + a\right),$$
$$0 \geq -aF_{gy} - bF_{gx} + \tau - cm_f g. \tag{A.28}$$

From (A.2), (A.5) and (A.3), (A.6),

$$0 \geq (-a)\left\{m\ddot{y}_{\mathrm{CM}} + \left(m_f + m\right)g\right\} - b\left(m\ddot{x}_{\mathrm{CM}}\right) + \tau - cm_f g,$$
$$-am\ddot{y}_{\mathrm{CM}} - bm\ddot{x}_{\mathrm{CM}} + \tau \leq a\left(m_f + m\right)g + cm_f g \tag{A.29}$$
$$-am\left(A_1\ddot{\theta} + B_1\dot{\theta}^2\right) - bm\left(A_x\ddot{\theta} + B_x\dot{\theta}^2\right) + \tau \leq K_4$$
$$\ddot{\theta}E_1 + \tau + \dot{\theta}^2 D_1 \leq K_4,$$

where,

$$E_1 = -amA_1 - bm\left(A_2 - \mu A_1\right),$$
$$D_1 = -amB_1 + bm\left(B_2 + \mu B_1\right), \tag{A.30}$$
$$K_4 = a\left(m_f + m\right)g + cm_f g.$$

From (A.1),

$$(\tau - mlJ)\,E_1 + \tau ml^2 \leq ml^2\left(K_4 - \dot{\theta}^2 D_1\right); \tag{A.31}$$

solving for τ

$$\tau\left(ml^2 + E_1\right) \leq ml^2\left(K_4 - \dot{\theta}^2 D_1\right) + mlJE_1,$$
$$\tau \leq \frac{ml^2\left(K_4 - \dot{\theta}^2 D_1\right) + mlJE_1}{\left|ml^2 + E_1\right|}, \quad \text{for } ml^2 + E_1 > 0,$$
$$\tau \geq \frac{ml^2\left(K_4 - \dot{\theta}^2 D_1\right) + mlJE_1}{\left|ml^2 + E_1\right|}, \quad \text{for } ml^2 + E_1 < 0. \tag{A.32}$$

For the COP after the toe condition, (A.9) becomes

$$0 < \mathrm{COP}. \tag{A.33}$$

Equation (A.4) becomes

$$0 < l_f - \left(\frac{bF_{gx} - \tau + cm_f g}{F_{gy}} + a\right),$$
$$0 < \left(l_f - a\right)F_{gy} - bF_{gx} + \tau - cm_f g. \tag{A.34}$$

From (A.2), (A.5) and (A.3), (A.6),

$$0 < \left(l_f - a\right)\left(m\ddot{y}_{\mathrm{CM}} + \left(m_f + m\right)g\right) - b\left(m\ddot{x}_{\mathrm{CM}}\right) + \tau - cm_f g,$$
$$\left(l_f - a\right)m\ddot{y}_{\mathrm{CM}} - bm\ddot{x}_{\mathrm{CM}} + \tau \geq -\left(l_f - a\right)\left(m_f + m\right)g + cm_f g,$$
$$m\left(l_f - a\right)\left(A_1\ddot{\theta} + B_1\dot{\theta}^2\right) - mb\left(A_x\ddot{\theta} + B_x\dot{\theta}^2\right) + \tau \geq K_5$$
$$\ddot{\theta}E_2 + \tau + \dot{\theta}^2 D_2 \geq K_5, \tag{A.35}$$

where,

$$E_2 = m\left(l_f - a\right)A_1 - mb\left(A_2 - \mu A_1\right),$$
$$D_2 = m\left(l_f - a\right)B_1 + mb\left(B_2 + \mu B_1\right), \tag{A.36}$$
$$K_5 = -\left(l_f - a\right)\left(m_f + m\right)g + cm_f g.$$

From (A.1)

$$(\tau - mlJ)\,E_2 + \tau ml^2 + \geq ml^2\left(K_5 - \dot{\theta}^2 D_2\right). \tag{A.37}$$

Solving for τ,

$$\tau\left(ml^2 + E_2\right) \geq ml^2\left(K_5 - \dot{\theta}^2 D_2\right) + mlJE_2,$$

$$\tau \geq \frac{ml^2\left(K_5 - \dot{\theta}^2 D_2\right) + mlJE_2}{\left|ml^2 + E_2\right|}, \quad \text{for } ml^2 + E_2 > 0,$$

$$\tau \leq \frac{ml^2\left(K_5 - \dot{\theta}^2 D_2\right) + mlJE_2}{\left|ml^2 + E_2\right|}, \quad \text{for } ml^2 + E_2 < 0. \tag{A.38}$$

Conflict of Interests

The authors confirm that there is no conflict of interests in relation to this work.

Acknowledgment

This work was supported in part by the Ministry of Education, Culture, Sports, Science and Technology of Japan under a grant-in-aid for challenging exploratory research.

References

[1] C. A. M. Doorenbosch, "Two strategies of transferring from sit-to-stand; the activation of monoarticular and biarticular muscles," *Journal of Biomechanics*, vol. 27, no. 11, pp. 1299–1307, 1994.

[2] M. M. Gross, P. J. Stevenson, S. L. Charette, G. Pyka, and R. Marcus, "Effect of muscle strength and movement speed on the biomechanics of rising from a chair in healthy elderly and young women," *Gait and Posture*, vol. 8, no. 3, pp. 175–185, 1998.

[3] Y.-C. Pai and K. Iqbal, "Simulated movement termination for balance recovery: can movement strategies be sought to maintain stability in the presence of slipping or forced sliding?" *Journal of Biomechanics*, vol. 32, no. 8, pp. 779–786, 1999.

[4] J.-Y. You, Y.-L. Chou, C.-J. Lin, and F.-C. Su, "Effect of slip on movement of body center of mass relative to base of support," *Clinical Biomechanics*, vol. 16, no. 2, pp. 167–173, 2001.

[5] T. Bhatt and Y.-C. Pai, "Long-term retention of gait stability improvements," *Journal of Neurophysiology*, vol. 94, no. 3, pp. 1971–1979, 2005.

[6] T. Bhatt, J. D. Wening, and Y.-C. Pai, "Influence of gait speed on stability: recovery from anterior slips and compensatory stepping," *Gait and Posture*, vol. 21, no. 2, pp. 146–156, 2005.

[7] G. Barton, P. Lisboa, A. Lees, and S. Attfield, "Gait quality assessment using self-organising artificial neural networks," *Gait and Posture*, vol. 25, no. 3, pp. 374–379, 2007.

[8] Y.-C. Pai and J. Patton, "Center of mass velocity-position predictions for balance control," *Journal of Biomechanics*, vol. 30, no. 4, pp. 347–354, 1997.

[9] A. L. Hof, M. G. J. Gazendam, and W. E. Sinke, "The condition for dynamic stability," *Journal of Biomechanics*, vol. 38, no. 1, pp. 1–8, 2005.

[10] F. Mourey, A. Grishin, P. D'Athis, T. Pozzo, and P. Stapley, "Standing up from a chair as a dynamic equilibrium task: a comparison between young and elderly subjects," *Journals of Gerontology A*, vol. 55, no. 9, pp. B425–B431, 2000.

[11] M. Fujimoto and L.-S. Chou, "Dynamic balance control during sit-to-stand movement: an examination with the center of mass acceleration," *Journal of Biomechanics*, vol. 45, no. 3, pp. 543–548, 2012.

[12] T. Bhatt, F. Yang, M. K. Y. Mak, C. W. Y. Hui-Chan, and Y. C. Pai, "Effect of externally cued training on dynamic stability control during the sit-to-stand task in people with Parkinson disease," *Physical Therapy*, vol. 93, no. 4, pp. 492–503, 2013.

[13] E. Papa and A. Cappozzo, "A telescopic inverted-pendulum model of the musculo-skeletal system and its use for the analysis of the sit-to-stand motor task," *Journal of Biomechanics*, vol. 32, no. 11, pp. 1205–1212, 1999.

[14] M. J. Pavol, T. M. Owings, and M. D. Grabiner, "Body segment inertial parameter estimation for the general population of older adults," *Journal of Biomechanics*, vol. 35, no. 5, pp. 707–712, 2002.

[15] R. L. Waters and S. Mulroy, "The energy expenditure of normal and pathologic gait," *Gait and Posture*, vol. 9, no. 3, pp. 207–231, 1999.

[16] M.-A. Brehm, D. L. Knol, and J. Harlaar, "Methodological considerations for improving the reproducibility of walking efficiency outcomes in clinical gait studies," *Gait and Posture*, vol. 27, no. 2, pp. 196–201, 2008.